CHALMERS
UNIVERSITY OF TECHNOLOGY

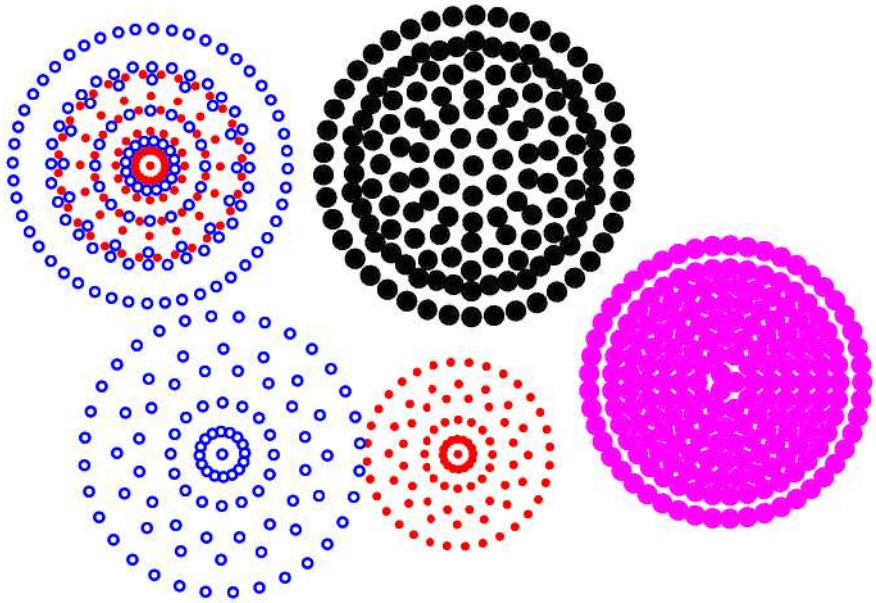

Properties of Sparse Array Antennas – A trade-off investigation

Thesis for the Degree of Master of Science

MARIKA SVENSSON

Department of Signals and Systems
CHALMERS UNIVERSITY OF TECHNOLOGY
Gothenburg, Sweden 2016

Master's thesis 2016:NN

Properties of Sparse Array Antennas – A trade-off investigation

MARIKA SVENSSON

CHALMERS
UNIVERSITY OF TECHNOLOGY

Department of Signals and Systems
Division of Antenna Systems
Chalmers University of Technology
Gothenburg, Sweden 2016

Properties of Sparse Array Antennas
– A trade-off investigation
MARIKA SVENSSON

Supervisor: Dr. Johan Wettergren, RUAG space
Co-Supervisor: Carlo Bencivenni, department of Signals and Systems
Co-Supervisor: Assist. Prof. Rob Maaskant, department of Signals and Systems
Examiner: Assoc. Prof. Dr. Marianna Ivashina, department of Signals and Systems

Master's Thesis 2016:NN
Department of Signals and Systems
Division of Antenna Systems
Chalmers University of Technology
SE-412 96 Gothenburg
Telephone +46 31 772 1000

Cover: Shows three types of sparse array antennas obtained through convex optimisation and one density tapered array.

Typeset in LaTeX
Printed by Chalmers University of Technology
Gothenburg, Sweden 2016

Abstract

Sparse array antennas employ fewer elements than non-sparse array antennas and can therefore provide less costly solutions without necessarily compromising the high degree of functionality. A trade-off investigation, conducted for RUAG space, of sparse array antennas focusing on satellite communication (SATCOM) applications is presented in this MSc thesis. Of primary importance are the number of elements and controls required which depends on the side lobe level, gain loss, Field of View (FoV), inter-beam distance, total aperture size, element positioning and element size. Furthermore the number of elements depends also on weather one common element or two separate elements are employed for the receive (RX) and transmit (TX).

The methodology for obtaining sparse array antennas utilises convex optimisation while including Mutual Coupling (MC) effects and allowing multi-beam optimisation. Additionally, by integrating the full-wave EM simulation software FEKO MC effects are accounted for accurately. Moreover, the convex optimised array antennas are compared to Taylor synthesised and density tapered array antennas.

The synthesis problem turned out intractable for full size array antenna cases making it necessary to exclude MC effects. However, when MC effects are small, accurate results can be obtained while simultaneously reducing computations in the order of weeks. Such is the case for the array antenna, with the FoV 4° and inter-beam distance 1°, with separate RX/TX apertures and elements where as for the array antenna with common RX/TX apertures and separate RX/TX elements the radiation patterns violated the radiation mask, which can be attributed to the higher element number density of the shared RX/TX aperture.

Results indicate that the convex optimised array antennas lie in the region of 100–1000 elements when varying the FoV between $4\,°-8\,°$ and inter-beam distance between $0.5\,°-1\,°$. Furthermore, Taylor synthesised array antennas are comparable to convex optimised array antennas with respect to the number of elements, while the density tapered array antennas requires significantly denser array antennas. Moreover, by employing common RX/TX elements the number of elements were reduced significantly compared to array antennas of separate RX/TX elements, with a drawback of rendering it more difficult to obtain solutions through the convex optimisation. Furthermore, when employing shared RX/TX apertures and separate RX/TX elements the total aperture size is reduced significantly compared to array antennas with separate RX/TX apertures and elements. In conclusion, the array configurations with common RX/TX apertures proved to be the most desirable due to the total aperture size, gain and number of elements.

Keywords: sparse array antenna, trade-off study, FEKO, convex optimisation, antenna array synthesis, RUAG space.

Acknowledgments

I would like to thank Dr. Johan Wettergren for guidance and interest given to this project, as well as my colleagues at RUAG space whom welcomed me warmly into the field of space technology and wireless communication. Furthermore, I would like to thank Carlo Bencivenni for giving me advice and guiding me in the array antenna synthesis. I would also like to thank Assist. Prof. Rob Maaskant for giving me advice when writing the report and Assoc. Prof. Dr. Marianna Ivashina for welcoming me to the department of Signals and Systems.

Foremost, I would like to thank Peter Broere for relentlessly supporting me and making my world a great place to be.

Marika Svensson, Gothenburg, March 2016

List of Publications

Poster

Johan Wettergren, Marika Svensson and Carlo Bencivenni, "Footprint Sharing Sparse Arrays for 20 and 30 GHz", AntennEMB Symposium at the Swedish Microwave Days 15-16 March 2016.

Acronyms

HPBW	Half Power Beam Width
FNBW	First Null Beam Width
FEKO	FEldberechning für Körper mit beliebiger Oberfläche
MoM	Method of Moments
FEM	Finite Element Method
SLL	Side Lobe Level
EoC	Edge of Coverage
AoC	Area of Coverage
OoC	Out of Coverage
FoV	Field of View
EEP	Embedded Element Pattern
IEP	Isolated Element Pattern
IAC	Initial Array Configuration
EM	ElectroMagnetic
MC	Mutual Coupling

Contents

List of Tables

1
Introduction

A brief introduction to the subject of array antennas and the main focus of the report will be provided in this chapter. First, the background to this project is presented which is followed up by the purpose and limitations of the thesis which is finally concluded with the thesis outline.

1.1 Background

There are several benefits of using array antennas in satellite communication (SATCOM) applications, including the prospect of increasing the overall gain as well as the functionality of steering the main beam in a desired direction. Furthermore, the main motivation for designing optimal sparse array antennas is that they present the possibility of having antennas with high degree of functionality while lessening the number of elements in comparison with non-sparse array antennas, as the manufacturing costs are reduced significantly. Of importance is that the reduction in the number of elements does not necessarily compromise the degree of functionality of the sparse array antennas compared to the non-sparse array antennas. Indeed, some non-sparse array antennas would prove too expensive and possibly too heavy to be realised for the targeted applications [1]. It is therefore of interest to research and improve the performance of array antennas to RUAG space.

The approaches previously used to design sparse array antennas can be categorised into two approaches. The first approach is referred to as the Sparse Array approach and the second is referred to as the Thinned Array approach. These approaches encompasses various number of mathematical techniques, for example stochastic, analytical and deterministic methods [2]. The stochastic techniques often utilises genetic algorithms, particle swarm or ant colony. These algorithms are, rather computationally demanding which makes them a poor choice for optimising large array antenna problems [3]. The analytical implementation utilises methods such as Matrix Pencil Beam Method and Almost Different Sets. These approaches are computationally inexpensive, making them suitable for large array antenna problems, although the analytical methods usually assumes no Mutual Coupling (MC) effects. [2]. Finally, deterministic methods are for example that of density tapering [4] and Taylor synthesis [5], these approaches also do not consider MC effects but are computationally inexpensive.

The methodology employed for designing optimum array antennas in this thesis has

been established at the department of Signals and Systems at Chalmers, it utilises convex optimisation and undertakes the problem of accounting for realistic antenna elements, i.e. including MC effects in the optimisation. The method minimises the number of elements while simultaneously allowing for multi-beam optimisation if desired. As a comment, the reader may bare in mind that the previous mentioned approaches to sparse array antennas often only consider simplified situations or resort to exclude MC effects altogether [6].

Furthermore, RUAG Space is currently in cooperation with Chalmers University of Technology, Royal Institute of Technology and Ericsson, within Chalmers Antenna Systems Excellence Centre (CHASE). The main interest for RUAG lies thus in developing sparse array antennas for SATCOM applications that are more cost-effective. This MSc thesis will therefore be focused on finding sparse array antenna designs with requirements for SATCOM applications through techniques previously developed at Chalmers.

1.2 Purpose and Limitations

With newly developed theory and methodology further array antenna designs and analysis were possible to investigate for SATCOM applications, making the objective of this thesis to complete a trade-off investigation where multiple array antennas will be designed. The trade-offs that will be considered for the investigation are:

- Number of elements and controls depending on the coverage, the latter which is also referred to as the Field of View (FoV)
- Total aperture size
- Element positioning
- Element size versus number of elements
- Number of elements versus side lobe level (SLL) and gain loss
- Effects of changed coverage or inter-beam distance
- Common versus separate RX and TX elements

The convex optimised array antennas will furthermore be compared to deterministically determined array antennas. In particular these are classically Taylor synthesised array antennas with the Tschebyscheff-error as well as density tapered array antennas. As an addition to the existing code and developed method, the commercial software FEKO will be interfaced with MATLAB to simulate the MC effects, as this would provide results with a fully-fledged calculation tool.

1.3 Thesis Outline

The chapters that will follow the Introduction are Theory, Method, Results, Discussion, Conclusions and lastly Future Recommendations. Moreover, an appendix is provided with more detailed results from the trade-off investigation.

An introduction to antenna theory will be given Ch. 2. That in Sec. 2.1 begins with theory dealing with general electromagnetism and antenna concepts such as the field regions, far-field function, directivity and radiation patterns. In particular, in Sec. 2.1.7 is the terminology used for radiation pattern characteristics presented. This will be followed up in Sec. 2.2 by theory on array antennas where concepts such as the far-field function of array antennas, beam scanning and MC effects will be discussed. Concluding Ch. 2 is Sec. 2.3 where the deterministic procedures, Taylor synthesis and density tapering, of array antennas are described.

In Ch. 3 will the methodology of the trade-off investigation be presented, which includes the three array antenna configurations, array element types with their construction in FEKO, convex optimisation algorithm as well as the modifications considered to the initial algorithm and synthesis procedure. In particular, in Sec. 3.1 are the details for the trade-off investigation presented, which accounts for antenna specifications as well as the imposed radiation masks.

The numerical results, radiation patterns and array antenna designs from the trade-off investigation will be presented in Ch. 4. Additionally, simulations including MC effects in the post-evaluation are also presented for case where the FoV is 4° and the inter-beam distance is 1° of array antenna configurations 1 and 2. These results are discussed in Ch. 5 leading up to the conclusions and recommendations for future research, in Ch. 6 and Ch. 7, respectively. Concluding the thesis, is the Appendix in Sec. A where radiation patterns and array antenna designs are given for FoV 5°-7°.

2

Theory

Theory for obtaining a good insight in the results and simulations of sparse array antennas is presented in this chapter. Sec. 2.1 includes a basis to antenna theory and electromagnetism with the concepts of the employed units and EM field quantities, field regions in space, the far-field function of antennas, antenna polarisation, radiated power, directivity, gain, antenna efficiency, S-parameters, Z-parameters and radiation patterns.

Afterwards, in Sec. 2.2, theoretical details regarding array antennas are provided which includes the far-field function for linear and planar array antennas, steering the main beam of array antennas and MC effects. Lastly, the procedures of the deterministic approaches to array antennas are presented in Sec. 2.3, which encompasses Taylor synthesis and density tapering.

2.1 Antennas and Electromagnetism

It is common to use SI-units or units derived from SI-units when working with antennas and EM field theory. The most common quantities and their units used in this thesis are given below in Table 2.1 [7].

Table 2.1: Relevant quantities and units of antenna and EM field theory.

Electric field **E**	[V/m]
Far-field function **G**	[V]
Magnetic field **H**	[A/m]
Wave impedance η	[Ω]
Electric current I	[A]
Electric impedance Z	[Ω]
Wave number k	[1/m]
Wavelength λ	[m]
HPBW θ_{HPBW}	[deg]
FNBW θ_{FNBW}	[deg]
Instantaneous power density vector **W**	[W/m^2]
Power density vector $\mathbf{W}_{\text{ave}}$	[W/m^2]
Radiation intensity U	$\left[\frac{\text{W}}{\text{unit solid angle}}\right]$
Voltage V	[V]
Radiated power P_{rad}	[W]
Instantaneous radiated power P	[W]
Directive gain D_0	[dBi]
Maximum gain G_0	[dBi]

2.1.1 Field Regions and the Far-field Function

The volume enclosing a radiating object can be separated into three regions, these are commonly referred to as the reactive near-field region, the radiating near-field region and the far-field region. The latter two are regions where the Fresnel and Fraunhofer approximations hold, respectively [8]. The antenna theory can be greatly simplified by the fact that the EM field and derived quantities are typically considered in the far-field region. The far-field region can be described as the region where the angular field distribution is considered independent of the distance from the observation point to the antenna. This distance, r, is known to be

$$r > \frac{2D^2}{\lambda} \tag{2.1}$$

where D is the largest diameter size of the antenna, λ is the wavelength and r is the distance from the antenna to the observation point [7]. In Fig. 2.1 are the field regions depicted with the approximative limits

$$|\mathbf{r}_1| = 0.62\frac{\sqrt{D^3}}{\lambda} \text{ and } |\mathbf{r}_2| = \frac{2D^2}{\lambda} \tag{2.2}$$

for the radiating near-field region and the far-field region, respectively. The antenna has an aperture diameter D and its phase reference point is placed in the centre of the aperture.

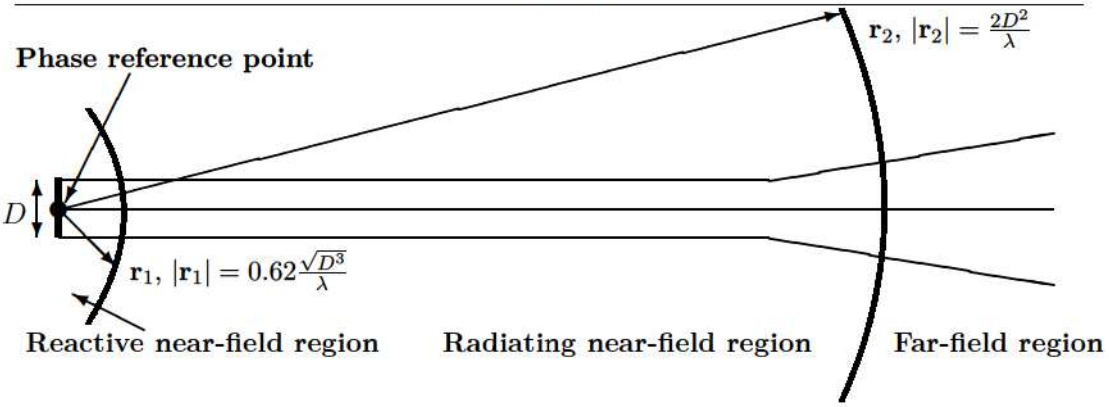

Figure 2.1: Illustration of the field regions surrounding an antenna with diameter D and phase reference point in the centre of the antenna.

The region in space where the far-field region commences can not be definitely defined, as it can be required larger or smaller than $2D^2/\lambda$ depending on what type of antenna is considered. Furthermore, for SATCOM applications will the observation point will clearly lie in the far-field region as the wavelength will be in the order of 10^{-2} m, while the distance from the Earth of the antenna will be in the order of 10^7 m and the diameter of the array antennas will be in the order of 10^0 m.

Next, the antenna far-field function $\mathbf{G}(\hat{\mathrm{r}})$ and its radiated electric field, $\mathbf{E}(\mathbf{r})$, are presented of an arbitrary antenna by considering it for an observation point $\mathbf{r}$ in the far-field region, i.e.

$$\mathbf{r} = \mathbf{R} + \mathbf{r}_0. \tag{2.3}$$

As the distance from the antenna to the observation point and angular dependencies become separable in the far-field region, the following expression is obtained for the electric field of an antenna positioned in the origin and with its phase reference point in the origin and observation point $\mathbf{r}$ as

$$\mathbf{E}(\mathbf{r}) = \mathbf{G}(\hat{\mathrm{r}})\frac{e^{-jkr}}{r} \iff \mathbf{E}(r,\theta,\phi) = \mathbf{G}(\theta,\phi)\frac{e^{-jkr}}{r}, \tag{2.4}$$

where $\hat{\mathrm{r}} = \mathbf{r}/|\mathbf{r}| = \mathbf{r}/r$ is the normalised vector of $\mathbf{r}$. Continue by considering the electric field when the phase reference point is moved from the origin to $\mathbf{r}_0$, which is depicted in Fig. 2.2.

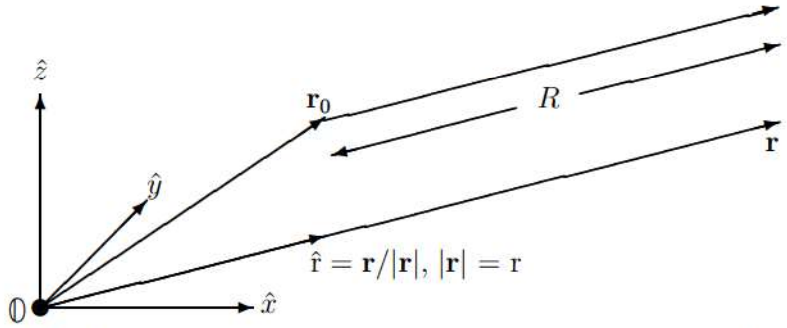

Figure 2.2: A Coordinate system with the observation point $\mathbf{r}$ and phase reference point $\mathbf{r}_0$.

As the electric field should not change if the phase reference point is moved, the electric field can be expressed in terms of R, θ and ϕ as

$$\mathbf{E}(r,\theta,\phi) = \mathbf{E}(R,\theta,\phi) = \mathbf{G}'(\theta,\phi)\frac{e^{-jkR}}{R}, \tag{2.5}$$

where R is approximately the distance $|\mathbf{r} - \mathbf{r}_0|$ in the far-field region and $\mathbf{G}'(\theta,\phi)$ is unknown. It is desired to express the electric field only in the known far-field function, $\mathbf{G}(\theta,\phi)$, introduced at the very beginning. By considering the Fraunhofer approximations,

$$\begin{cases} \frac{1}{r} \approx \frac{1}{R} & \text{for the amplitude and} \\ r \approx R + \mathbf{r}_0 \cdot \hat{\mathrm{r}} & \text{for the phase,} \end{cases} \tag{2.6}$$

the RHS of Eq. (2.5) may be rewritten as

$$\mathbf{G}'(\theta,\phi)\frac{e^{-jkR}}{R} = \mathbf{G}(\theta,\phi)e^{-jk(r-R)}\frac{e^{-jkR}}{R} = \mathbf{G}(\theta,\phi)e^{-jk(\mathbf{r}_o\cdot\hat{\mathrm{r}})}\frac{e^{-jkR}}{R}. \tag{2.7}$$

This gives the final expression of the electric field and far-field function as

$$\begin{cases} \mathbf{E}(R,\theta,\phi) = \mathbf{G}(\theta,\phi)e^{-jk(\mathbf{r}_o\cdot\hat{\mathrm{r}})}\frac{e^{-jkR}}{R} \\ \mathbf{G}'(\theta,\phi) = \mathbf{G}(\theta,\phi)e^{-jk(\mathbf{r}_o\cdot\hat{\mathrm{r}})} \end{cases} \tag{2.8}$$

To obtain the expression when the antenna is positioned in a point in space $\mathbf{r}_n$ with its phase reference point in the origin $-\mathbf{r}_0$ is substituted with $\mathbf{r}_n$. The expressions for the electric field and far-field function is then derived as

$$\begin{cases} \mathbf{E}_{\mathbf{r}_n}(r,\theta,\phi) = \mathbf{G}(\theta,\phi)e^{jk(\mathbf{r}_n\cdot\hat{\mathrm{r}})}\frac{e^{-jkr}}{r} \\ \mathbf{G}_{\mathbf{r}_n}(\theta,\phi) = \mathbf{G}(\theta,\phi)e^{jk\mathbf{r}_n\cdot\hat{\mathrm{r}}}. \end{cases} \tag{2.9}$$

It is thus possible to express the far-field generated by several antennas placed in arbitrary positions [8].

2.1.2 Antenna Polarisation

The polarisation performance is an important antenna characteristic as the electric field radiated by an antenna can have various polarisation states. In particular the orthonormal co- and cross- polarisation vectors are to be considered, which may be viewed as the polarisation states which are desired and not desired, respectively. It is thus required to suppress the cross polarisation component relative to the co polarisation component. The co- and cross- polarisation vectors for linear polarisation are generally defined as

$$\hat{\mathrm{co}} = \cos(\phi-\epsilon)\hat{\theta} - \sin(\phi-\epsilon)\hat{\phi}, \tag{2.10}$$

$$\hat{\mathrm{xp}} = -\sin(\phi-\epsilon)\hat{\theta} - \cos(\phi-\epsilon)\hat{\phi} \tag{2.11}$$

where ϵ can be chosen to achieve various polarisations. In order to achieve linear x-polarisation ϵ is set to 0 and to achieve y-polarisation ϵ is set to $\pi/2$. Furthermore,

for the Right Hand Circular Polarisation (RHCP) the co- and cross- polarisation vectors are written as

$$\begin{cases} \hat{\text{co}} = e^{-j\phi}/\sqrt{2}(\hat{\theta} - j\hat{\phi}) \\ \hat{\text{xp}} = e^{j\phi}/\sqrt{2}(\hat{\theta} + j\hat{\phi}) \end{cases} \text{or} \begin{cases} \hat{\text{co}} = 1/\sqrt{2}(\hat{x} - j\hat{y}) \\ \hat{\text{xp}} = 1/\sqrt{2}(\hat{x} + j\hat{y}) \end{cases} \tag{2.12}$$

and for the Left Hand Circular Polarisation (LHCP) the vectors instead are written as

$$\begin{cases} \hat{\text{co}} = e^{j\phi}/\sqrt{2}(\hat{\theta} + j\hat{\phi}) \\ \hat{\text{xp}} = e^{-j\phi}/\sqrt{2}(\hat{\theta} - j\hat{\phi}) \end{cases} \text{or} \begin{cases} \hat{\text{co}} = 1/\sqrt{2}(\hat{x} + j\hat{y}) \\ \hat{\text{xp}} = 1/\sqrt{2}(\hat{x} - j\hat{y}) \end{cases} \tag{2.13}$$

for the cross- and co- polarisation components [8]. Finally, the far-field function may be expressed in the co- and cross- polarisation vectors as

$$\mathbf{G} = G_{\text{co}}\hat{\text{co}} + G_{\text{xp}}\hat{\text{xp}}, \tag{2.14}$$

$$\tag{2.15}$$

with

$$G_{\text{co}} = \mathbf{G}_{\text{co}} \cdot \hat{\text{co}}^*, \tag{2.16}$$

$$G_{\text{xp}} = \mathbf{G}_{\text{co}} \cdot \hat{\text{xp}}^*, \tag{2.17}$$

which will render a clear insight into the polarisation characteristics [1].

2.1.3 Total Radiated Power

The radiated power of an antenna is necessary to introduce for the concepts of directivity, gain and radiation patterns. Hence, a brief derivation of the radiated power of an antenna is conferred is this section. Firstly, the instantaneous power density, P, is evaluated through an integral of the instantaneous power density vector, $\mathbf{W}$, over a closed surface, S. The expression of the instantaneous power density is given as

$$P = \oiint_S \mathbf{W} \cdot \mathbf{ds} = \oiint_S \mathbf{W} \cdot \hat{n} da, \tag{2.18}$$

where da is the infinitesimal area of the closed surface and $\hat{n}$ the outward pointing normal to the closed surface S [7]. However, in antenna theory it is of interest to compute the averaged radiated power, as opposed to the instantaneous one, which is computed from the averaged power density vector $\mathbf{W}_{\text{ave}}$ [8]

$$\mathbf{W}_{\text{ave}} = \frac{1}{2}\text{Re}[\mathbf{E} \times \mathbf{H}^*] = \left[\mathbf{H} = \frac{1}{\eta}\hat{\text{r}} \times \mathbf{E}\right] = \frac{1}{2\eta}|\mathbf{E}|^2\hat{\text{r}} = \frac{1}{2\eta r^2}|\mathbf{G}|^2\hat{\text{r}}. \tag{2.19}$$

From this point it is handy to introduce the radiation intensity U, which can be expressed as [7]

$$U(\theta, \phi) = r^2\mathbf{W}_{\text{ave}} \cdot \hat{\text{r}} = \frac{r^2}{2\eta}|\mathbf{E}(r, \theta, \phi)|^2 = \frac{1}{2\eta}(|G(\theta, \phi)_{\text{xp}}|^2 + |G(\theta, \phi)_{\text{co}}|^2), \tag{2.20}$$

where the wave impedance in free space is $\eta = 120\pi\,\Omega$. From this equation it is rather easy to compute the average radiated power accordingly

$$P_{\text{ave}} = \oiint_{S_\infty} (\mathbf{W}_{\text{ave}} \cdot \hat{\mathrm{r}}) da = \int_0^{2\pi} \int_0^{\pi} (\mathbf{W}_{\text{ave}} \cdot \hat{\mathrm{r}}) r^2 \sin\theta d\theta d\phi = \int_0^{2\pi} \int_0^{\pi} U(\theta, \phi) \sin\theta d\theta d\phi, \tag{2.21}$$

where the integration is taken over the far-field sphere, for which $\hat{n} = \hat{\mathrm{r}}$. The total radiated power can finally be computed, by considering equation (2.20), as

$$P_{\text{rad}} = P_{\text{ave}} = \frac{1}{2\eta} \int_0^{2\pi} d\phi \int_0^{\pi} d\theta \sin\theta \left(|G_{\text{co}}(\theta, \phi)|^2 + |G_{\text{xp}}(\theta, \phi)|^2 \right), \tag{2.22}$$

making the total radiated power dependent on the far-field function only [8].

2.1.4 Antenna Directivity and Antenna Gain

The directive gain, D_0, and the directivity, $D(\theta, \phi)$, are measurements of how the antenna distributes the radiated power in the volume surrounding the antenna [7]. The ideal directive gain of an antenna is defined as

$$D_0 = \frac{4\pi}{\lambda^2} A_{\text{aperture}}, \tag{2.23}$$

where A_{aperture} is the area aperture of the antenna. This is, however, not an exact value as array antennas will suffer from for example phase errors [1]. The directivity is defined generally as the ratio of the radiation intensity in a given direction to the radiation intensity averaged over all directions. This may be expressed as

$$D(\theta, \phi) = \frac{4\pi}{P_{\text{rad}}} U(\theta, \phi) = \frac{U(\theta, \phi)}{U_0}. \tag{2.24}$$

The directive gain can then instead be found as

$$D_0 = \frac{U_{\text{max}}}{U_0}, \tag{2.25}$$

which typically gives a more accurate value, but requires a numerical integration over the far-field sphere.

The maximum antenna gain, G_0, and gain, $G(\theta, \phi)$, on the other hand combines the directivity properties of the antenna with its efficiency. The efficiency of the antenna is characterised by a coefficient ϵ_0 which is the total efficiency of the antenna and may be linked to two main sources; reflections due to mismatch between the connecting antenna and the transmission line and ohmic losses, also referred to as I^2R losses. The total efficiency coefficient of the antenna is written as

$$\epsilon_0 = \epsilon_r \epsilon_c \epsilon_d, \tag{2.26}$$

where $\epsilon_r = (1 - |\Gamma|^2)$ is the reflection efficiency coefficient and Γ is the voltage reflection coefficient at the input of the antenna. To clarify Γ is defined as

$$\Gamma = \frac{z_{\text{in}} - z_0}{z_{\text{in}} + z_0}, \tag{2.27}$$

where z_{in} is the input impedance to the antenna and z_0 is the characteristic impedance of the antenna. The latter two efficiency coefficients in Eq. 2.26 are the conduction efficiency, ϵ_c, and the dielectric efficiency, ϵ_d. Often the total efficiency coefficient can be written as

$$\epsilon_0 = (1 - |\Gamma|^2)\epsilon_{\text{cd}} \tag{2.28}$$

because measurements usually determines the combined efficiency coefficient ϵ_{cd}, i.e the total ohmic losses. Due to these losses in the antenna, the power that is radiated will not be the the total input power but rather $P_{\text{rad}} = \epsilon_0 P_{\text{in}}$. Finally the gain can be expressed in terms of the efficiency coefficient and radiation intensity as

$$G(\theta, \phi) = \frac{4\pi}{P_{\text{in}}} U(\theta, \phi) = \epsilon_{\text{cd}}(1 - |\Gamma|^2) D(\theta, \phi). \tag{2.29}$$

The maximum gain is subsequently found as [7]

$$G_0 = \epsilon_{\text{cd}}(1 - |\Gamma|^2) D_0. \tag{2.30}$$

2.1.5 Scattering and Impedance Parameters

The scattering and impedance parameters, often referred to as S- and Z- parameters, are considered for the antenna efficiency in terms of mismatch between the transmission line and the antenna. It will be shown that the S- and Z- parameters can relate to the reflection coefficient which in turn can be related to the reflection efficiency coefficient, as described in the previous section.

As an example a two-port network will be studied and is illustrated conceptually in Fig. 2.3.

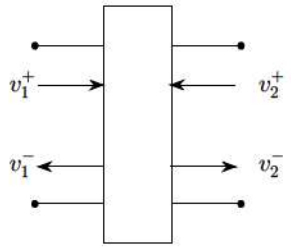

Figure 2.3: Depicts a two-port system.

The S-parameters for such a network can be written as

$$v_1^- = s_{11} v_1^+ + s_{12} v_2^+, \tag{2.31}$$
$$v_2^- = s_{21} v_1^+ + s_{22} v_2^+, \tag{2.32}$$

where the total voltage in port i is the sum $v_i = v_i^+ + v_i^-$ and the corresponding current is $i_i = i_i^+ - i_i^-$. The relation between the voltage to the S-parameters can be written in matrix form as

$$V^- = SV^+ \text{ where } s_{ij} = \frac{v_i^-}{v_j^+}. \tag{2.33}$$

Furthermore, the current can be related to the voltage and characteristic impedance as

$$i_i^{\pm} = \frac{v_i^{\pm}}{z_0} \tag{2.34}$$

leading to the current $i_i = \frac{1}{z_0}(v_i^+ - v_i^-)$ making it possible to calculate S- and Z-parameters in matrix form as [9]

$$S = (Z + z_0\mathbb{1})^{-1}(Z - z_0\mathbb{1}) \tag{2.35}$$

$$Z = z_0(\mathbb{1} + S)(\mathbb{1} - S)^{-1}. \tag{2.36}$$

From here the reflection coefficient for the input can be computed as

$$\Gamma = \frac{z_{\text{in}} - z_0}{z_{\text{in}} + z_0} = s_{11}, + \frac{s_{12}s_{21}\Gamma_{\text{L}}}{1 - s_{22}\Gamma_{\text{L}}}, \tag{2.37}$$

where Γ_{L} is the reflection in the load of the antenna [10]. The reflection efficiency coefficient of the antenna can thus be computed as $\epsilon_r = (1 - |\Gamma|^2)$.

2.1.6 Radiation Patterns

The radiation pattern is defined as the mathematical function of the radiation properties of space coordinates. It is often evaluated in the far-field region and may be visualised in various scales. A logarithmic scale is often used as it shows details well [7]. The radiation pattern may further be visualized in terms of the co- and cross-polarisation components separately, giving a further insight to the performance of the antenna for a particular polarisation. The definition of the co polarisation logarithmic radiation pattern is

$$D_{\text{co}}(\theta,\phi) = 10 \cdot {}^{10}\log\left(\frac{4\pi|G_{\text{co}}(\theta,\phi)|^2}{P_{\text{rad}}2\eta}\right) = 20 \cdot {}^{10}\log\left(\sqrt{\frac{4\pi}{P_{\text{rad}}2\eta}}|G_{\text{co}}(\theta,\phi)|\right). \tag{2.38}$$

Subsequently the definition for the cross polarisation must be

$$D_{\text{xp}}(\theta,\phi) = 10 \cdot {}^{10}\log\left(\frac{4\pi|G_{\text{xp}}(\theta,\phi)|^2}{P_{\text{rad}}2\eta}\right) = 20 \cdot {}^{10}\log\left(\sqrt{\frac{4\pi}{P_{\text{rad}}2\eta}}|G_{\text{xp}}(\theta,\phi)|\right). \tag{2.39}$$

The units of this pattern is given in dBi which means that the radiation pattern is normalised with respect to an isotropic antenna. The pattern may also be expressed in dB or dBp which corresponds to an arbitrary rescaling factor and a dipole antenna, respectively [8].

2.1.7 Radiation Pattern Characteristics

When an antenna is designed certain characteristics are desired, depending on the application, which are manifested in the radiation mask. For array antennas in this thesis the radiation mask will be given in the parameters of Side Lobe Level (SLL), Edge of Coverage (EoC), Out of Coverage (OoC) and Field of View (FoV). For a cell system that is hexagonal these parameters can be defined accordingly:

- OoC is the angle that is placed nearest to the EoC and lies in the same channel, also referred to as colour
- SLL is the level which is defined as the maximum gain in the region outside the FoV
- EoC is defined as the angle where the edges of the beams cross over, this can be better understood in Fig. 3.1, where for a hexagonal cell system EoC has the value inter-beam distance over $\sqrt{3}$
- FoV, also referred to as coverage, is the angle where the gain is no longer constricted by the gain specified after OoC

In addition the OoC region can be established as the region from OoC to FoV, the radiation pattern is constrained to have a maximum level in this region. Also an EoC region may be referred to as the region from the center of the main beam to EoC, which has a minimum requirement for the radiation pattern [1]. A conceptual radiation mask is presented in Fig. 2.4 as a clarification to the reader. In the figure EoC, OoC, FoV and SLL are displayed, i.e. the radiation pattern must be larger than the EoC gain, smaller than the OoC gain and the SLL in order to be a truly successful design.

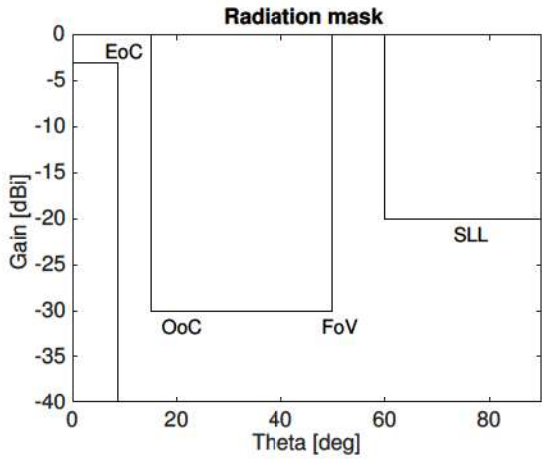

Figure 2.4: Shows the concept of a radiation mask.

2.1.7.1 Beam Parameters

The main beam in the radiation pattern is characterised by the half power beam width (HPBW) and the first null beam width (FNBW). The HPBW is defined as

the angle where the beam contains half of its power and the FNBW is defined as the angle where the first null of the radiation pattern occurs [7]. The HPBW and FNBW are depicted in Fig. 2.5 along with the main beam, side lobes and back lobe in units of dBi. For a circular aperture the diameter, D, is related to the HPBW as

$$D = 0.886\frac{\lambda}{\theta_{\text{HPBW}}} \tag{2.40}$$

where θ_{HPBW} is the angle where the radiation pattern has dropped 3 dB in strength [1]. Furthermore, the first null can be related to the diameter of the aperture, D, as

$$\theta_{\text{FNBW}} = 1.226\frac{\lambda}{D}. \tag{2.41}$$

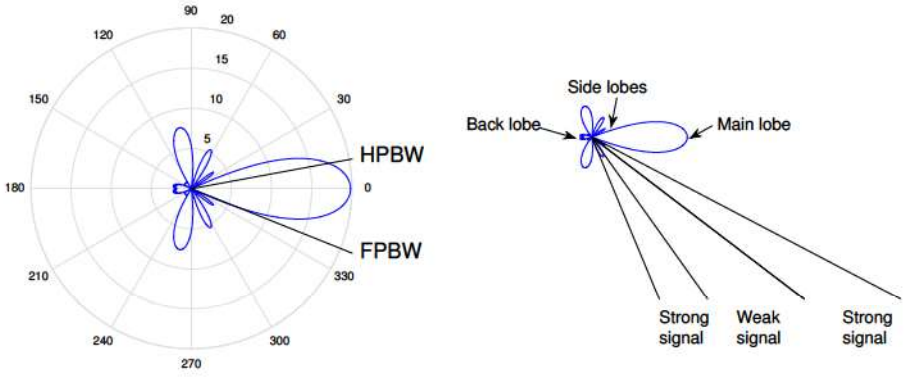

Figure 2.5: Illustrates the FNBW, HPBW, main lobe, back lobe and side lobes in the radiation pattern and how it corresponds to the strength of the signal.

Thus, the FNBW and HPBW are shown to determine the shape of the main beam and furthermore the aperture size [7].

2.2 Array Antennas

An array antenna is a set of several smaller antenna elements, which allows for various radiation patterns to be formed without necessarily demanding very complex array antenna elements. The radiation patterns of array antennas will be shown to depend on the type of chosen array antenna element, the current excitation and the positioning of array antenna elements.

This section will thus undertake the concepts of the far-field function of linear and planar array antennas, for these are the type of antennas which will be the main focus in the thesis. Of course non-planar antennas can be assembled, it is however, not expected that a non-planar array antenna would be significantly better than that of a planar [11]. The section will also present concepts of the array factor (AF) and MC effects.

2.2.1 The Far-Field Function of Linear Array Antennas

A linear array with N elements is now to be considered. The electric field of the n:th array element positioned in $\mathbf{r}_n$ of such an array antenna is generally expressed as

$$\mathbf{E}_n(r,\theta,\phi) = \frac{1}{r}e^{-jkr}\mathbf{G}_n(\theta,\phi)e^{jk\mathbf{r}_n\cdot\hat{\mathbf{r}}}. \tag{2.42}$$

By combining all array elements the far-field function of the array antenna, $\mathbf{G}_\mathrm{A}(\theta,\phi)$, can be computed as

$$\mathbf{G}_\mathrm{A}(\theta,\phi) = \sum_{n=1}^{N} A_n e^{j\phi_n}\mathbf{G}_n(\theta,\phi)e^{jk\mathbf{r}_n\cdot\hat{\mathbf{r}}}, \tag{2.43}$$

where $A_n e^{j\phi_n}$ is the amplitude and phase of the excitation current of element n, $\mathbf{G}_n$ is the far-field function of element n and $e^{jk\mathbf{r}_n\cdot\hat{\mathbf{r}}}$ is the factor which makes up for the fact that the array element placed in $\mathbf{r}_n$ instead of the origin.

If the array pattern for the array elements are identical the summation can be simplified as $\mathbf{G}_n = \mathbf{G}\ \forall\ n \in 1,...,N$. It should noted that MC effects are ignored for this case. In this situation the AF is commonly used as a simplification of the far-field function and gives rise to the expression

$$\mathbf{G}_\mathrm{A}(\theta,\phi) = \mathbf{G}(\theta,\phi)AF \tag{2.44}$$

as the isolated radiation pattern is taken out of the summation in Eq. (2.43). The expression for the AF is thus

$$AF(\theta,\phi) = \sum_{n=1}^{N} A_n e^{j\phi_n}e^{jk\mathbf{r}_n\cdot\hat{\mathbf{r}}} = \sum_{n=1}^{N} w_n e^{jk\mathbf{r}_n\cdot\hat{\mathbf{r}}} \tag{2.45}$$

where w_n denotes the complex excitation current of element n in the array. As mentioned in Ch. 1 an array antenna has the ability to steer the main beam, and even shape it, in a particular direction $\hat{\mathrm{r}}_s$, or simply (θ_s,ϕ_s) which also can be referred

to as the scanning angle [12]. This means that the main beam of every element is directed along a particular steering vector with fixed angles by altering the phase of the excitation current, which is written as [2]

$$w_n^s = w_n e^{-jk\mathbf{r}_n \cdot \hat{\mathbf{r}}_s}. \tag{2.46}$$

The expression of the array factor when steered thus changes to

$$AF(\theta, \phi) = \sum_{n=1}^{N} w_n e^{jk(\mathbf{r}_n \cdot \hat{\mathbf{r}} - \mathbf{r}_n \cdot \hat{\mathbf{r}}_s)}. \tag{2.47}$$

Going back to the far-field function in general the steering beam would change the far-field function accordingly

$$\mathbf{G_A}(\theta, \phi) = \sum_{n=1}^{N} w_n \mathbf{G}_n(\theta, \phi) e^{jk(\mathbf{r}_n \cdot \hat{\mathbf{r}} - \mathbf{r}_n \cdot \hat{\mathbf{r}}_s)}. \tag{2.48}$$

2.2.1.1 Steered Uniform Linear Array Antennas

Consider a linear array with N_x elements of length L_x placed symmetrically on the x-axis which is equidistant, has a uniform excitation current amplitude and a linear phase dependence. In addition the array is steered in direction (θ_s, ϕ_s). The length can thus be written as $L_x = N_x d_x$ and the excitation current as $w_n = w \ \forall$ $n = 1, ..., N_x$. This enables us to express the array factor as

$$AF = w \sum_{n=1}^{N_x} e^{jknd_x(u - u_s)} \tag{2.49}$$

where $u = \sin\theta\cos\phi$ and $\phi = 0$ as the array in positioned along the x-axis [12]. Furthermore, the normalised array factor can be expressed as

$$|AF| = \left| \frac{1}{N_x} \frac{\sin(N_x \Psi_x / 2)}{\sin(\Psi_x / 2)} \right|, \text{ with} \tag{2.50}$$

$$\begin{cases} \Psi_x = kd_x u - \beta_x \\ \beta_x = kd_x u_s. \end{cases} \tag{2.51}$$

If the array is placed along the y-axis the AF can be written as

$$AF = w \sum_{n=1}^{N_y} e^{jknd_y(v - v_s)} \tag{2.52}$$

where $v = \sin\theta\sin\phi$ and $\phi = \pi/2$. The normalised AF can for this case be written as

$$|AF| = \left| \frac{1}{N_y} \frac{\sin(N_y \Psi_y / 2)}{\sin(\Psi_y / 2)} \right|, \text{ with} \tag{2.53}$$

$$\begin{cases} \Psi_y = kd_y v - \beta_y \\ \beta_y = kd_y v_s. \end{cases} \tag{2.54}$$

Finally, if the array is positioned along the z-axis the array factor may be written as

$$AF = w \sum_{n=1}^{N_z} e^{jknd_z(\cos\theta - \cos\theta_s)} \tag{2.55}$$

which may be written, in a normalised form, as

$$|AF| = \left| \frac{1}{N_z} \frac{\sin(N_z\Psi_z/2)}{\sin(\Psi_z/2)} \right| \text{ , with} \tag{2.56}$$

$$\begin{cases} \Psi_z = kd_z\cos\theta - \beta_z \\ \beta_z = kd_z\cos\theta_s \quad . \end{cases} \tag{2.57}$$

It should be noted again that MC effects are ignored for this case [13].

2.2.2 The Far-Field Function of Planar Array Antennas

Consider now a planar array antenna instead with N elements along the x-axis and M elements along the y-axis, which are symmetrically placed. It can easily be understood that the far-field function of the planar array antenna is expressed accordingly [14]

$$\mathbf{G_A}(\theta,\phi) = \sum_{n=1}^{N}\sum_{m=1}^{M} A_{nm}e^{j\Phi_{nm}}\mathbf{G}_{nm}(\theta,\phi)e^{jk\mathbf{r}_{nm}\cdot\hat{\mathbf{r}}} = \sum_{n=1}^{N}\sum_{m=1}^{M} w_{nm}\mathbf{G}_{nm}(\theta,\phi)e^{jk\mathbf{r}_{nm}\cdot\hat{\mathbf{r}}}. \tag{2.58}$$

Additionally, if all the elements in the array are identical the same simplification as for linear array holds, $\mathbf{G_A}(\theta,\phi) = \mathbf{G}(\theta,\phi)AF$ [12] for which the array factor is expressed as

$$AF(\theta,\phi) = \sum_{n=1}^{M}\sum_{n=1}^{N} A_{nm}e^{j\phi_{nm}}e^{jk\mathbf{r}_{nm}\cdot\hat{\mathbf{r}}} = \sum_{n=1}^{M}\sum_{n=1}^{N} w_{nm}e^{jk\mathbf{r}_{nm}\cdot\hat{\mathbf{r}}}, \tag{2.59}$$

where w_{nm} denotes the excitation current for element in position $\mathbf{r}_{nm}$. For a planar steered array the excitation current is written as

$$w_{nm}^{s} = w_{nm}e^{-jk\mathbf{r}_{nm}\cdot\hat{\mathbf{r}}_s} \tag{2.60}$$

along with the array factor

$$AF(\theta,\phi) = \sum_{n=1}^{M}\sum_{n=1}^{N} w_{nm}e^{jk(\mathbf{r}_{nm}\cdot\hat{\mathbf{r}}-\mathbf{r}_{nm}\cdot\hat{\mathbf{r}}_s)}. \tag{2.61}$$

However, if the elements are not identical the far-field function of the array can generally be computed as

$$\mathbf{G_A}(\theta,\phi) = \sum_{n=1}^{N}\sum_{m=1}^{M} w_{nm}\mathbf{G}_{nm}(\theta,\phi)e^{jk(\mathbf{r}_{nm}\cdot\hat{\mathbf{r}}-\mathbf{r}_{nm}\cdot\hat{\mathbf{r}}_s)}, \tag{2.62}$$

where MC effects can be considered [2].

2.2.2.1 Steered Uniform Planar Array Antennas

As a clarification of the steered beam the corresponding example, in Sec. 2.2.1.1, for the linear case will be shown with a planar array antenna. The length of the array antenna is L_x, L_y with intermediate spacing d_x, d_y and N, M as the number of elements along the x- and y- axis, separately. The array factor and far-field function may then be written as

$$AF = w \sum_{n}^{N} \sum_{m}^{M} e^{jk[nd_x(u-u_s)+md_y(v-v_s)]}, \tag{2.63}$$

with the coordinates $u = \sin\theta\cos\phi$ and $v = \sin\theta\sin\phi$ [14]. Assuming that the sums are separable the AF is expressed as

$$AF = w \left[\sum_{n}^{N} e^{jk[nd_x(u-u_s)]}\right] \left[\sum_{m}^{M} e^{jk[md_y(v-v_s)]}\right]. \tag{2.64}$$

Similarly to the linear case the normalised array factor may now be written as

$$|AF| = \left|\frac{\sin(Nkd_x(u-u_s)/2)}{N\sin(kd_x(u-u_s)/2)}\right| \cdot \left|\frac{\sin(Mkd_y(v-v_s)/2)}{M\sin(kd_y(v-v_s)/2)}\right| \Rightarrow \tag{2.65}$$

$$|AF| = \left|\frac{\sin(N\Psi_x/2)}{N\sin(\Psi_x/2)}\right| \cdot \left|\frac{\sin(M\Psi_y/2)}{M\sin(\Psi_y/2)}\right| \tag{2.66}$$

with

$$\begin{cases} \Psi_x = kd_x u - \beta_x \\ \beta_x = kd_x u_s \end{cases} \text{ and } \begin{cases} \Psi_y = kd_y v - \beta_y \\ \beta_y = kd_y v_s. \end{cases} \tag{2.67}$$

Similarly to the the linear case the current excitation is assumed to be uniform with respect to amplitude. [15].

2.2.3 Mutual Coupling (MC)

In array antennas MC will often greatly affect the radiation patterns as it changes the currents and the radiated fields in magnitude, phase and distribution. A simple way to describe MC is by considering the impedance, voltage and current of the elements in an array antenna. These quantities can be connected according to the following relation

$$v_m = \sum_{n}^{N} z_{mn} i_n, \tag{2.68}$$

where v_m is the applied voltage and i_n the excitation current of element n, where the total number of elements are N. What the equation tells us is that the isolated case corresponds to when the impedance matrix Z is a diagonal matrix of equal values of $z_{nn} = z$ [16]. The effects of MC are illustrated in Fig. 2.6 for an array antenna where the dashed lines correspond to the isolated radiation pattern of an array of the first element and the filled lines represent the embedded radiation pattern for the initial element.

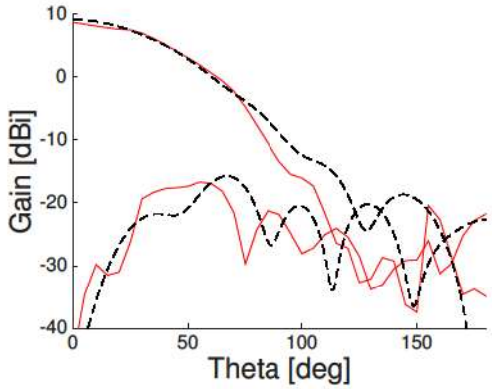

Figure 2.6: Example of the effects of MC. The dashed dark lines represent the isolated co- and cross- polarisation radiation pattern, the filled lines represents the embedded co- and cross polarisation radiation pattern.

2.3 Array Antenna Synthesis

In order to enhance the performance of array antennas, particular current distributions can be utilised in contrast to utilising an excitation current of uniform amplitude. In this section two methods of enhancing the antenna performance will be shown. Firstly, the synthesis procedure of an array antenna with a Taylor distributed current is presented, referred to as Taylor synthesised array antennas. Secondly, an array antenna with a Taylor distributed current of equivalent aperture is presented, referred to as density tapered array antennas. This section will furthermore extend the concept of AF to the space factor, SF, which corresponds to a discrete aperture and continuous aperture, respectively [17].

2.3.1 Taylor Synthesised Array Antennas

The Taylor distribution has the advantage of allowing the FNBW of the radiation pattern to be the smallest possible depending on what highest allowed side lobe level is chosen, making it suitable as a reference to convex optimised array antennas [5]. This section will provide the procedure proposed by Taylor [18] which incorporates the Tschebyscheff-error for a line source, and then extending it to a planar array antenna. This synthesis also has the advantage of being applicable to asymmetric array antenna patterns, which is suitable for the possibility of changing the radiation mask [19].

It is known that for an continuous line source of length $2a$ and its distribution $a(x)$ that the space factor can be written as a function of $v = \cos\theta$ written as

$$SF(v) = k \int_{-a}^{a} a(x) e^{jkxv} dx \tag{2.69}$$

by Fourier transform. By making the substitutions $u = \frac{2av}{\lambda}$ and $p = \frac{\pi x}{a}$ the space

factor can be written as

$$SF(u) = \frac{2a}{\lambda}\int_{-\pi}^{\pi} a(p)e^{jpu}dp = \frac{2a}{\lambda}F(u). \tag{2.70}$$

Generally for antenna synthesis the distribution is required to be single valued, piecewise continuous in the interval $-\pi < p < \pi$ and uniformly bounded [18]. Furthermore, it was shown by [20] that the ideal space factor of an Dolph-Tschebyscheff arrays becomes

$$F(u) = \cos\pi\sqrt{u^2 - A^2}. \tag{2.71}$$

as the number of elements goes to infinity [20]. In the works of [7], the ideal space factor from the Dolph-Tschebyscheff array is written as

$$SF(u, A) = \frac{\cosh\left[\sqrt{(\pi A)^2 - u^2}\right]}{\cosh(\pi A)} \tag{2.72}$$

for a linear array antenna of length l, where $u = \frac{\pi l}{\lambda}\cos\theta$, and is referred as the ideal pattern in this section. The constant A is given by $\cosh(\pi A) = R_0$, where R_0 is the maximum desired value of SLL [5].

However, the ideal SF violates the requirement for having a uniformly bounded distribution, and is thus unreleasable. This can be understood as outer side lobes do not decay and the member of the n:th zero pair are asymptotic to $\pm[n - (1/2)]$, as showed by Taylor [18]. Since this SF is not possible to realise, it can be approximated the with the Tschebyscheff-error given as

$$SF(u) = \frac{\sin(u)}{u}\frac{\prod_{n=1}^{\bar{n}-1}\left[1 - (\frac{u}{u_n})^2\right]}{\prod_{n=1}^{\bar{n}-1}\left[1 - (\frac{u}{\pi n})^2\right]}, \tag{2.73}$$

where $u_n = \pi v_n = \frac{l\pi}{\lambda}\cos\theta_n$ and $u = \pi v = \frac{l\pi}{\lambda}\cos\theta$. Along with the the parameter

$$\sigma = \frac{\bar{n}}{\sqrt{A^2 + (\bar{n} - 1/2)^2}} \tag{2.74}$$

which has the property of fusing inner nulls with the outer nulls in the radiation pattern, creating a smooth radiation pattern for a Taylor distributed current. $\bar{n}$ is a chosen parameter and the nulls are found as

$$u_n = \begin{cases} \pm\pi\sigma\sqrt{A^2 + (n - 1/2)^2} & \text{where} \quad 1 \leq n < \bar{n} \\ \pm\pi n & \text{where} \quad \bar{n} \leq n \leq \infty. \end{cases} \tag{2.75}$$

Lastly the current distribution is found as

$$i(x) = \frac{\lambda}{l}\left[1 + 2\sum_{p=1}^{\bar{n}-1} SF(p, A, \bar{n})\cos(2\pi px/l)\right] \text{ with} \tag{2.76}$$

$$SF(p, A, \bar{n}) = \begin{cases} \frac{[(\bar{n}-1)!]^2}{(\bar{n}-1+p)!(\bar{n}-1-p)^2}\prod_{m=1}^{\bar{n}-1}\left[1 - (\frac{\pi p}{u_m})^2\right] & \text{where} \quad |p| < \bar{n} \\ 0 & \text{where} \quad |p| \geq \bar{n} \end{cases} \tag{2.77}$$

where l is the length of the array and the $SF(p, A, \bar{n})$ is an even function. By assuming that the excitation vectors are separable for the x- and y- directions the current distribution of a planar array antenna can be found as

$$i(x, y) = i(x)i(y). \tag{2.78}$$

$i(x, y)$ will thus constitute the excitation current w_{nm} in the expression for the far-field function in Sec. (2.62) of an array antenna [5].

2.3.2 Density Tapered Array Antennas

If the array antenna has uniform excitation current amplitudes the ohmic losses can be reduced [4]. Therefore will an array antenna that is Taylor distributed with respect to equivalent aperture be considered in this section. The idea of tapering the array antenna with respect to element density is to satisfy the following condition

$$\frac{\text{integral over area}}{\text{integral over the antenna aperture}} = \frac{\text{elements in area}}{\text{elements in the antenna aperture}}. \tag{2.79}$$

This synthesis will be concerned with the ideal radiation pattern of the array antenna, F_0, and ideal excitation current, i_0, as well as the approximated array antenna radiation pattern F_a (or AF) and approximated excitation current i_a. Initially it can be beneficial to consider a linear array antenna with N elements and length $2a$ placed symmetrically along the x-axis. For such an array antenna are the ideal and approximated radiation patterns expressed as

$$F_0(u) = \int_{-a}^{a} i_0(x) e^{jkxu} dx \tag{2.80}$$

$$AF(u) = \sum_{n=1}^{N} a_n e^{jkx_n u}, \tag{2.81}$$

where $i_0(x)$ is the continuous current distribution and a_n are the amplitude coefficients, that is the discrete current. With these expressions in mind the synthesis of the array can commence accordingly:

- Firstly, divide the area in to slices according to the excitation current distribution, shown in Fig. 2.7a. Secondly, place an element at the median of every slice with assigned amplitude coefficients, a_k

With the current distribution $i_0(x)$ in mind and its cumulative distribution function, computed as

$$I(x) = \int_{-a}^{x} i(\eta) d\eta, \tag{2.82}$$

the synthesis can also be achieved in two equivalent steps:

- Firstly, divide the vertical axes of the cumulative distribution function according to the amplitude coefficients, as depicted in Fig. 2.7b Secondly, place an array antenna element at the middle of each vertical slice of assigned amplitude excitation [21]

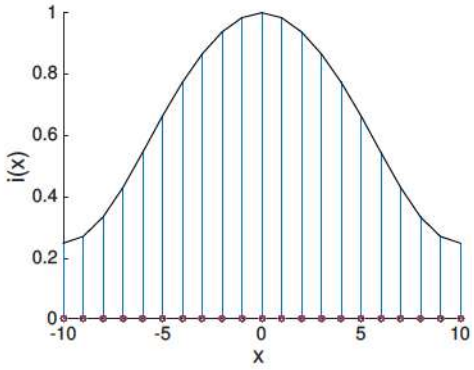

(a) Distribution function.

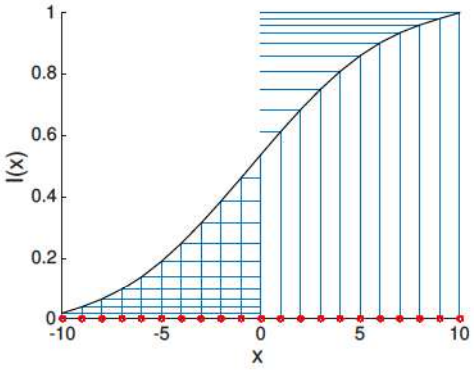

(b) Cumulative distribution function.

A procedure will now be presented for tapering a planar circular array antenna. For such an array antenna are the radiation pattern and excitation current symmetric with respect to rotation. The ideal radiation pattern is thus evaluated as

$$F_0(u) = H_0(i_0(\rho)) = 2\pi \int_0^\infty i_0(\rho)\rho J_0(ku\rho)d\rho \tag{2.83}$$

where $u = \sin\theta$, H_0 is the Hankel function and J_0 is the Bessel function of 0:th order. Furthermore, the cumulative distribution functions and array antenna patterns are related as

$$\int_0^\infty \frac{|F_0(u) - F_a(u)|^2}{(ku)^2} udu = \int_0^\infty \frac{2\pi|I_0(\rho) - I_a(\rho)|^2}{k\rho^2}\rho d\rho, \tag{2.84}$$

which represents the weighted mean square errors with an inverse quadratic weighting function of the radiation pattern and cumulative distribution function, respectively [4].

Assume now that an array antenna has N rings that are assigned with power excitations $\{p_k\}_{k=1}^N$ of unknown ring radii $\{r_k\}_{k=1}^N$, unknown element diameter $\{\Delta r_k\}_{k=1}^N$ and unknown ring area $A_k = 2\pi r_k \Delta r_k$. The approximative excitation current and radiation pattern of such an array antenna can be expressed as

$$i_a(\rho) = \sum_{k=1}^N b_k i_k(\rho) \quad \text{and} \quad F_a(u) = \sum_{k=1}^N b_k g_k(u). \tag{2.85}$$

Here i_k, g_k are the aperture fields and b_k amplitude coefficient of the k:th ring. Assume additionally that i_k will have a squared shaped silhouette, i.e.

$$i_k(\rho) = \Theta\left[\rho - \left[r_k - \frac{\Delta r_k}{2}\right]\right] - \Theta\left[\rho - \left[r_k + \frac{\Delta r_k}{2}\right]\right] \tag{2.86}$$

where Θ is the unit step function. Moreover, the aperture field g_k is determined as

$$g_k(u) = 2\pi \int_0^\infty i_k(\rho)\rho J_0(ku\rho)d\rho = \tag{2.87}$$

$$\pi\left(\left(r_k+\frac{\Delta r_k}{2}\right)^2 \Lambda_1\left(ku\left(r_k+\frac{\Delta r_k}{2}\right)\right) - \left(r_k-\frac{\Delta r_k}{2}\right)^2 \Lambda_1\left(ku\left(r_k-\frac{\Delta r_k}{2}\right)\right)\right) \tag{2.88}$$

where the Λ is defined as

$$\Lambda_p(x) = 2^p\Gamma(p+1)\frac{J_p(x)}{x^p} \text{ and } \Lambda_p(0) = 1. \tag{2.89}$$

The coefficients of the radiated power of ring k is computed from the integral of the amplitude coefficient and approximative excitation current over the element boundaries as

$$p_k = 2\pi \int_{r_k-\frac{\Delta r_k}{2}}^{r_k+\frac{\Delta r_k}{2}} |b_k i_k(\rho)|^2 \rho d\rho = 2\pi |b_k|^2 r_k \Delta r_k = |b_k|^2 A_k. \tag{2.90}$$

The assumption that the approximate cumulative distribution function is equal to the ideal cumulative distribution function enables us to express the difference between the ideal and approximative cumulative distribution function in ρ_k and ρ_{k-1} as

$$I_0(\rho_k) - I_0(\rho_{k-1}) = I_a(\rho_k) - I_a(\rho_{k-1}) = \int_{\rho_{k-1}}^{\rho_k} i_a(\rho)\rho d\rho = b_k r_k \Delta r_k. \tag{2.91}$$

By approximating that $r_k = \bar{p}_k = \frac{\rho_{k-1}+\rho_k}{2}$ and $\Delta r_k = \Delta\rho_k$ the relation

$$i_0(r_k)\Delta\rho_k = b_k \Delta r_k \tag{2.92}$$

can be combined to express the ideal excitation current as

$$i_0(r_k)\Delta\rho_k = \sqrt{\frac{p_k \Delta r_k}{2\pi r_k}}. \tag{2.93}$$

It is thus possible to relate the ideal excitation current, by substituting the Δr_k with $\Delta\rho_k$, as

$$2\pi i_0^2(r_k) r_k \Delta\rho_k = p_k. \tag{2.94}$$

By noting the following relation

$$2\pi \int_{\rho_{k-1}}^{\rho_k} i_0^2(\eta)\eta d\eta \approx 2\pi i_0^2(r_k) r_k \Delta\rho_k = p_k \tag{2.95}$$

the synthesis can be initiated by considering the grading function $E(\rho) = \int d\rho\rho i_0^2(\rho)$ and inverting it, leaving us to compute the boundaries, ρ_k, for the rings accordingly

$$\left\{\rho_k : \frac{\int_0^{\rho_k} \rho i_0^2(\rho)d\rho}{\int_0^\infty \rho i_0^2(\rho)d\rho} = \frac{\sum_{n=1}^k p_n}{\sum_{n=1}^N p_n}\right\} \qquad \forall\ k = 1, ..., N. \tag{2.96}$$

The diameters of the rings are determined with the expression of the amplitude coefficients a_k

$$a_k = I_0(\rho_k) - I_0(\rho_{k-1}) \tag{2.97}$$

and the feasibility condition

$$\Delta r_k \leq \Delta r_k^{max} = 2\min((r_k - \rho_{k-1}), (\rho_k - r_k)). \tag{2.98}$$

The diameters of the elements are finally be determined as

$$\Delta r_k = \frac{\frac{a_k^2}{p_k r_k}}{\max\left(\frac{a_k^2}{p_k r_k}\frac{1}{\Delta r_k^{max}}\right)}. \tag{2.99}$$

As this step is completed the amplitude coefficients, b_k, and the approximative radiation pattern, F_a can be computed according to the equations presented previously in this section. Furthermore, we will consider utilising assigned average powers $\{q_k\}_{k=1}^N$ for the elements in th k:th ring. The amplitude coefficients b_k must now obey the relation

$$b_k = \sqrt{\frac{p_k}{A_k^{RE}}} \tag{2.100}$$

where A_k^{RE} is the radiating area of an array antenna element. In addition the number of elements in the k:th ring should be

$$N_k \approx \frac{2\pi r_k}{\Delta r_k}. \tag{2.101}$$

where the power excitation of a the k:th ring is

$$p_k \approx N_k q_k \approx \frac{2\pi r_k}{\Delta r_k} q_k. \tag{2.102}$$

This results in the relation of the ideal excitation current with the element power excitation as

$$i_0(r_k)\Delta\rho_k = \sqrt{\frac{p_k \Delta r_k}{2\pi r_k}} = \sqrt{q_k}. \tag{2.103}$$

The synthesis can finally initiated by determining the boundaries, ρ_k, according to the inverted grading function as

$$\left\{\rho_k : \frac{\int_0^{\rho_k} i_0(\rho)d\rho}{\int_0^{\infty} i_0(\rho)d\rho} = \frac{\sum_{n=1}^{k}\sqrt{q_n}}{\sum_{n=1}^{N}\sqrt{q_n}}\right\} \qquad \forall\ k = 1, ..., N. \tag{2.104}$$

At this point the necessary quantities can be obtained from the previously presented equations [4].

The results of this array design and synthesis was computed with a -25 dB maximum side lobe level and 8 rings with a maximum aperture radius of $22\,\lambda$, as was done by [4], for the purpose of verifying the implementation. First an array antenna with constricted element diameter of $2\,\lambda$ was synthesised. The first case is depicted

in Fig. 2.7, where the ideal cumulative distribution function, ideal and approximative current distribution, array antenna design and radiation patterns are shown. Secondly, in Fig. 2.7 the results were depicted for the maximum diameter $3.4\,\lambda$. Finally, an array antenna, depicted in Fig. 2.9, was synthesised with no constraints for the element diameters. The test cases agreed well with those presented by [4]. It can be noted that the approximative radiation patterns are more similar to the ideal radiation patterns when there are no constraints than with constraints of the element diameters.

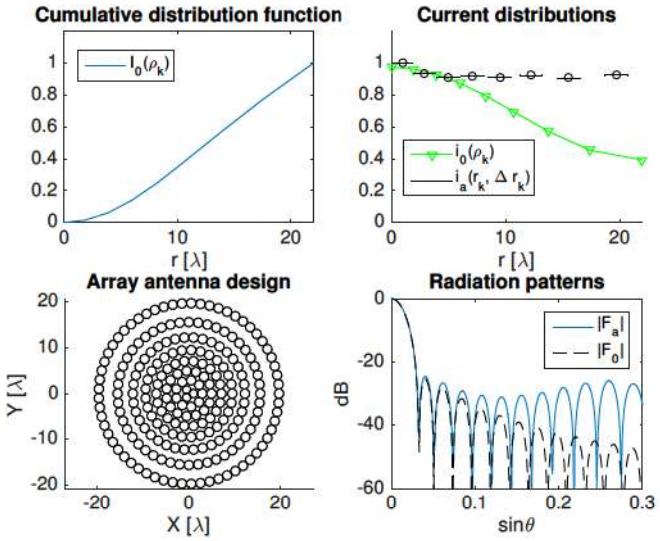

Figure 2.7: Shows the synthesised array antenna pattern when the element diameter is constricted to $2\,\lambda$ as the maximum diameter.

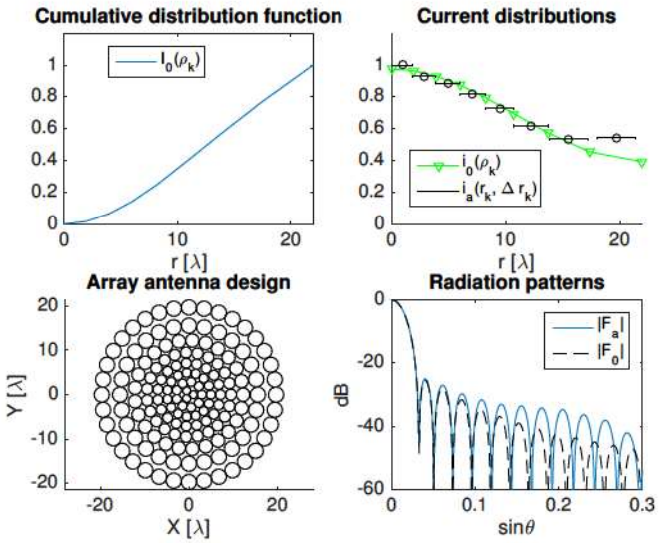

Figure 2.8: Shows the synthesised array antenna pattern when the element diameter is constricted to $3.4\,[\lambda]$ as the maximum diameter.

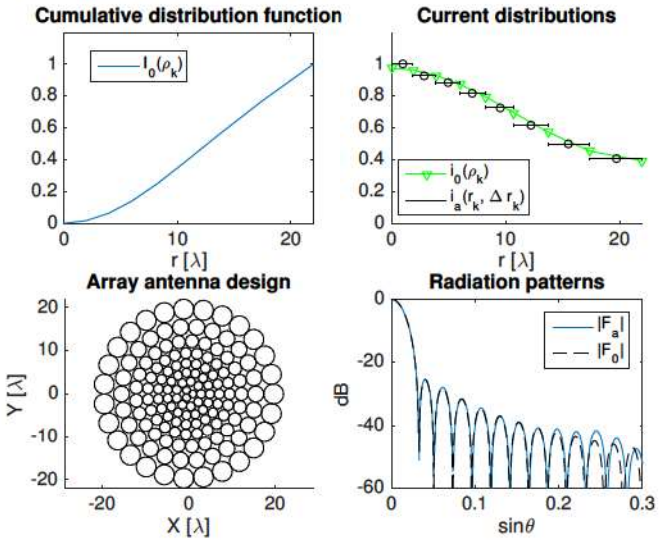

Figure 2.9: Shows the synthesised array antenna pattern when the element diameter is not constricted. It can be noted that the circular array antenna has the best performance when the element diameter is not limited.

3
Method

The aim of this chapter is to give the reader a deeper insight to the development of the results presented in Ch. 4. To begin the antenna specifications given by RUAG will be presented in Sec. 3.1. This is followed by the utilised array antenna configurations and array antenna elements for the trade-off investigation in Sec. 3.2. In Sec. 3.3 is the software FEKO and its implementation into the convex optimisation algorithm presented, which is followed by Sec. 3.4 where the algorithm for obtaining sparse array antennas through convex minimisation, as well as the needed modifications of the method are given. Concluding this chapter will be the modification of the density tapered arrays, presented in Sec. 3.5.

3.1 Antenna Specifications

The specifications for the array antennas that RUAG space desired to investigate are summarised in Table 3.1. These specifications will be the foundation for the trade-off investigation.

Table 3.1: Requirements of array antennas to be investigated in the trade-off investigation for RUAG space.

TX frequency	17.7–20.2 GHz
RX frequency	27.5–30.0 GHz
Polarisation	RHCP and LHCP
Coverage/FoV	Circular with semi angle 4°–8 °
Inter-beam distance	0.5°–1°
Cell system	Hexagonal, 4-colour
Gain	EoC gain critical point is the crossover gain divided by $\sqrt{3}$
OoC gain	$\leq$ 30 dB below maximum gain

The FoV is depicted in Fig. 2.4, which is one of the parameter varied in the specifications presented in Table 3.1. The reason for the variation of the FoV is that not all applications must cover the whole Earth, but will suffice with a portion of the Earth's surface. For the considered SATCOM applications the geostationary orbit of the Earth was of main focus. Furthermore, the required FoV to cover the Earth can be calculated by considering the average orbit radius, 35786 km, and the radius of the Earth, 6371 km, which gives the FoV semi angle as

$$\arcsin\left(\frac{6371}{6371+35786}\right) = 8.69°. \tag{3.1}$$

The maximum required FoV can thus be assumed to be 8° [1].

Moreover, the inter-beam distance, the second parameter to be varied, will influence the value of OoC. The OoC may be determined by considering the hexagonal four colour cell system illustrated in Fig. 3.1 where the OoC is specified to be the distance from the center of the beam of colour i to the point where the colour i reappears. For the four colour hexagonal system this implies that the OoC angle is related to the inter-beam distance as

$$\theta_{\text{OoC}} = 1.4224\theta_{\text{inter-beam}}. \tag{3.2}$$

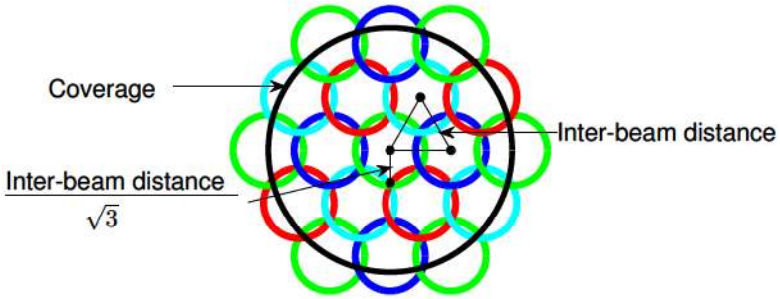

Figure 3.1: Shows the definition of coverage (also referred to as FoV), EoC and inter-beam distance for a hexagonal four colour cell system.

The aperture diameter must not be given to be too large in order to meet the requirement of OoC and EoC. For the lowest frequency, 17.7 GHz, this corresponds approximately to 0.84 m and 1.68 m for inter-beam distance 1° and 0.5°, respectively. For the highest frequency, 30 GHz, it corresponds approximately to 0.49 m and 0.99 m for inter-beam distance 1° and 0.5°, respectively.

3.2 Element Types and Antenna Configurations

The different types of array elements, previously developed at RUAG space, are presented in this section. The element types, i.e. the separate RX/TX elements and the common RX/TX element, could in turn yield the array configurations presented in Sec. 3.2.1. Furthermore, the characteristics of the array element types are presented in further details in Sec. 3.2.2 and Sec. 3.2.3.

3.2.1 Array Antenna Configurations

In a previous investigation of array antennas conducted for RUAG space by [1] the following three different array antenna configurations were proposed:

- Separate RX/TX apertures with separate RX/TX elements
- Common RX/TX apertures with separate RX/TX elements
- Common RX/TX apertures with combined RX/TX elements

These configurations were considered in this thesis as well and will be referred to as configuration 1, 2 and 3 for brevity. The concept for the first configuration is visualised in Fig. 3.2a, which is to use two types of array elements and two separate apertures, one for the TX and another for the RX. This configuration should exhibit less the MC effects than that of array configuration 2 but also demands a bigger total aperture. The considered second configuration is depicted in Fig. 3.2b, where the reader can see that two types of array elements are employed similarly to array configuration 1 while the RX and the TX apertures are shared.

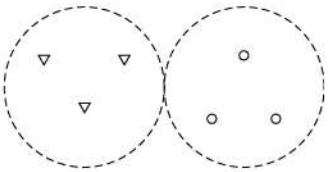

(a) Array antenna with separate RX/TX apertures and separate RX/TX elements.

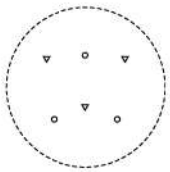

(b) Array antenna with common RX/TX apertures and separate RX/TX elements.

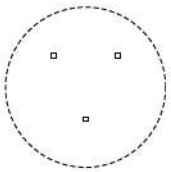

(c) Array antenna with common RX/TX apertures and common RX/TX elements.

Figure 3.2: Shows three different types of array antenna configurations.

The third array configuration is the case when the aperture is shared by both the TX and RX frequencies but also the array elements share the RX and TX, as shown in Fig. 3.2c.

3.2.2 Separate RX/TX Elements

A pipehorn antenna was chosen to create the first and second array configuration, scaled with a radius of 12.74 mm for the TX frequency band and 7.79 mm for the RX frequency band. The geometry of the pipehorn is depicted in Fig. 3.3a with FEKO. Further, the isolated pattern was plotted in Fig. 3.3b for 20 GHz which lies in the TX frequency, as the horn is simply scaled for the RX frequency the isolated pattern has the same characteristics as the isolated pattern of the TX.

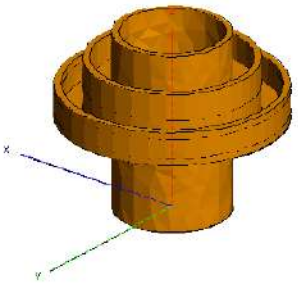

(a) Pipehorn antenna designed for 20 GHz or 30 GHz depending on the scaling factor. The figure is constructed in CADFEKO and visualised in POSTFEKO.

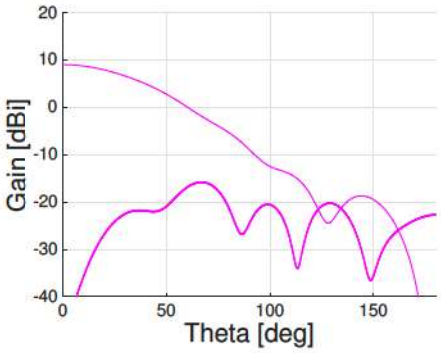

(b) Isolated radiation pattern of the separate RX/TX element excited with a waveguide port when transmitting in 20 GHz.

Figure 3.3: Separate RX/TX element with the isolated radiation pattern.

The pipehorn has a maximum gain of 9 dBi. Furthermore, it can be noted that the pipehorn is not very directive as when $\theta = 40°$ the gain has only decreased by about 4 dB, therefore MC effects may be exhibited in a non-trivial manner.

3.2.3 Common RX/TX Element

A corrugated pipehorn antenna was chosen to create the third array configuration. This array antenna element is capable of having a shared RX and TX and was also constructed in FEKO. Furthermore, the horn was visualised with the help of FEKO in Fig. 3.4. The largest radius of the element is 24.4 mm, making the common RX/TX elements significantly larger than the separate RX/TX elements.

Figure 3.4: Common RX/TX element constructed in CADFEKO and visualised in POSTFEKO.

The isolated radiation patterns were plotted in Fig. 3.5a and Fig. 3.5b for the TX

and RX, respectively. It can be noted that this array element is far more directive than the separate RX/TX elements where the maximum gain in 20 GHz, i.e. TX frequency, is 16.6 dBi and 19 dBi in 30 GHz, i.e. RX frequency. As this pipehorn is rather directive, arrays with common RX/TX elements are expected to exhibit less MC effects than array antennas that consist of separate RX/TX elements.

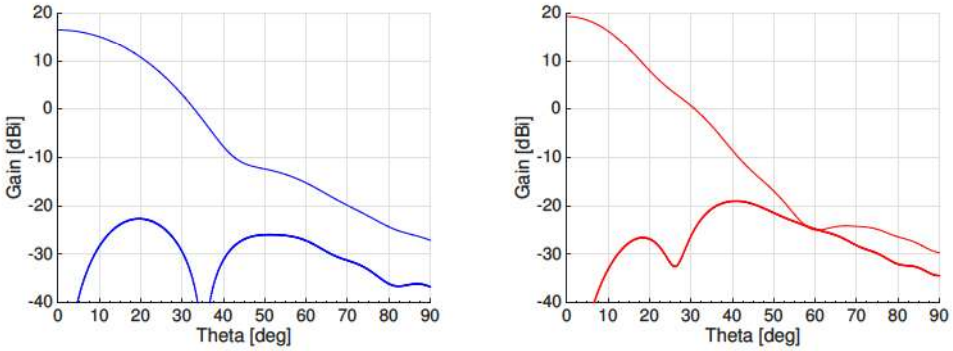

(a) Isolated radiation pattern of the common RX/TX element when transmitting in 20 GHz.

(b) Isolated radiation pattern of the common RX/TX element when transmitting in 30 GHz.

Figure 3.5: Isolated radiation patterns of the common RX/TX element.

3.3 Array Antenna Simulations with FEKO

In order to simulate array antennas while accounting for MC effects FEKO was interfaced with the convex optimisation algorithm and will be discussed in this section. FEKO is an electromagnetic multi-purpose calculation tool where array antenna elements can be constructed as well as simulated in a realistic manner. The software offers several solver types for the electromagnetic problems, which includes MoM (Method of Moments), FEM (Finite Element Method), Physical Optics (PO), Multi-level Fast Multi-pole Method (MLFMM), Geometrical Optics (GO), Uniform Theory of Diffraction (UTD) and Finite Difference Time Domain (FDTD). For the purposes of full-wave simulations of array antennas FEKO mainly uses MoM and MLFMM [22]. The methods scales rather badly with respect to time as the number of elements increase, which had a significant effect on the simulations.

Moreover, the specifications for the array antennas defined the polarisation to be circular, which rendered two approaches of exciting the array elements in FEKO, as the circular polarisation consists of an electric field with two perpendicular components that are separated 90° in phase with equal amplitudes. The first method will be denoted as the edge port excitation and the second as the waveguide port excitation.

3.3.1 Edge Port Excitation

By utilising two edge ports a circular polarisation could be obtained. Furthermore, the entire configuration with respect to excitation was possible to vary in one FEKO script which computed the Embedded Element Patterns (EEPs). Subsequently the computational time was reduced as the geometry was created in FEKO only once. Additionally, MLFMM rather than MoM was possible to employ and as MLFMM is faster than MoM the computational time as well as the memory requirements were reduced further.

The simulation times for a set of arrays of different sizes with respect to the number of elements are listed in Table 3.2. It can be noted that the simulation time

Table 3.2: Simulation times for the edge port excitation method with MFLMM employed as solver.

No. of elements in array	Simulation time
1	48 s
8	457 s
71	2 h 17 min
148	16 h 45 min

scales poorly with respect to the number of elements, and as the number of elements were expected to be approximately 500 for full scale array antenna cases [1] the total simulation times needed to be investigated. The proposed convex optimisation algorithm, presented in details in Sec. 3.4.3, iterates until set of active elements remains the same for two consecutive iterations when including MC effects. The solution usually converges in 10 iterations giving a total simulation time for 148 elements to be at least 170 h $\approx$ 1 week (excluding the simulation time for convex minimisation). However, as this lies in the lower end of the expected number of elements for the convex optimised arrays, the expected simulation time for the largest array antenna cases would be in the order of months.

The S-parameters were also simulated in the TX frequency interval in FEKO for both methods. The results were plotted in Fig. 3.6, it can be noted that the S-parameters in general are higher for the edge port excitation than the waveguide port excitation.

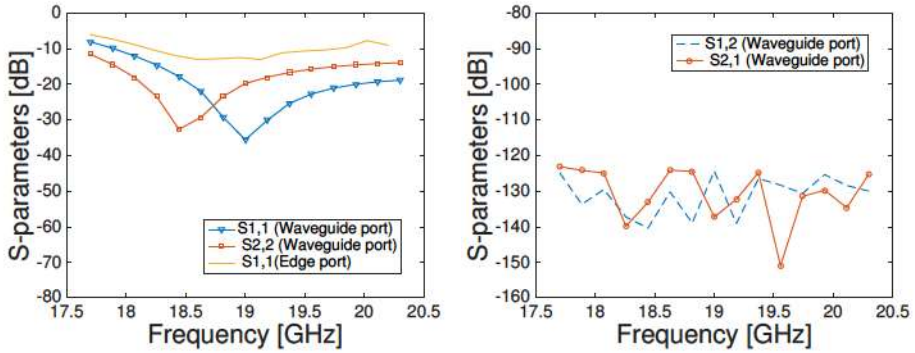

Figure 3.6: S-parameters simulated with FEKO of the pipehorn antenna with a waveguide port and two edge ports.

3.3.2 Waveguide Port Excitation

By utilising a waveguide port a circular polarisation could be obtained by using only one physical port in FEKO and exciting two perpendicular TE_{11} modes 90° out of phase. The current version of FEKO installed at RUAG did not present a possibility of changing the excitation configuration in one FEKO script. It was thus necessary to provide one script (and simulation) for every element in order to simulate the EEPs. As a consequence, the geometrical data must be constructed for every element, which is in itself a rather cumbersome task.

However, a cut-off radius was possible to introduce, in contrast to the edge port excitation. By implementing a cut-off radius in the simulations, the complexity and simulation time could be reduced which subsequently reduced the memory requirements in FEKO. A simulation for a linear array placed along the x-axis, depicted in Fig. 3.7b, was carried out in order to investigate the cut-off radius. The linear array used the separate RX/TX elements where the element radius was scaled to 12.74 mm. The intermediate element distance was set to 27 mm and the frequency was set to 20 GHz. In Fig. 3.7a are the embedded radiation patterns from the simulation with the cut-off radius 2, 5, 6, 8, 10, 15 and 20 λ depicted in addition to the isolated element pattern.

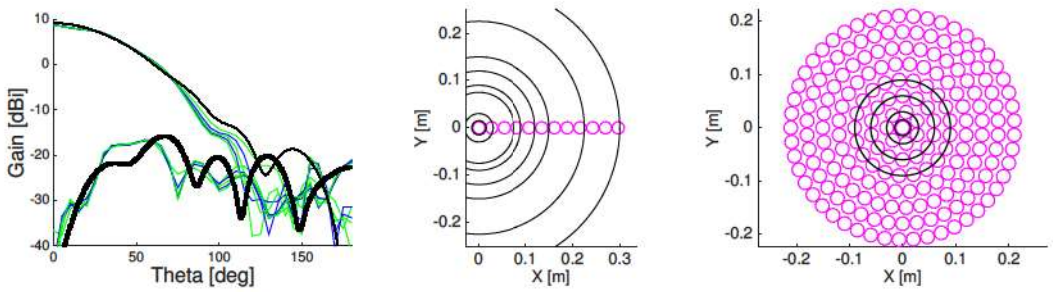

(a) Simulations with cut-off radius 1, 2, 5, 6, 8, 10, 15 and 20 λ in FEKO.

(b) Layout corresponding to simulations where the cut-off radius was 1, 2, 5, 6, 8, 10, 15, 20 λ.

(c) Layout corresponding to simulations with cut-off radius 1, 2, 4 and 6 λ.

Figure 3.7: Embedded radiation patterns and set up of simulations using a cut-off radius.

It can be noted that the radiation patterns diverges from each other after 70°. An additional simulation with the same array element and element spacing 27 mm was carried out for a circular array depicted in Fig. 3.7c along with the investigated cut-off radii in order to determine the expected total simulation times of the large array antenna cases of the convex optimisation algorithm. The simulation times for one element in these environments are shown in Table 3.3.

Table 3.3: Simulation times for one array element with respect to the number of elements in the array and cut-off radius, with MoM as solver.

Cut-off radius [λ]	Number of elements	Simulation time (1 element)
0	1	15.5 s
2	8	192.8 s
4	22	1888 s
6 and up	43 and up	out of memory

The cut-off radius of 4 λ was chosen in order to include the MC effects while not running out of computer memory. The waveguide excitation thus reduced the simulation time in FEKO to scale linearly with respect to the number of elements, i.e. the total simulation time in the worst case scenario should be $1888 \times N$ s, where N is the number of elements in the array antenna. Thus, for an array antenna with 148 elements, the simulation time could be 776 hours $\approx$ 32.3 days, assuming the convex optimisation algorithm converges in 10 iterations (excluding simulation time for the convex minimisation).

3.4 Convex Optimised Array Antennas

The method of creating the sparse irregular array antennas was an iterative convex minimisation procedure. First, in Secs. 3.4.1 and 3.4.2, will the software CVX used together with MATLAB and FEKO be presented along with the mathematical

formulation of the minimisation problem. In the following subsection, Sec. 3.4.2.1, will the formulation of the problem when reduced through symmetry be presented. Finally will the entire algorithm of convex optimised array antennas as well as a needed simplification of the originally proposed method be given.

3.4.1 Convex Programming

The utilised software package together with MATLAB and FEKO for the convex optimised arrays is called CVX. This package allows the user to obtain solutions for convex minimisation problems, and combines the following methods:

- Least square, LS, method
- Linear programming, LP
- Quadratic programming, QP

Before using CXV it is of great importance that the problem is properly formulated as convex as CVX does not offer any tool for checking this. Indeed, if the model of the optimisation problem is incorrect the result will subsequently be false [23]. The most important observation to make is that CVX allows the problem (3.6) subject to the set of constraints to be solved [6].

3.4.2 Convex Minimisation in the l_1-norm and l_0-norm

The l_0-norm minimisation is normally a solution to the electromagnetic problem of optimising sparse array antennas and is formulated according to equations (3.3)-(3.5)

$$\begin{aligned} &\text{argmin} \quad ||\mathbf{w}||_{l_0} \ \ \forall\, \mathbf{w} \in \mathbb{C}^N \text{ s.t.} && (3.3)\\ &G_{co}(\hat{r}_s) = 1, && (3.4)\\ &|G_v(\hat{r})|^2 \leq M_v(\hat{r}) \ \ \forall\, \hat{r} \in \text{ radiation mask}, && (3.5) \end{aligned}$$

where $\mathbf{w}$ is the excitation current, M_v is the radiation mask that is desired and $\mathbf{G}$ is the far-field function. The intrinsic issue for this problem is that it can't be solved in the l_0-norm but must be approximated by a solution in the l_1-norm. Fortunately, the initial problem may be reformulated in the l_1-norm accordingly

$$\begin{aligned} &\text{argmin} \quad ||Z^i\mathbf{w}^i||_{l_1} \ \ \forall\, \mathbf{w}^i \ \in \mathbb{C}^N \text{ s.t.} && (3.6)\\ &G_{co}(\hat{r}_s) = 1, && (3.7)\\ &|G_v(\hat{r})|^2 \ \leq M_v(\hat{r}) \ \forall\, \hat{r} \ \in \text{ radiation mask}, && (3.8) \end{aligned}$$

where the matrix Z^i is defined as

$$z_m^i = \frac{1}{|w_m^{(i-1)}| + \epsilon}. \tag{3.9}$$

Z^i has the property of allowing elements which in previous iterations have been determined inactive to become active. Furthermore, the Nyquist sampling condition

requires that the intermediate distance of the sample points are $\leq 0.1\lambda$ [6]. It should be noted that the consequence of the Nyquist sampling condition together with the convex formulation of the problem does not allow for a constraint that eliminates the possibility of array elements to be placed equal or closer than the element aperture diameter D. If such solutions are obtained, these would be non-physical.

3.4.2.1 Symmetry

In computationally demanding simulations computer memory and speed are of interest. The computational limitations can be rather neatly handled by imposing symmetry on circular apertures. Consider a circular planar array antenna, where rotational symmetry holds and can thus be divided into sections of the ϕ-plane. The symmetry renders the following relation of the far-field function of the array as

$$\mathbf{G}_A^{scan}(\theta,\phi) = \sum_{n=1}^{N} w_n \mathbf{G}_n^{scan}(\theta,\phi) \tag{3.10}$$

where N is the number of elements in the symmetry region. The total far-field function of element n can be expressed in the number of symmetries, $N_{\text{sym}}(n)$, as

$$\mathbf{G}_n^{scan} = \sum_{s=1}^{N_{\text{sym}}(n)} \mathbf{G}_{n,s} e^{-jk\Phi_{n,s}^{scan}}. \tag{3.11}$$

The iterative l_1-norm optimisation will consequently also be modified and changes the Z^i matrix accordingly

$$z_m^i = \frac{1}{\sum_{s=1}^{N_{sym}(m)} |w_m^{(i-1)}| + \epsilon} = \frac{1}{N_{sym}(m)|w_m^{(i-1)}| + \epsilon}. \tag{3.12}$$

This will reduce the simulation time for CVX substantially as the array will merely constitute a piece of the array antenna. The symmetry will reduce the problem as $1/N_{sym}$ and the simulation time will therefore scale as $1/N_{sym}^2$ [6].

3.4.3 Convex Optimisation Algorithm

The algorithm is divided into two parts that are separately involved with the isolated and embedded radiation patterns, respectively. A flowchart for the algorithm may be viewed in Fig. 3.8.

Firstly in Step 1, the Isolated Element Pattern (IEP) are simulated with FEKO. When the IEP are obtained the iterative l_1-norm minimisation is initiated, which enables for the element positions, i.e. set of active elements, to be determined, denoted Initial Array Configuration (IAC). After Step 1 is finished Step 2 is initiated, where firstly the EEPs are computed from the IAC in FEKO. When the EEPs are found new element positions are determined through the iterative l_1-norm minimisation. These positions constitutes an approximate Final Array Configuration (FAC) and if the set of active elements, i.e. new element positions, remaine the same compared to the former iteration of IAC the algorithm is finished. If, on the other hand, the set of active elements changed Step 2 is repeated with the FAC until the set of active elements remained the same for two consecutive iterations [6].

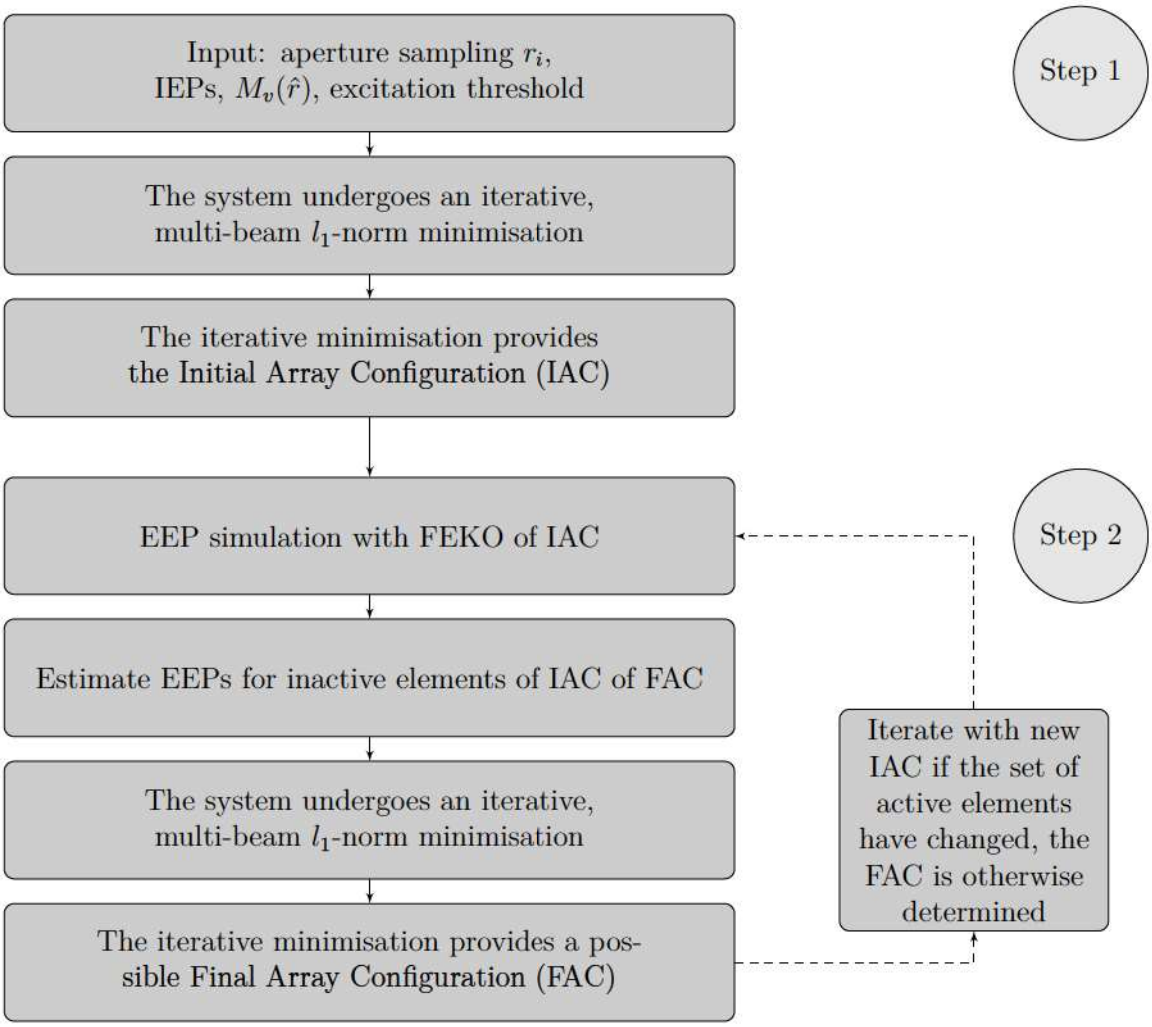

Figure 3.8: The flowchart depicts the algorithm that shows how sparse array antennas can determined through convex minimisation that optimises for multiple scanning beams and also undertakes the issue of MC effects.

3.4.3.1 Modified Convex Optimisation Algorithm

It quickly arose issues regarding the simulation time for array antennas in FEKO as the simulation times would be in the order of weeks. This can easily be seen from the proposed optimisation method, presented in details in Sec. 3.4.3, which iterates until set of active elements remains the same for two consecutive iterations when including MC effects. Furthermore, it can easily be seen that Step 2 of the algorithm depicted in Fig. 3.8 was the bottleneck in the process and finally it was concluded that the problem was intractable for the anticipated large array antennas. Thus, the modification of Step 2 of the algorithm depicted in Fig. 3.8 will be discussed in this section.

The algorithm had to be changed in two ways. For the first and third array configurations the procedure was only slightly modified as second step was simply reduced to simulating the EEPs. For the second array configuration Step 1 of the algorithm in Fig. 3.8 optimised first either for the TX or RX, Step 1 was then repeated in order to optimise with a reduced area for the RX or TX. The modification of the algorithm in the case of array configuration 2 is illustrated in Fig. 3.9 when the TX is optimised first and the RX is optimised secondly. The initial given area of the TX is shown as the lighter and biggest circle, the array elements are shown with black dots for the TX array solution and the aperture area given to Step 1 for the RX is thus the darker smaller area.

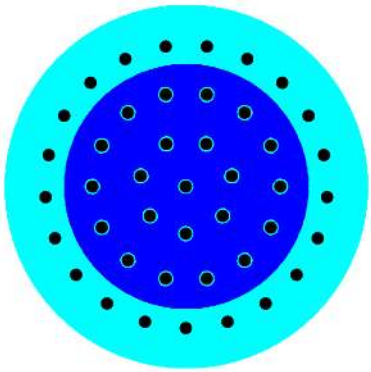

Figure 3.9: Shows the modified method for convex optimised array antennas of configuration 2. The lighter circular area is the initial given area for the TX problem where the black dots represent the array elements in the TX solution. Lastly, the initial area for the RX problem is the darker circular area.

When both the RX and TX solutions are determined, the EEPs could be simulated with FEKO. The modifications were a significant change from initially proposed method, as it meant that the optimisation had a high probability of not meeting the requirements of the radiation mask when MC effects were accounted for.

3.5 Modification of Density Tapered Array Antennas

The procedure of density tapered array antennas developed by [4] faced feasibility issues in determining the diameters of the array elements. This issue was due to that the elements could initially be chosen as small as desired. However, for the purposes of this project array elements were constricted to a constant diameter. Where the element diameter was either 2·7.79 mm, 2·12.74 mm or 2·24.4 mm depending on weather the separate RX/TX elements were employed or the common RX/TX element. Initially the boundaries for the elements were computed as

$$\left\{ \rho_k : \frac{\int_0^{\rho_k} i_0(\rho) d\rho}{\int_0^{\infty} i_0(\rho) d\rho} = \frac{\sum_{n=1}^{k} \sqrt{q_n}}{\sum_{n=1}^{N} \sqrt{q_n}} \right\} \qquad \forall k = 1, ..., N. \tag{3.13}$$

To solve the feasibility issue, i.e. allowing the use of a constant diameter $\Delta r_k = r \; \forall \; k = 1, ..., N$, the condition

$$\rho_k - \rho_{k-1} > D \tag{3.14}$$

was imposed where D is the diameter of the array antenna element.

4

Results

This chapter will present results with the methodology introduced in Ch. 3 and 2.3 of the trade-off investigation given in Ch. 1 and Ch. 3 in four separate sections. These results encompasses FoV 4° and 8° as well as inter-beam distance 0.5° and 1°. Furthermore, in Appx. A results for FoV 5°–7° and inter-beam distance 0.5°–1° are given as well.

Firstly, array configuration 1, which is array antennas employing separate RX/TX apertures and elements, of Taylor synthesised and density tapered array antennas will be presented. The first section also presents the convex optimised array antennas with configurations 1 and 2, where the second configuration are array antennas of common RX/TX apertures and separate RX/TX elements. The section is followed up with results of the third array configuration; array antennas employing common RX/TX apertures and elements for both convex optimised, Taylor synthesised and density tapered array antennas. The third part will give a summary for the entire trade-off investigation and finally the MC effects are presented for array configurations 1 and 2 with FoV 4° and inter-beam distance 1°.

The results will be presented with radiation patterns for the RX and the TX, that is 30 GHz and 20 GHz, along with the radiation mask. The separate RX elements will be depicted with filled circles and the separate TX elements will be represented with empty circles for the separate RX/TX elements. For the case of the common RX/TX elements these will be depicted with semi filled circles.

4.1 Array Antennas Utilising Common and Separate RX/TX Apertures and Separate RX/TX Elements

The radiation pattern and array designs will be given as results, where in the case of array configuration 1 simply one pattern is presented as it represents both the RX and the TX frequencies. Configuration 1 is presented for both the deterministic approaches as well as the convex optimised array antennas, while configuration 2 was achieved only for the convex optimised array antennas.

4.1.1 Taylor Synthesised Array Antennas

The Taylor synthesised array antennas with the Tschebyscheff-error are presented firstly with inter-beam distance 1 ° and secondly with inter-beam distance 0.5 °.

4.1.1.1 Inter-beam Distance 1 °

The array designs are given for the FoV 4 ° and 8 °. Furthermore, in Appx. A.1.1.1 further array designs are presented to the reader for classically Taylor synthesised array antennas. In Fig. 4.1 are the radiation pattern and array design with the FoV 4 ° and inter-beam distance 1 ° depicted. The array consisted of 71 array elements for the TX array and the RX array respectively, thus the array antenna in total consisted of 142 elements. The corresponding maximum gain was 26.4 dBi.

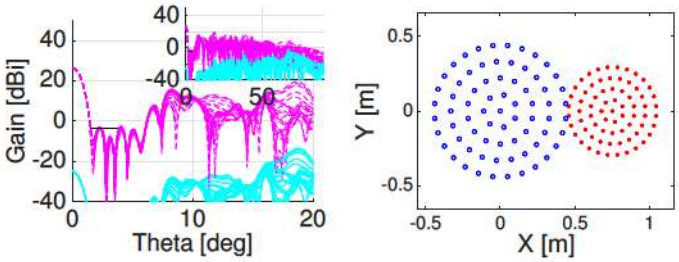

(a) Radiation pattern for the TX and the RX. (b) Array configuration 1.

Figure 4.1: Array design of the Taylor synthesised arrays and radiation pattern with inter-beam distance 1° and the FoV 4°.

In Fig. 4.2 are the radiation pattern and array design with the FoV 8 ° and inter-beam distance 1 ° depicted. The array consisted of 128 array elements for the TX array and the RX array respectively, and the maximum gain 29.9 dBi. Thus, the total number of elements were 256 for the array antenna.

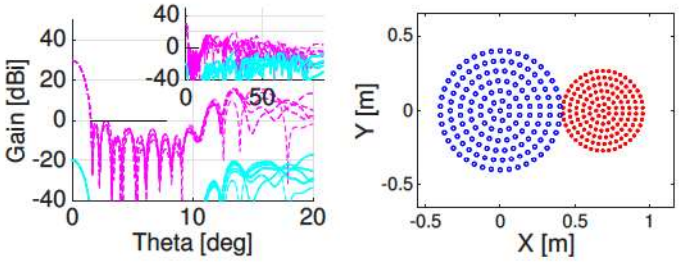

(a) Radiation pattern for the TX and the RX. (b) Array configuration 1.

Figure 4.2: Array design of the Taylor synthesised arrays and radiation pattern with inter-beam distance 1° and the FoV 8°.

4.1.1.2 Inter-beam Distance 0.5°

The corresponding results with inter-beam distance 0.5° are presented for the Taylor synthesised array antennas, with additional results in Appx. A.1.1.2. The arrays are here expected to have a diameter that is approximately double that of the aperture diameter for arrays of inter-beam distance 1°. In Fig. 4.3 are the radiation pattern and array design with the FoV 4° and inter-beam distance 0.5° depicted. The array consisted of 106 array elements for the TX array and the RX array, respectively. The total number of elements were thus 212 with the maximum gain 28.5 dBi for the array antenna.

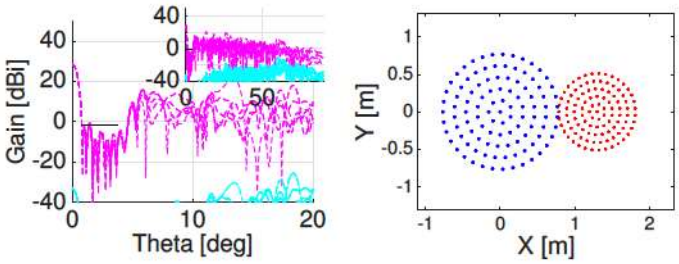

(a) Radiation pattern for the TX and the RX.

(b) Array configuration 1.

Figure 4.3: Array design of the Taylor synthesised arrays and radiation pattern with inter-beam distance 0.5° and the FoV 4°.

In Fig. 4.4 are the radiation pattern and array design with the FoV 8° and inter-beam distance 0.5° depicted. The array consisted of 316 array elements for the TX array and the RX array respectively, meaning that the total number of elements were 632 for the array antenna. The corresponding maximum gain was 33.5 dBi for this array antenna.

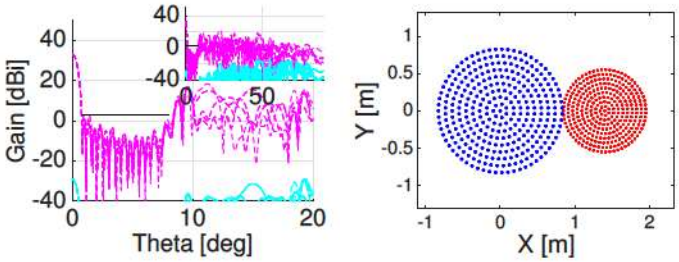

(a) Radiation pattern for the TX and the RX.

(b) Array configuration 1.

Figure 4.4: Array design of the Taylor synthesised arrays and radiation pattern with inter-beam distance 0.5° and the FoV 8°.

4.1.2 Density Tapered Array Antennas

In this section the results from the density tapered array antennas will be presented, beginning with arrays that have inter-beam distance 1° and continuing with inter-

beam distance 0.5 °.

4.1.2.1 Inter-beam Distance 1 °

The array designs will be presented for the FoV $4-6\,^{\circ}$ and $7-8\,^{\circ}$, constituting the entire study with respect to FoV. Therefore, no further results are given in the appendix. In Fig. 4.5 are the radiation pattern and array design with the FoV $4-6\,^{\circ}$ and inter-beam distance $1\,^{\circ}$ depicted. The array consisted of 356 array elements, for the TX array and the RX array, respectively. The maximum gain was 34.8 dBi and the total number of elements for the antenna were thus 712.

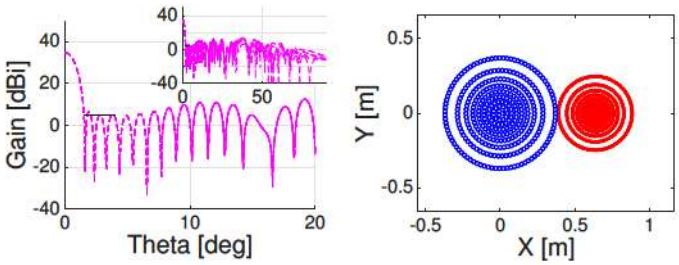

(a) Radiation pattern for the TX and the RX.

(b) Array configuration 1.

Figure 4.5: Array design of density tapered arrays and radiation pattern with inter-beam distance 1° and the FoV 4°-6°.

In Fig. 4.6 are the radiation pattern and array design with the FoV $7\,^{\circ}-8\,^{\circ}$ and inter-beam distance $1\,^{\circ}$ depicted. The array consisted of 391 array elements for the TX array and the RX array, respectively. The maximum gain was 34.9 dBi and the array antenna had in total 782 elements.

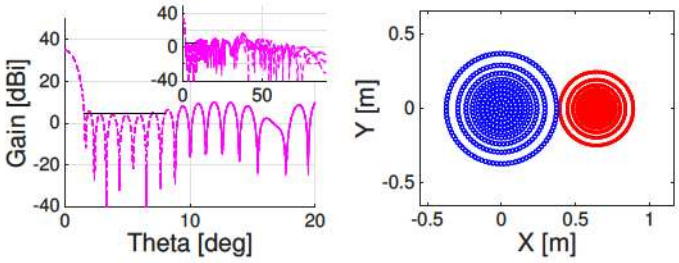

(a) Radiation pattern for the TX and the RX.

(b) Array configuration 1.

Figure 4.6: Array design of the density tapered arrays and radiation pattern with inter-beam distance 1° and the FoV 7° and 8°.

4.1.2.2 Inter-beam Distance 0.5°

The array designs will be presented for the FoV $4\,^{\circ}$ and $8\,^{\circ}$. In Appx. A.1.2 further results are presented to the reader for density tapered array antennas of inter-beam

distance 0.5°. In Fig. 4.7 are the radiation pattern and array design with the FoV 4° and inter-beam distance 0.5° depicted. The array antenna consisted of 1748 elements in total, or 874 array elements for the TX array and the RX array, respectively. The maximum gain for the TX and the RX was 38.5 dBi.

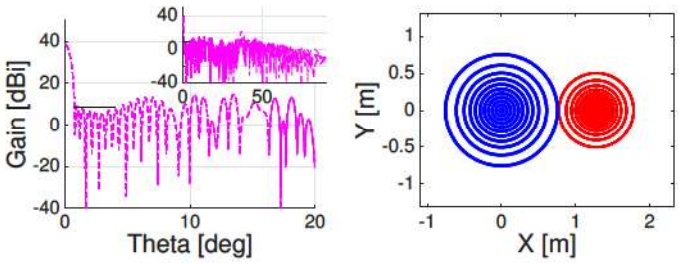

(a) Radiation pattern for the TX and the RX.

(b) Array configuration 1.

Figure 4.7: Array design of the density tapered arrays and radiation pattern with inter-beam distance 0.5° and the FoV 4°.

In Fig. 4.8 are the radiation pattern and array design with the FoV 8° and inter-beam distance 0.5° depicted. The array consisted of 1331 array elements, for the TX array and the RX array, respectively, and the maximum gain 40.3 dBi. In total array antenna consisted of 2662 elements.

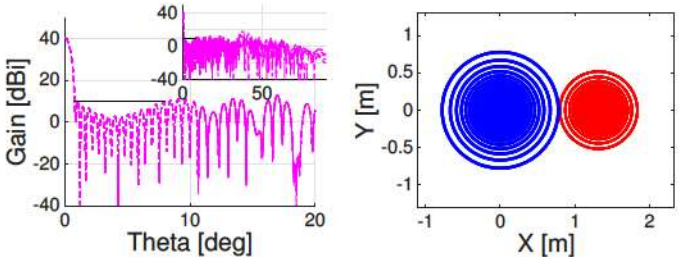

(a) Radiation pattern for the TX array and the RX array.

(b) Array configuration 1.

Figure 4.8: Array design of the density tapered arrays and radiation pattern with inter-beam distance 0.5° and the FoV 8°.

4.1.3 Convex Optimised Array Antennas

In this section will the convex optimised array antennas, as described in Ch. 3, be presented beginning with array antennas of inter-beam distance 1° and continuing with inter-beam distance 0.5°. For the array antenna of configuration 2 there are two separate radiation patterns as results, one for the RX and one for the TX. For the first configuration, either the radiation pattern of the RX or the TX will correspond to the array designs. Moreover, two different radiation masks were used. The first mask presented suppresses the radiation pattern up to 8° and will be referred to as

the short mask. The second mask suppresses the radiation pattern up to 15 °, this radiation mask is referred to as the long mask.

4.1.3.1 Inter-beam Distance 1°

The array designs will be presented for the FoV 4 ° and 8 ° while in Appx. A.1.3 results for the FoV 5°-7° are presented. In Fig. 4.9 are the array designs and the corresponding radiation patterns depicted for the FoV 4° and inter-beam distance 1° with the short mask. For the array antenna of configuration 2, the number of elements were 208 with the maximum gain 27.8 dBi for the RX array 28.3 dBi for the TX array. For the array antenna of configuration 1 the number of elements were 192 with maximum gain 27.8 dBi for both the TX and the RX, where the radiation pattern corresponds to the RX array.

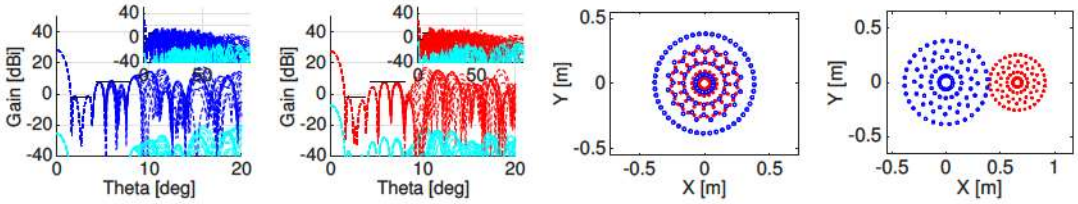

(a) Radiation pattern for the TX. (b) Radiation pattern for the RX. (c) Array configuration 2. (d) Array configuration 1.

Figure 4.9: Array designs for convex optimised arrays and radiation patterns of inter-beam distance 1°, the FoV 4° and radiation mask range 8°.

In Fig. 4.10 are the array designs and the corresponding radiation patterns depicted for the FoV 4° and inter-beam distance 1° with the long radiation mask. For the array antenna of configuration 2 the number of elements were 397 with maximum gain 26.5 dBi for the TX and 30.8 dBi for the RX. The array antenna of configuration 1 corresponds to the TX design, which gives a total number of elements of 310 and 26.5 dBi as maximum gain.

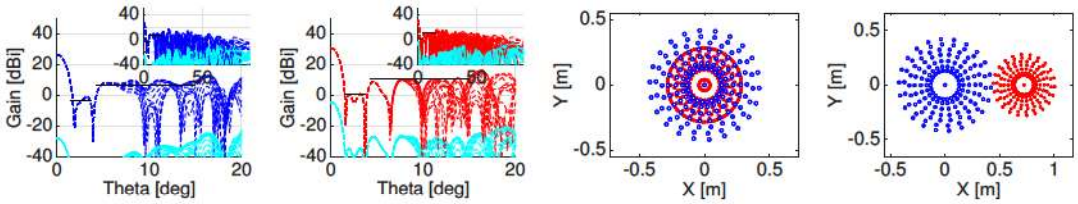

(a) Radiation pattern for the TX. (b) Radiation pattern for the RX. (c) Array configuration 2. (d) Array configuration 1.

Figure 4.10: Array designs for convex optimised arrays and radiation patterns of inter-beam distance 1°, the FoV 4° and radiation mask range 15°.

In Fig. 4.11 are the array designs and the corresponding radiation patterns depicted for the FoV 8° and inter-beam distance 1° with the short mask. For the array antenna of configuration 2 the number of elements were 257 with the maximum

gain 28.9 dBi for the RX array and 29.0 dBi for the TX array. For the array antenna of configuration 1, with radiation pattern corresponding to the RX case in this instance, the number of elements were 256, with maximum gain 28.9 dBi.

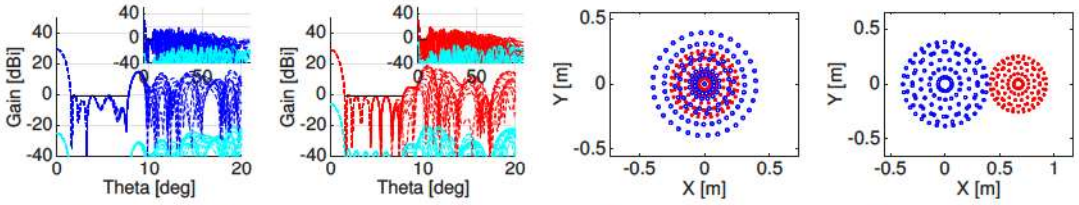

(a) Radiation pattern for the TX. (b) Radiation pattern for the RX. (c) Array configuration 2. (d) Array configuration 1.

Figure 4.11: Radiation pattern and array designs for an convex optimised array with inter-beam distance 1°, the FoV 8° and the radiation mask range is 8°.

In Fig. 4.12 are the array designs and the corresponding radiation patterns depicted for the FoV 8° and inter-beam distance 1° with the long mask. For the array antenna of configuration 2 the number of elements were 485 with the maximum gain 31.5 dBi for the RX array and 30.6 dBi for the TX array. For the array antenna of configuration 1, corresponding to the TX case, the number of elements were 442 with maximum gain 30.6 dBi for both the RX and the TX.

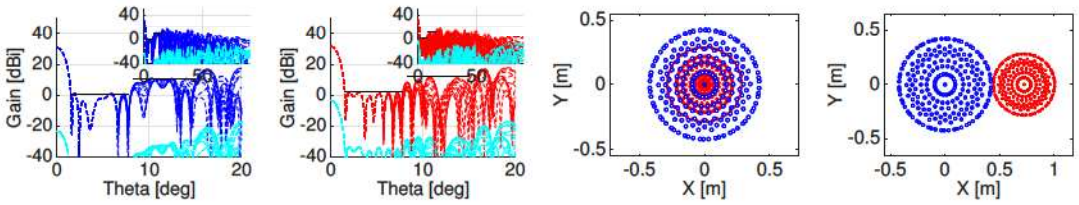

(a) Radiation pattern for the TX. (b) Radiation pattern for the RX. (c) Array configuration 2. (d) Array configuration 1.

Figure 4.12: Array designs for convex optimised arrays and radiation patterns of inter-beam distance 1°, the FoV 8° and radiation mask range 15°.

4.1.3.2 Inter-beam Distance 0.5°

The convex optimised array designs will be presented for the FoV 4° and 8°. In Appx. A.1.3 the results for the FoV 5°-7° are given additionally. In Fig. 4.13 are the array designs and the corresponding radiation patterns depicted for the FoV 4° and inter-beam distance 0.5° with the short radiation mask. For the array antenna of configuration 2 the number of elements were 451 with the maximum gain 31.8 dBi for the RX array and 28.9 dBi for the TX array. The array antenna of configuration 1, which corresponds to the RX case, had 434 elements with maximum gain 28.9 dBi.

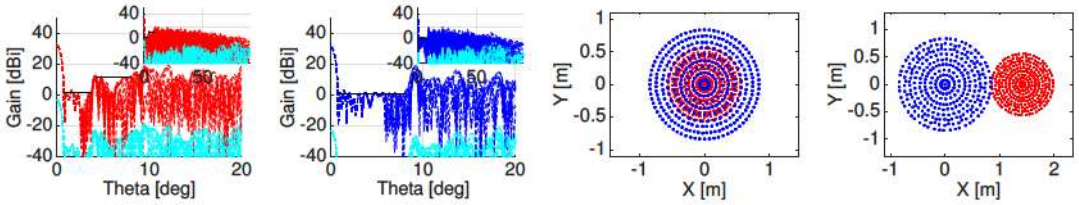

(a) Radiation pattern for the RX. (b) Radiation pattern for the TX. (c) Array configuration 2. (d) Array configuration 1.

Figure 4.13: Array designs for convex optimised arrays and radiation patterns of inter-beam distance 0.5°, the FoV is 4° and radiation mask range 8°.

In Fig. 4.14 are the array designs and the corresponding radiation patterns depicted for the FoV 4° inter-beam distance 0.5° with the long mask. For the array antenna of configuration 2 the number of elements were 617 with the maximum gain 32.9 dBi for the RX array 31.6 dBi for the TX array. For the array antenna of configuration 1, corresponding to the TX case, the number of elements were 618 and maximum gain 31.6 dBi.

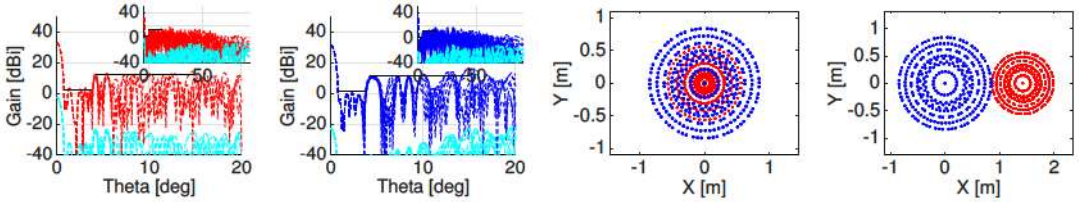

(a) Radiation pattern for the RX. (b) Radiation pattern for the TX. (c) Array configuration 2. (d) Array configuration 1.

Figure 4.14: Array designs for convex optimised arrays and radiation patterns of inter-beam distance 0.5°, the FoV is 4° and radiation mask range 15°.

In Fig. 4.15 are the array designs and the corresponding radiation patterns depicted for the FoV 8° inter-beam distance 0.5° with the short mask. For the array antenna of configuration 2 the number of elements were 685 with the maximum gain 32.8 dBi for the RX array and 30.9 dBi for the TX array. For the array antenna of configuration 1, which corresponds to the RX case, the number of elements were 650 with maximum gain 32.8 dBi.

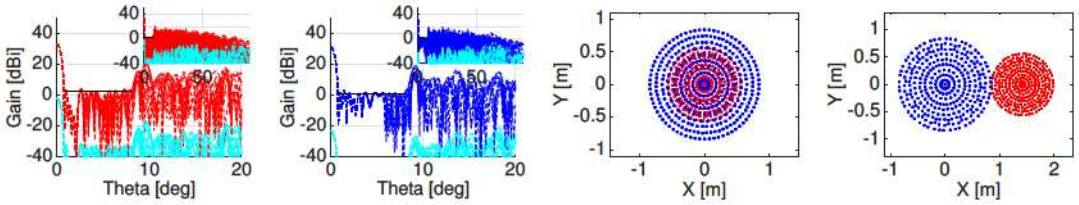

(a) Radiation pattern for the RX. (b) Radiation pattern for the TX. (c) Array configuration 2. (d) Array configuration 1.

Figure 4.15: Array designs for convex optimised arrays and radiation patterns of inter-beam distance 0.5°, the FoV 8° and radiation mask range 8°.

In Fig. 4.16 are the array designs and the corresponding radiation patterns depicted for the FoV 8° inter-beam distance 0.5° with the long radiation mask. For the array antenna of configuration 2 the number of elements were 903 with the maximum gain 34.4 dBi for the RX array and 33.4 dBi for the TX array. For the array antenna of configuration 1 the number of elements were 926 with maximum gain 33.4 dBi, as it is represented by the TX array.

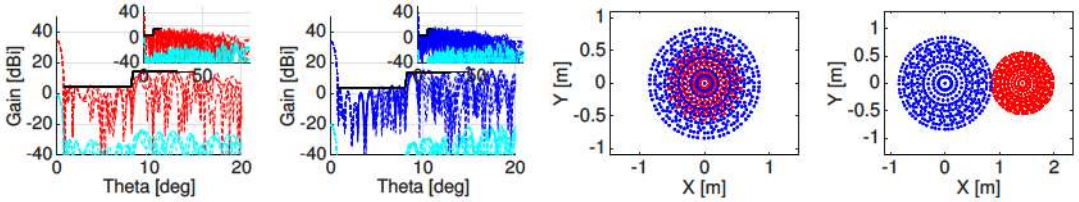

(a) Radiation pattern for the RX. (b) Radiation pattern for the TX. (c) Array configuration 2. (d) Array configuration 1.

Figure 4.16: Array designs for convex optimised arrays and radiation patterns of inter-beam distance 0.5°, the FoV 8° and radiation mask range 15°.

4.1.4 Summary

As a summary the four Tables 4.1- 4.4 are presented that corresponds to the inter-beam distances 0.5° and 1° and the different radiation masks. The tables show the numerical values of the maximum gain in units of dBi and the number of elements.

Table 4.1: Shows the maximum gain in dBi as well as the number of elements for convex optimised array antennas of configuration 1 and 2, Taylor synthesised array antennas of configuration 1 and density tapered array antennas of configuration 1 with inter-beam distance 1 °, for short radiation masks.

FoV	G_0^{TX}	G_0^{RX}	$N_{conf.2}^{conv.opt.}$	$G_0^{RX/TX}$	$N_{conf.1}^{conv.}$	$G_0^{RX/TX}$	$N_{conf.1}^{Taylor}$	$G_0^{RX/TX}$	$N_{conf.1}^{den.}$
4°	28.3	27.8	208	27.8	192	26.4	142	34.8	712
5°	29.0	27.1	225	27.1	194	26.7	142	34.8	712
6°	29.4	28.1	241	28.1	226	28.3	212	34.9	782
7°	29.2	28.6	240	28.6	224	28.5	212	34.9	782
8°	29.0	28.9	257	28.9	256	29.9	256	34.9	782

Table 4.2: Shows the maximum gain in dBi as well as the number of elements for convex optimised array antennas of configuration 1 and 2 with inter-beam distance 1 °, with the long radiation mask.

FoV	G_0^{TX}	G_0^{RX}	$N_{conf.2}^{conv.}$	$G_0^{RX/TX}$	$N_{conf.1}^{conv.}$
4°	26.5	30.8	397	26.5	310
5°	30.1	30.8	419	30.1	398
6°	29.5	31.0	441	29.5	442
7°	30.6	31.9	263	30.6	442
8°	30.6	31.5	485	30.6	442

Table 4.3: Shows the maximum gain in dBi as well as the number of elements for convex optimised array antennas of configuration 1 and 2, Taylor synthesised array antennas of configuration 1 and density tapered array antennas of configuration 1 with inter-beam distance 0.5 °, with short radiation masks.

FoV	G_0^{TX}	G_0^{RX}	$N_{conf.2}^{conv.}$	$G_0^{RX/TX}$	$N_{conf.1}^{conv.}$	$G_0^{RX/TX}$	$N_{conf.1}^{Taylor}$	$G_0^{RX/TX}$	$N_{conf.1}^{den.}$
4°	28.9	31.8	451	28.9	434	28.5	212	38.5	1748
5°	28.6	31.3	469	28.6	434	29.7	296	39.0	1902
6°	30.0	31.3	559	30.0	579	31.0	394	39.4	2222
7°	30.7	33.2	613	30.7	614	32.0	504	39.4	2378
8°	30.9	32.8	685	30.9	650	33.5	632	40.3	2662

Table 4.4: Shows the maximum gain in dBi as well as the number of elements for convex optimised array antennas of configuration 1 and 2 with inter-beam distance 0.5 °, with the long radiation mask.

FoV	G_0^{TX}	G_0^{RX}	$N_{conf.2}^{conv.}$	$G_0^{RX/TX}$	$N_{conf.1}^{conv.}$
4°	31.6	32.9	617	31.6	618
5°	32.8	33.1	727	32.8	706
6°	32.3	33.3	771	32.3	706
7°	32.3	34.3	771	32.3	706
8°	33.4	34.4	903	33.4	926

It can be noted that the number of elements for Taylor synthesised arrays lied in the region $142-265$ and $212-632$ for inter-beam distances $1\,^\circ$ and $0.5\,^\circ$, respectively. Thus, the number of elements increases as the FoV increases and as the inter-beam distance decreases. The gain lied in the region $26.4-29.9\,\mathrm{dBi}$ and $28.5-33.5\,\mathrm{dBi}$ for inter-beam distances 1° and 0.5°, respectively. The array antennas are therefore more directive as the FoV in increased and the inter-beam distance decreases.

The density tapered array antennas exhibit a similar behavior, but demanded significantly more elements for all arrays. The number of elements for the density tapered arrays lied in the region $712-782$ and $1748-2662$ for inter-beam distances $1\,^\circ$ and $0.5\,^\circ$, respectively. The method could only give two array antenna designs for inter-beam distance $1\,^\circ$ as the elements are confined to diameter $2\cdot 12.74\,\mathrm{mm}$ and to be placed in the xy-plane. For the smaller inter-beam distance, the aperture is bigger which gives a larger area to create the approximative current distribution more similar to the ideal current distribution and thus results for every FoV investigated were obtained. The gain lied in the region $34.8-34.9\,\mathrm{dBi}$ inter-beam distance $1\,^\circ$ and $38.5-40.3\,\mathrm{dBi}$ for inter-beam distance $0.5\,^\circ$, giving here as well a more directive pattern as the FoV in increased and the inter-beam distance decreased.

The convex optimised array antennas of configuration 1 with inter-beam distance 1° the total number of elements ranged between $192-256$ for the short radiation mask, and $310-442$ for the long radiation mask. For the corresponding array antennas of configuration 2 the number of elements varied from $208-257$ for the short radiation mask and $397-485$ for the long radiation mask. For inter-beam distance 0.5° the number of elements for convex optimised array antennas of configuration 1 varied from $434-650$ for the short mask and $618-926$ for the long radiation mask. For the array antennas of configuration 2 the number of elements lied in the region $451-685$ for the short radiation mask and $617-903$ for the long radiation mask. It can further be noted that the maximum gain depends on the FoV and inter-beam distance as the Taylor synthesised and density tapered array antennas. Furthermore, the maximum gain varied for the RX and the TX which depended on what solution had the most elements which in turn depended on weather the RX or the TX was optimised first. In addition the maximum gain varied slightly when the longer radiation mask was applied, the larger effect to note is the number of elements which increased significantly.

4.2 Array Antennas Utilising Common RX/TX Apertures and Common RX/TX Elements

The third and last configuration considered was array antennas with common RX/TX apertures in combination with the common RX/TX element. First the results of the Taylor synthesised array antennas will be conferred, which will be followed by the density tapered array antennas and finally the results of the convex optimised array antennas will be presented.

4.2.1 Taylor Synthesised Array Antennas

In this section will the Taylor synthesised array antennas with Tschebyscheff-error be presented. Beginning with array antennas of inter-beam distance 1 ° and continuing with inter-beam distance 0.5 °, the array designs will be presented for the FoV 4 ° and 8 °. Furthermore, in Appx. A.2.1 further results are presented to the reader for the FoV 5°-7°.

4.2.1.1 Inter-beam Distance 1°

In Fig. 4.17 are the radiation patterns and array design with the FoV 4 ° and inter-beam distance 1 ° shown. The array antenna consisted of 71 array elements and the maximum gain 34.1 dBi and 37.3 dBi for the TX and the RX, respectively.

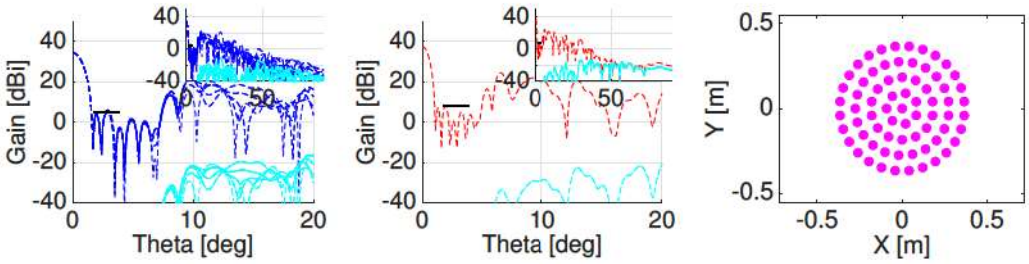

(a) Radiation patterns for the RX.

(b) Radiation patterns for the TX.

(c) Array configuration 3.

Figure 4.17: Array design of a Taylor synthesised array antenna and radiation patterns with inter-beam distance 1° and the FoV 4°.

In Fig. 4.18 are the radiation patterns and array design with the FoV 8 ° and inter-beam distance 1 ° depicted. The array antenna consisted of 148 array elements and the maximum gain 37.6 dBi and 41.0 dBi for the TX and the RX, respectively.

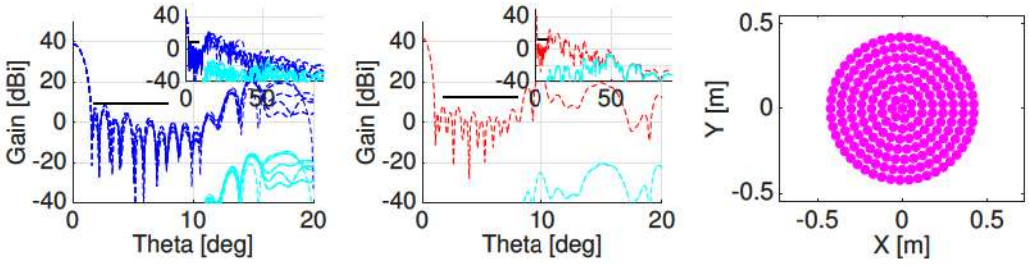

(a) Radiation patterns for the RX.

(b) Radiation patterns for the TX.

(c) Array configuration 3.

Figure 4.18: Array design of a Taylor synthesised array antenna and radiation patterns with inter-beam distance 1° and the FoV 8°.

4.2.1.2 Inter-beam Distance 0.5 °

In Fig. 4.19 are the radiation patterns and array design with the FoV 4 ° and inter-beam distance 0.5 ° depicted. The array antenna consisted of 148 array elements

and the maximum gain 37.0 dBi and 40.0 dBi for the TX and the RX, respectively.

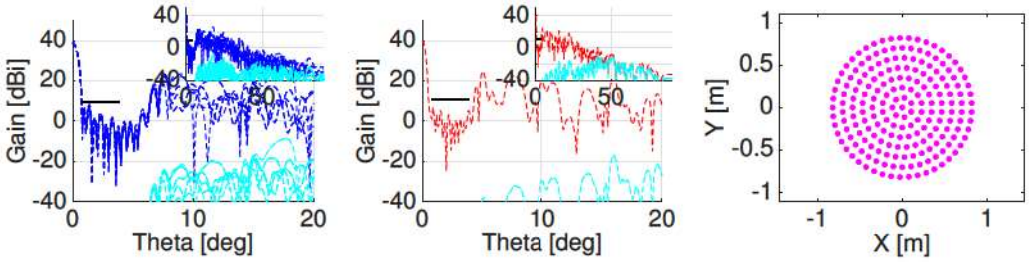

(a) Radiation patterns for the RX.

(b) Radiation patterns for the TX.

(c) Array configuration 3.

Figure 4.19: Array design of a Taylor synthesised array antenna and radiation patterns with inter-beam distance 0.5° and the FoV 4°.

In Fig. 4.20 are the pattern and array design with the FoV 8 ° and inter-beam distance 0.5 ° depicted. The array antenna consisted of 547 array elements and the maximum gain 44.7 dBi and 47.0 dBi for the TX and the RX, respectively.

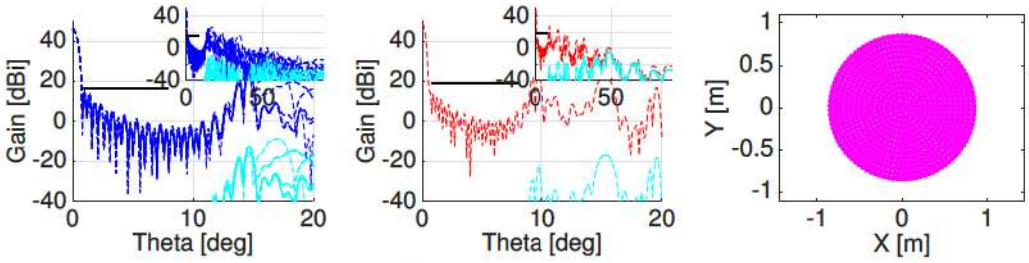

(a) Radiation patterns for the RX.

(b) Radiation patterns for the TX.

(c) Array configuration 3.

Figure 4.20: Array design of a Taylor synthesised array antenna and radiation patterns with inter-beam distance 0.5° and the FoV 8°.

4.2.2 Density Tapered Array Antennas

In this section will the density tapered array antennas be presented, beginning with arrays that have inter-beam distance 1 ° and continuing with inter-beam distance 0.5 °.

4.2.2.1 Inter-beam Distance 1°

The array designs will be presented for the FoV 4 ° – 8 ° with one array design, as the method could not handle a variation of FoV. In Fig. 4.21 are the radiation patterns and array design with the FoV 4°–8 ° and inter-beam distance 1 ° shown. The array antenna consisted of 209 array elements and the maximum gain 38.8 dBi and 41.6 dBi for the TX and the RX, respectively.

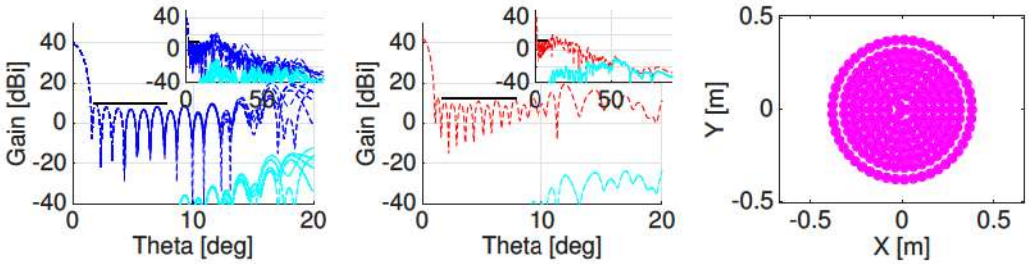

(a) Radiation patterns for the TX.

(b) Radiation patterns for the RX.

(c) Array configuration 3.

Figure 4.21: Array design of a density tapered array antenna and radiation patterns with inter-beam distance 1° and FoV 4° – 8°.

4.2.2.2 Inter-beam Distance 0.5°

The array designs will be presented for the FoV 4° and 8°. The remaining results for the FoV 5° – 7° can be viewed in Appx. A.2.2 . In Fig. 4.22 are the radiation patterns and array design with the FoV 4° and inter-beam distance 0.5° shown. The array antenna consisted of 524 array elements and the maximum gain 43.5 dBi and 46.3 dBi for the TX and the RX, respectively.

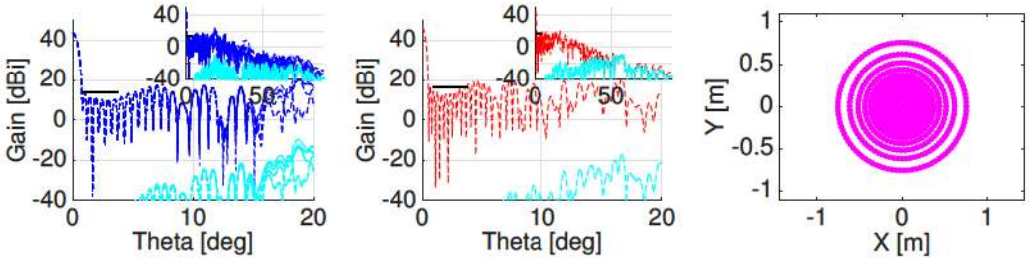

(a) Radiation patterns for the TX.

(b) Radiation patterns for the RX.

(c) Array configuration 3.

Figure 4.22: Array design of a density tapered array antenna and radiation patterns with inter-beam distance 0.5° and FoV 4°.

In Fig. 4.23 are the radiation patterns and array design with the FoV 8° and inter-beam distance 0.5° depicted. The array antenna consisted of 748 array elements and the maximum gain 44.9 dBi and 47.6 dBi for the TX and the RX, respectively.

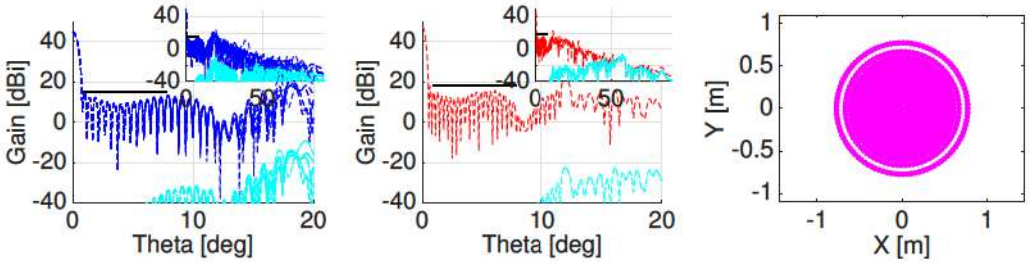

(a) Radiation patterns for the TX.

(b) Radiation patterns for the RX.

(c) Array configuration 3.

Figure 4.23: Array design of a density tapered array antenna and radiation patterns with inter-beam distance 0.5° and FoV 8° .

4.2.3 Convex Optimised Array Antennas

In this section will the convex optimised array antennas be presented, beginning with array antennas that have inter-beam distance 1 ° and continuing with inter-beam distance 0.5 °.

4.2.3.1 Inter-beam Distance 1°

The array designs will be presented for the FoV 4 ° and 8 ° while in Appx. A.2.3.1 more results are displayed to the reader. In Fig. 4.24 are the radiation patterns and array design shown for the FoV 4° and inter-beam distance 1°. For this array antenna the number of elements were 85 with the maximum gain 33.0 dBi and 38.8 dBi for the TX and the RX, respectively.

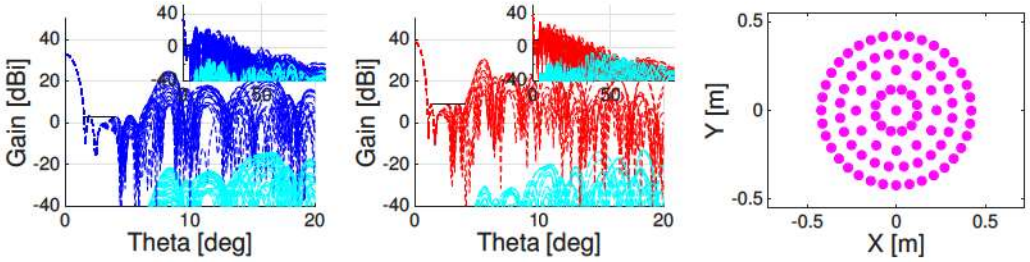

(a) Radiation pattern for the RX.

(b) Radiation pattern for the TX.

(c) Array configuration 3.

Figure 4.24: Array design and radiation patterns of a convex optimised array antenna with the inter-beam distance 1° and the FoV 4°.

In Fig. 4.25 are the corresponding radiation patterns shown for the FoV 8° and inter-beam distance 1°. For this array antenna the number of elements were 191 with the maximum gain 38.0 dBi and 43.8 dBi for the TX and the RX, respectively. It should be noted that some of the elements overlap, which is an unphysical solution.

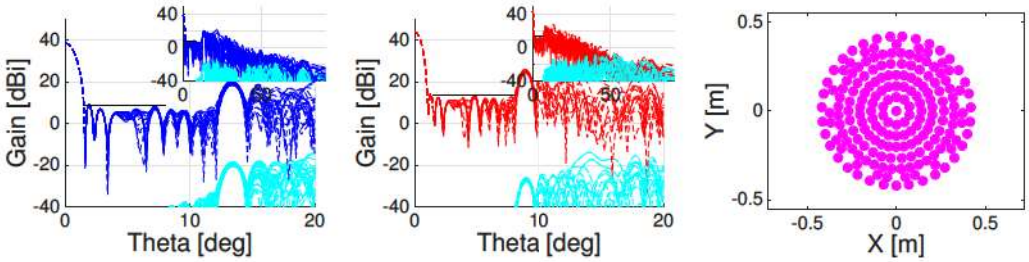

(a) Radiation pattern for the RX.

(b) Radiation pattern for the TX.

(c) Array configuration 3.

Figure 4.25: Array design and radiation patterns of a convex optimised array antenna with the inter-beam distance 1° and the FoV 8°.

4.2.3.2 Inter-beam Distance 0.5°

The array designs will be presented for the FoV 4° and 8° where more results are given to the reader in Appx. A.2.3.2. In Fig. 4.26 are the radiation patterns and array design shown with inter-beam distance 0.5° and the FoV 4°. For this array antenna the number of elements were 193 with the maximum gain 43.7 dBi for both the TX and the RX.

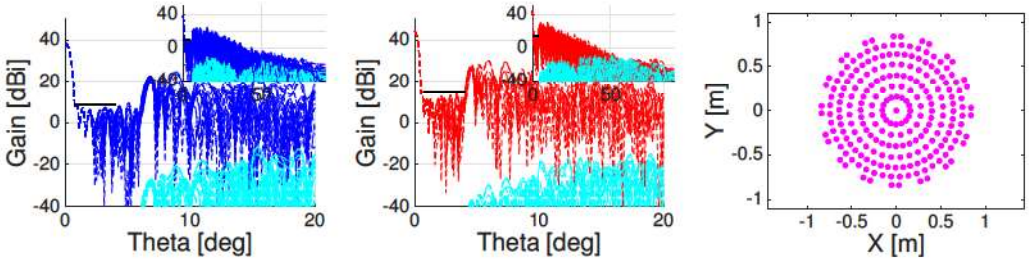

(a) Radiation pattern for the TX.

(b) Radiation pattern for the RX.

(c) Array configuration 3.

Figure 4.26: Array design and radiation patterns of a convex optimised array antenna with inter-beam distance 0.5° and the FoV 4°.

In Fig. 4.27 are the corresponding radiation patterns shown with inter-beam distance 0.5° and the FoV 8°. For this array antenna the number of elements were 545 with the maximum gain 48.2 dBi and 48.5 dBi for the TX and the RX, respectively.

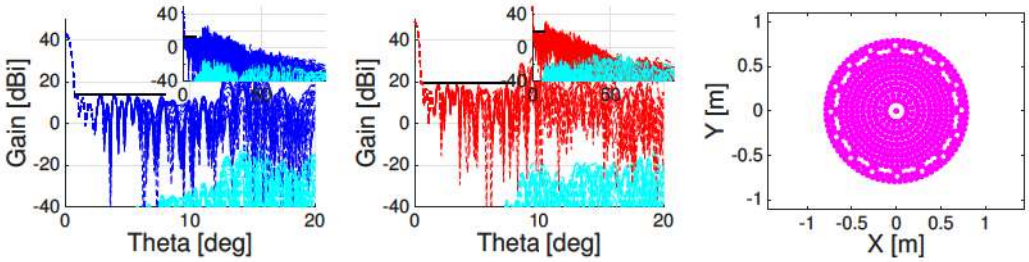

(a) Radiation pattern for the TX.

(b) Radiation pattern for the RX.

(c) Array configuration 3.

Figure 4.27: Array design and radiation patterns of a convex optimised array with inter-beam distance 0.5° and the FoV 8°.

4.2.4 Summary

A summary of the convex optimised and synthesised array antennas are given Tables 4.5 and 4.6 with inter-beam distance 1 ° and 0.5 °, respectively. It can be noted that the number of elements required for Taylor synthesised array antennas lied in the region 71−148 and 148−547 with inter-beam distances 1 ° and 0.5 °, respectively. For inter-beam distance 1° the maximum gain lied in the region 34.1–37.6 dBi and 37.3–41.0 dBi for the TX and the RX, respectively. Correspondingly, for inter-beam distance 0.5° the maximum gain varied as 37.0–44.7 dBi and 40.0–47.0 dBi for the TX and the RX, respectively. Thus, the maximum gain is larger for these array antennas than the first and second array configurations, whilst having less elements.

For the density tapered array antennas only one solution for the bigger inter-beam distance was obtained with 209 elements with gain 38.8 dBi for the TX and 41.6 dBi for the RX. This can be expected as the current distribution differ more from the ideal excitation current on the smaller aperture area. For inter-beam distance 0.5 ° the number of elements required lied in the region 524−748 with the maximum gain 43.5–44.9 dBi for the TX and 46.3–47.6 dBi for the RX. It can be noted that the number of elements required are significantly higher than for the Taylor synthesised array antennas.

It was not possible to suppress the side lobes outside FoV for the convex optimised array antennas, as the convex optimisation method would provide non-physical solutions where the elements were placed on top of each other if a longer radiation mask was applied. For inter-beam distance 1° the number of elements ranged as 85–191 and the maximum gain lied in the region 33.0–38.0 dBi for the TX and 38.8–43.8 dBi for the RX. The number of elements varied as 193−545 with inter-beam distance 0.5°, the corresponding gain lied in the region 43.7–48.2 dBi for the TX and 43.7–48.5 dBi for the RX.

Table 4.5: Shows the maximum gain in dBi as well as the number of elements for convex optimised, density tapered and Taylor synthesised array antennas of configuration 3 with inter-beam distance 1 °, while having a mask for the radiation pattern up to FoV °.

FoV	G_0^{TX}	G_0^{RX}	$N_{conf.3}^{conv.}$	G_0^{TX}	G_0^{RX}	$N_{conf.3}^{Taylor}$	G_0^{TX}	G_0^{RX}	$N_{conf.3}^{den.}$
4°	33.0	38.8	85	34.1	37.3	71	38.8	41.6	209
5°	35.0	40.4	109	34.4	37.7	71	38.8	41.6	209
6°	36.4	42.0	148	35.9	38.6	106	38.8	41.6	209
7°	37.3	42.9	169	36.6	39.3	106	38.8	41.6	209
8°	38.0	43.8	191	37.6	41.0	148	38.8	41.6	209

Table 4.6: Shows the maximum gain in dBi as well as the number of elements for convex optimised, density tapered and Taylor synthesised array antennas of configuration 3 with inter-beam distance 0.5 °, while having a mask for the radiation pattern up to FoV °.

FoV	G_0^{TX}	G_0^{RX}	$N_{conf.3}^{conv.}$	G_0^{TX}	G_0^{RX}	$N_{conf.3}^{Taylor}$	G_0^{TX}	G_0^{RX}	$N_{conf.3}^{den.}$
4°	43.7	43.7	193	37.0	40.0	148	43.5	46.3	524
5°	45.3	45.3	273	38.7	42.0	197	44.3	47.0	661
6°	46.4	46.6	337	40.0	43.0	253	44.3	47.0	662
7°	48.2	48.2	497	42.0	44.7	386	44.9	47.6	749
8°	48.2	48.5	545	44.7	47.0	547	44.9	47.6	748

A similar pattern for the FoV and inter-beam distance parameters can be noted in the tables for convex optimised, Taylor synthesised, density tapered array antennas as for the previous array configurations, where the number of elements and the maximum gain increases as the FoV increases and the inter-beam distance decreases. As the common RX/TX element is more directive than the separate RX/TX elements the maximum gain was also higher for these array antennas while utilising less elements. It should be noted that for the FoV 8° and inter-beam distance 1° that the elements actually overlap, which is not a physical solution.

4.3 Summary of Trade-off Investigation

A summary for the convex optimised array antennas and synthesised array antennas in the possible configurations, inter-beam distances and FoVs are given for the maximum gain in Fig. 4.29 and number of elements in Fig. 4.28.

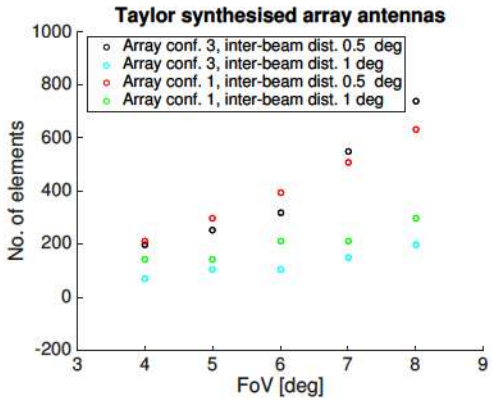

(a) Number of elements depending on the FoV for inter-beam distances 0.5° and 1° for Taylor synthesised array antennas.

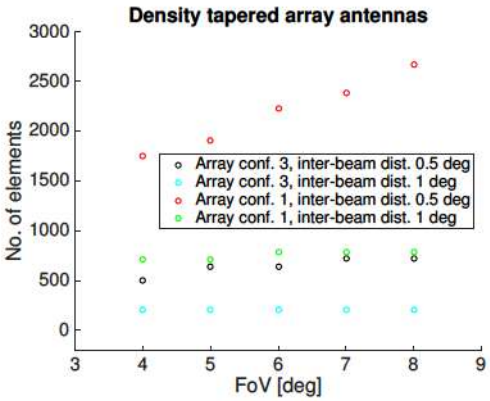

(b) Number of elements depending on the FoV for inter-beam distances 0.5° and 1° for density tapered array antennas.

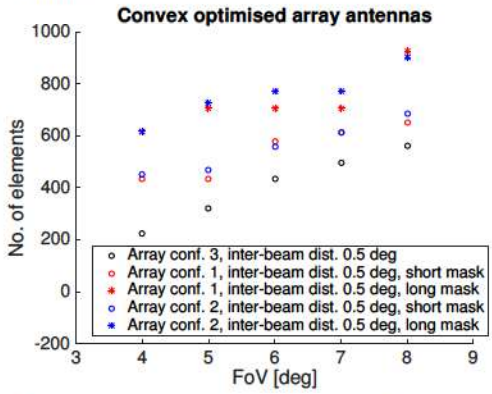

(c) Number of elements depending on the FoV for convex optimised array antennas of inter-beam distance 0.5°.

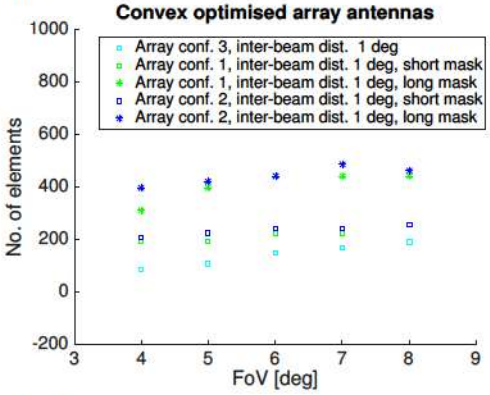

(d) Number of elements depending on the FoV for convex optimised array antennas of inter-beam distance 1°.

Figure 4.28: Number of elements and controls depending on the FoV and inter-beam distance.

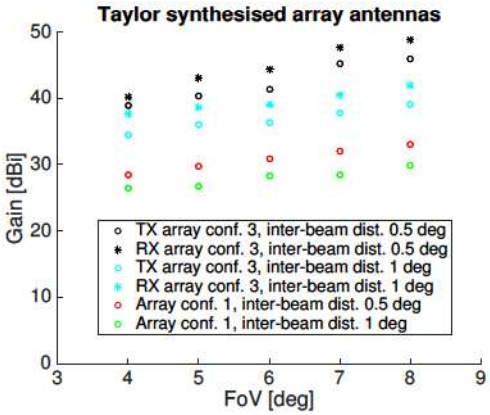

(a) Gain depending on the FoV for inter-beam distances 0.5° and 1° for Taylor synthesised array antennas.

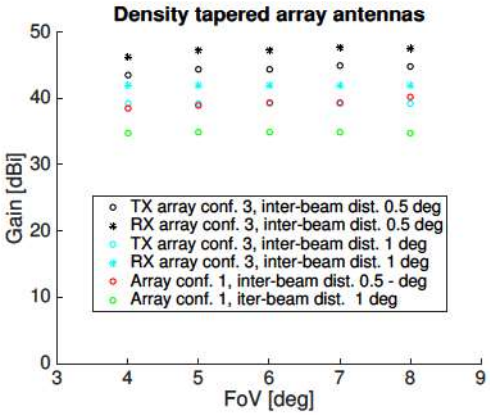

(b) Gain depending on the FoV for inter-beam distances 0.5° and 1° for density tapered array antennas.

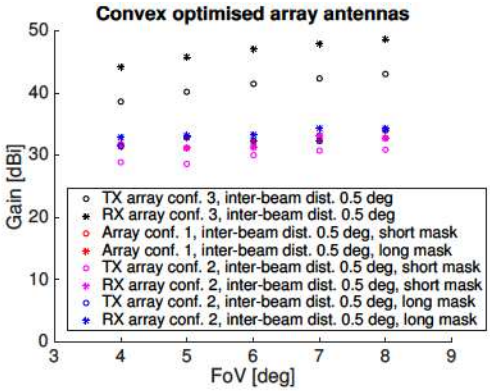

(c) Gain depending on the FoV for convex optimised array antennas of inter-beam distance 0.5°.

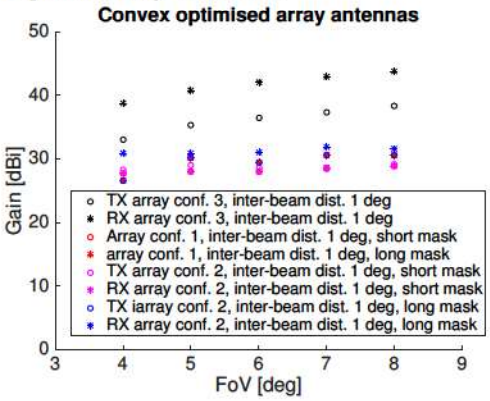

(d) Gain depending on the FoV for convex optimised array antennas of inter-beam distance 1°.

Figure 4.29: Gain depending on the FoV and inter-beam distance.

4.4 Effects of MC

The MC effects were investigated for array configuration 1 of the separate TX array of inter-beam distance 1° with the FoV 4°, depicted in Fig. 4.9d, while suppressing the rest of the radiation pattern up to 8°. This array contained 96 array elements for both the RX and the TX. The MC effects were accounted for by utilising FEKO for the waveguide port excitation and cut-off radius $6\,\lambda$. The radiation patterns with MC effects included are depicted in Fig. 4.30.

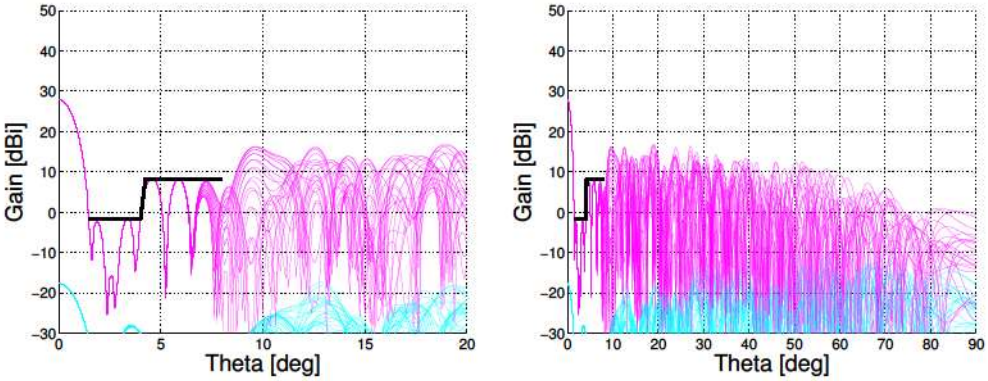

(a) Shows the radiation pattern for the TX array up to 20°.

(b) Shows the radiation pattern for the TX array up to 90°.

Figure 4.30: Radiation pattern for array configuration 1 with MC effects included.

It can be noted that the mask still holds for the radiation pattern, as depicted in Fig. 4.30. In addition the array antenna of configuration 2, depicted in Fig. 4.9c, was simulated with FEKO for the same radiation mask, that contained 96 and 112 elements for the RX and the TX, respectively.

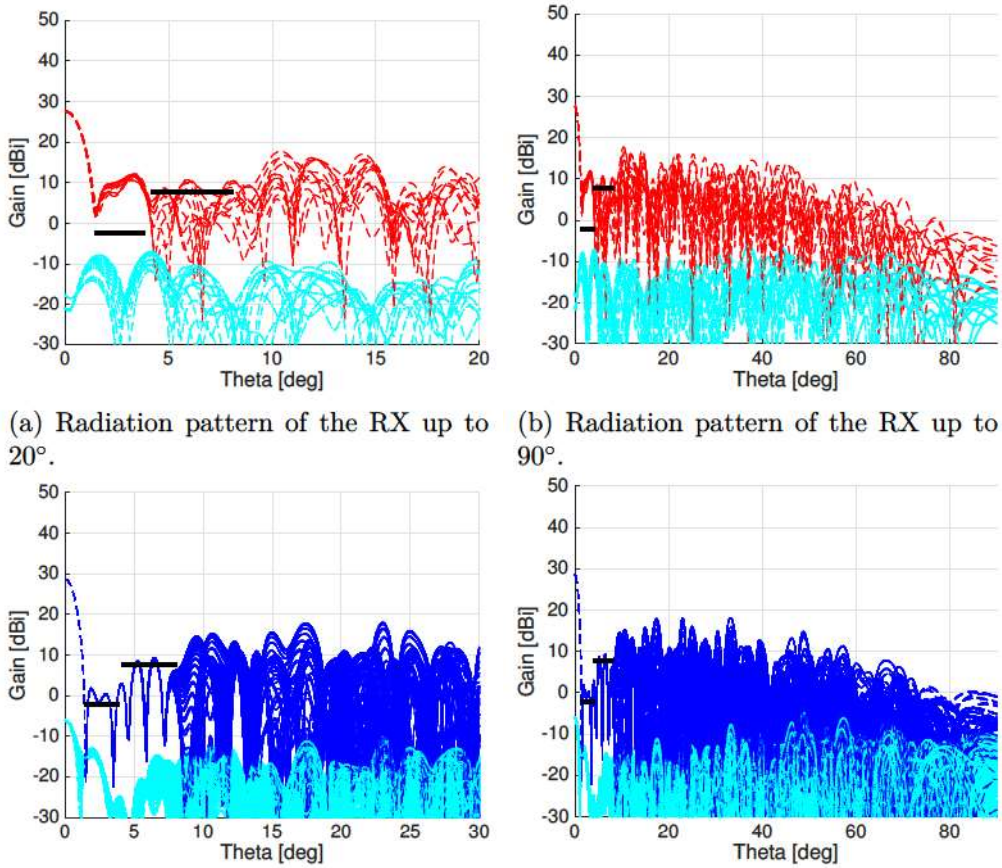

(a) Radiation pattern of the RX up to 20°.

(b) Radiation pattern of the RX up to 90°.

(c) Radiation pattern of the TX up to 20°.

(d) Radiation pattern of the TX up to 90°.

Figure 4.31: Radiation patterns for array configuration 2 with MC effects included.

It can be noted that the mask is violated for both TX and RX frequencies and that the pattern of the RX array is far more affected than the TX array as shown in Fig. 4.31. This is expected as the RX array is embedded in the TX array.

5

Discussion

In this section will the results be discussed further details, specifying on the trade-off points listed in chapter 1. Moreover, the results from the simulations in FEKO will also be discussed and what implications there may be for the simulations of array antennas.

5.1 Number of Elements and Controls compared to changed FoV

The FoV was varied from 4° to 8° in steps of 1° for the sparse array antennas. It can be noted that the antennas had to obey rather strict requirements, presented in Sec. 3.1, as the array antennas must be able to cope with rather narrow main beams and a steep drop from the maximum gain to the OoC gain.

The noted overall trend was that the number of elements and controls increase as the FoV increases for the deterministically synthesised array antennas as well as the convex optimised array antennas. The number of elements lied in the region 100–500 elements for the convex optimised array antennas of configuration 1 and 2 and Taylor synthesised array antennas of configuration 1, if the arrays are considered separately for the RX and the TX. That is, for the entire array antennas the number of elements lied in the region 200–1000 elements. In comparison the density tapered array antennas of configuration 1 lied in the region 700–2700 elements. For the array antennas of configuration 3 the number of elements lied in the region 100–600 for the convex optimised array antennas as well as the Taylor synthesised array antennas, where the density tapered array antennas lied in the region 200–800 elements.

The relation between FoV and the number of elements are shown in Fig. 4.28. In particular, the results are depicted for the convex optimised array antennas in Fig. 4.28c and Fig. 4.28d for inter-beam distance 0.5° and 1°, respectively. The results for Taylor synthesised array antennas are depicted in Fig. 4.28a for inter-beam distance 0.5°–1° and the density tapered array antennas are depicted in Fig. 4.28b for inter-beam distance 0.5°–1°. These are expected results as the radiation pattern is required to be 30 dB below maximum gain from OoC to FoV. The density tapered array antennas were required to have significantly (with the maximum individual array to have in the order of 1300 elements) more elements in order to meet the antenna requirements, but still showed the same trend the the convex optimised

and Taylor synthesised array antennas, as shown in Fig. 4.28b.

It can be noted that for array antennas of configuration 2 the number of elements would vary for the RX and the TX array antennas depending on which array was optimised first. This can be understood as the optimisation must be done twice and that the area which is given to the second optimisation is limited, as explained in Ch. 3. The effect of this approach is that array configuration 2 have a tendency to require more elements than the first configuration.

5.2 Effects of changed Inter-beam Distance

The investigated inter-beam distance was varied from 0.5° to 1°. The main observed effect was the significant enhancement in the number of elements and total aperture size. For inter-beam distance 1° the total aperture width (i.e. length along the x-axis) depending on if the configuration was either the latter two or 1 varied from 1.5 m to 0.9 m approximately, for inter-beam distance 0.5° the total aperture width changed to vary from 3 m to 1.8 m. Additionally the number of elements would approximately double for inter-beam distance 0.5° compared to the number of elements required for FoV 1°. The third effect was the increased maximum gain, however, this effect was not as significant as the other two.

5.3 Separate compared to Common RX/TX Elements and Element Sizes

The possibility of employing separate or common RX/TX elements are directly linked to the element size, as these effects can be seen in the usage of the separate or common RX/TX elements, where the common RX/TX element is the largest. The overall gain is higher for the array antennas of configuration 3, as depicted in Fig. 4.29. Furthermore, the number of elements for the array antennas were reduced significantly, often to half compared to configuration 1 and 2.

Array antennas of configuration 3 suffered from uncontrolled SLLs outside the FoV as the convex optimisation rendered solutions that were unphysical if the radiation pattern was extended further, i.e. elements were placed where they were overlapping. This issue is not as significant when using the separate RX/TX elements, as these elements are approximately half the size of the common RX/TX element. However, the number of elements required to suppress the radiation pattern further was significant, especially if compared to the increase in gain. An example of an unphysical solution for the array antenna of configuration 3 of inter-beam distance 1° and the FoV 8° is shown in Fig. 4.25.

5.4 SLL, Gain loss and Element Positioning

As SLLs were suppressed for the separate RX/TX element outside FoV the gain increased very little, as depicted in Fig. 4.29, often with the cost of 100–200 elements. This is a significant change as the number of elements to begin with are in the order of 200–300 and for the array antennas where the inter-beam distance is 1° and 400–700 elements for the array antennas where the inter-beam distance is 0.5°. As the gain is not greater in any significant manner, it is rather questionable if it is necessary to suppress the pattern outside FoV.

The total aperture width for configuration of the first compared to the latter two lied in the region 1.5 m–0.9 m and 3 m–1.8 m for inter-beam distance 1° and 0.5°, respectively. For the array antennas of configuration 1 the number of elements were lower in general than the array antennas of configuration 2 for inter-beam distance 0.5° and 1°, when suppressing the radiation pattern up to 8° and 15°, as shown in Fig. 4.28d. A bigger difference was observed for radiation mask range up to 15°, which may be due to that less area was given for the second array to be optimised. When the radiation pattern was suppressed to 8° the number of elements of array antennas of configuration 2 were closer to the array of configuration 1 for both inter-beam distances. Therefore are the array of configuration 2 preferable to the array antennas of configuration 1, as the aperture size is reduced significantly while only demanding slightly more elements.

5.5 Convex Optimised Array Antennas compared Taylor Synthesised Array Antennas and Density Tapered Array Antennas

For the Taylor synthesised array antennas well performing array antennas of configuration 1 could be obtained while the number of elements could compete with those of the convex optimised array antennas simultaneously. The element density tapered array antennas on the other hand demanded significantly more elements than both the convex optimised and Taylor synthesised array antennas. This is attributed to that the density tapering approach was initially designed to utilise different sizes of array elements, with respect to diameter. The functionality was implemented and presented in Ch. 2 but not used for the investigation as the given elements each have a constant radius in this thesis. It can be noted that the tapered array antennas had more difficulties for the larger inter-beam distance, as there is less area to obtain an approximative current distribution similar to the ideal current distribution.

Both the Taylor synthesised array antennas and the density tapered array antennas provided solutions of high element number density resulting in that array antennas of configuration 2 could not be obtained through these methods. It should be noted that the Taylor synthesised and density tapered array antennas in this thesis are optimised for the main beam only and are likely to perform worse in the scanning

mode. In the specification it is understood that the array should have the opportunity to steer the beam within the FoV, this should be better for the convex optimised array antennas.

5.6 MC Effects and Simulation Time

For the array antenna of configuration 1 the MC effects were included for the FoV 4° and inter-beam distance 1° where the simulation in FEKO showed that the radiation pattern complied with the requirements as depicted in Fig. 4.30. However, this array is one of the least dense array antennas and therefor may denser antenna designs violate the radiation mask when accounting for MC. It still suggests that MC effects are less than expected for the antennas employing separate RX/TX elements, which are the least directive compared to the common RX/TX element.

For the case of including MC effect for the array antenna of configuration 2, shown in Fig. 4.31, the radiation pattern violated the radiation mask for both the RX and the TX. It can be noted that the TX case violates the radiation mask less than the RX, which is expected because the RX array is embedded in the TX array causing the RX array to be in a denser environment. Although, the exhibited MC effects may be reduced for the RX case when the height of the RX elements are greater or equal to the height of the TX elements.

These results therefore present a possibility of obtaining realistic array antennas with significantly reduced simulation times, which would be in the order of weeks. However, further simulations with greater values of the FoV, inter-beam distance 0.5° and arrays with common RX/TX elements are needed to conclude this. Moreover, the results presented provides qualitatively interesting results, and possibly realistic results for many of the array antennas of configuration 3 and 1.

6

Conclusions

The array antennas antennas presented in the Ch. 4 utilises three array configurations which are schematically depicted in Fig. 3.2, where it additionally can be seen that the RX and TX apertures are circular. The first array configuration has two separate apertures as well as two separate array elements, presented in Sec. 3.2.2 for the RX and TX, where the RX frequency bandwidth is 27.5–30.0 GHz and the TX frequency bandwidth is 17.7–20.2 GHz. The second array configuration has one common aperture for the RX and the TX while still utilising two separate array element types. The third and last array configuration has one common aperture as well as one common array element type, presented in Sec. 3.2.3, for the RX and TX. Furthermore, the array designs were obtained through three different approaches where two of them are deterministic and the latter employ convex optimisation, described in Sec. 3.4, which optimises the element positions and excitation current to produce a radiation pattern which complies to the radiation mask. Of the deterministic approaches one is the density tapering, as described in Sec. 2.3.2, which utilises uniform element field amplitudes and creates an equivalent aperture to produce an excitation current that corresponds to the Taylor distribution. The other deterministic approach is that of the Taylor synthesis, as described in Sec. 2.3.1, which utilises uniformly placed elements and a varying element current excitation to produce a radiation pattern which has the most narrow beam-width for the highest allowed SLL.

The aperture diameters used for the simulations were for inter-beam distance 1° 2·0.45 m for the TX and 2·0.3 m for the RX. For the case of inter-beam distance 0.5° the diameters 2·0.9 m and 2·0.6 m were used for the TX and RX respectively. This subsequently means that for configuration 1 the spatial extension in x-direction will be 1.5 m and 0.9 m in the y-direction. The corresponding spatial extension for inter-beam distance 0.5° will be 1.8 m in the y-direction and 3 m in the x-direction. For configuration 2 and 3 the spatial extension of the antennas will be equal in both the x- and y- directions. Which for inter-beam distance 1° is 0.9 m and for inter-beam distance 0.5° is 1.8 m.

In conclusion, the maximum gain for array antennas of configurations 1 and 2 proved to be similar, usually varying as 0-4 dB from one another, as depicted in Fig. 4.29c and Fig. 4.29d for inter-beam distances 0.5° and 1° of convex optimised array antennas. These are expected results as the aperture area of the individual RX and TX arrays are equal for both configurations, where the only difference is that for configuration 2 both the RX and TX arrays share the aperture. Furthermore, the

first array configuration often achieves less total number of elements than the second configuration, in the region of 0-80 elements which is depicted in Fig. 4.28d and Fig. 4.28c. However, array antennas with configuration 2 achieves a smaller total aperture while exhibiting more MC effects, which degrades the radiation pattern in general as the SLLs are higher such that the radiation mask is violated, to a greater extent than the first array configuration. Moreover, the MC effects are of importance if the MC effects are not included in the synthesis procedures, i.e. the design procedure does not achieve optimum positions when accounting for MC effects such that the radiation pattern is not violated, as the radiation pattern becomes more degraded in this case. To achieve an optimum design of the array antennas the MC effects should be included, i.e. designing an array antenna which have elements placed such that the MC effects still obey the radiation mask, making the array with configuration 2 a conclusively better option with respect to the total aperture area, where the x-dimension is reduced from 1.5 m to 0.9 m and 3 m to 1.8 m for inter-beam distance 1° and 0.5°, respectively. Additionally, the number of elements can still be chosen equal or up to 80 more elements compared to configuration 1 while the gain is not significantly changed, but is increased in the region of 0-4 dB.

For the third array configuration the number of elements are reduced significantly, often close to 50% of the elements as compared to configurations 1 and 2. This is due to that the common RX/TX solution generates the radiation patterns in both frequencies, in contrast for array configurations 1 and 2 which demands two different solutions for the RX and the TX. The common RX/TX element is in addition more directive than the separate RX/TX elements and array antennas of configuration 3 and could therefore achieve higher maximum gain of the third array configuration. However, the convex optimisation showed difficulties in finding physical solutions, as elements were placed on top of each other, for array configuration 3 which forced the SLL outside Field of View (FoV) to be uncontrolled, where FoV is the angle which is no longer suppressed by the OoC gain requirement. It was on the other hand observed for the first and second array configurations that the number of elements required to suppress the SLL outside FoV were surprisingly large in comparison to the increase in gain. This makes the array antenna of configuration 3 a good candidate for SATCOM applications, with respect to the number of elements which ranges from 85–191 for inter-beam distance 1° and 193-545 for inter-beam distance 0.5° for the convex optimised array antennas, required aperture area, where the diameter is 0.9 m for inter-beam distance 1° and 1.8 m for inter-beam distance 0.5°. Finally, the gain is increased to lie in the region 33.0–38.0 dBi and 38.8–43.8 dBi for inter-beam distance 1° for the TX and RX, respectively, and 43.7–48.2 dBi 43.7–48.5 dBi for inter-beam distance 0.5° for the TX and RX, respectively.

When taking MC effects into account, in the post-evaluation for the previously convex optimised array antennas, the radiation patterns are expected to be degraded. For the case of array configuration 1 of FoV 4° and inter-beam distance 1° the radiation pattern, depicted in Fig. 4.30, complied with the applied radiation mask where as for array configuration 2 of FoV 4° and inter-beam distance 1° the radiation pattern, depicted in Fig. 4.31, violated the radiation mask. However, in the

case of array configuration 2, the MC effects might be reduced if the RX elements are raised to be higher or equal in height as the TX elements in the z-direction. It might therefore be possible to dramatically speed up the array simulations in the order of weeks while still obtaining realistic results for the array antennas of configuration 1 and 3, as the common RX/TX element is more directive and is expected to exhibit less MC effects. However, further simulations for configuration 3, wider FoV and narrower inter-beam distances are required to fully support this conclusion, as the requirements FoV 4° and inter-beam distance 1° have a lower element number density than that of the FoV 8° and inter-beam 1° for example. The array antennas are for the latter case forced to obey constraints which are stricter than FoV 4° as the radiation pattern is required to be below the OoC gain further, this pattern is depicted in Fig. 4.28.

The array antennas presented in Ch. 4 obtained through Taylor synthesis could meet the requirements presented in Sec. 3.1 with the number of elements in the same order as sparse array antennas obtained through convex optimisation where number of elements ranged from 71–547 for configuration 3 and 142-632 for configuration 1 of both inter-beam distance 1° and 0.5°. On the other hand, the density tapered array antennas encountered difficulties in meeting the stringent requirements presented in Sec. 3.1, resulting in significantly more array elements which ranged form 209 to 748 for configuration 3 and from 712 to 2662 for configuration 1. This is attributed to not using elements with varying diameters. In addition neither of the deterministic approaches could present solutions of array configuration 2, as the arrays were too dense with respect to the number of elements. Furthermore, array antennas of the deterministic approaches are optimised for the main beam only. Thus, when scanning for various angles they may perform worse than convex optimised array antennas.

To summarise, the convex optimised array antennas achieved good results for all configurations, albeit configurations 2 and 3 present more interesting advantages with respect to the number of elements, total aperture size and maximum gain than the first array configuration. Where for configuration 3 the number of elements reduces to close to half to that of configuration 1 and 2, while increasing the gain in the range of 10 dB. Although configuration 2 is still similar to configuration 1 with respect to number of elements it can require up to 80 elements more while the gain is increased up to 4dB. Lastly the total aperture area is reduced to 69% of the total aperture area of configuration 1, which is also true for configuration 3.

7

Future Recommendations

There are several aspects of this thesis that may be addressed where the most important part would be to complete the investigation while optimising with MC, as proposed in Ch. 3. As FEKO provides results for MC effects well, with less time constrictions, the results would be interesting to obtain. However, for further research the usage of the software CAESAR (CAESAR is a calculation tool developed at the department of Signals and Systems at Chalmers) instead of FEKO in the convex optimisation method would be beneficial. The main interest in doing so is that CAESAR is significantly faster than FEKO, albeit still in a developing phase. As RUAG space are interested in using a commercial EM calculation tool the EEPs could as a last step be simulated with FEKO of the optimised array in addition to the optimisation done with CAESAR. This approach would render two final radiation patterns, one with CAESAR and one with FEKO where the radiation pattern simulated with FEKO would serve as a reference.

Furthermore, it would be of interest for RUAG space to have the latest version of FEKO, which allows for the use of built in calculation tools of arrays in combination with waveguide ports. With the latest version FEKO presents the possibility of calculating the EEPs for the array antennas faster while providing a circular polarisation with waveguide ports instead of two edge ports.

For the density tapered array antennas it would be interesting to fully use the method, i.e. let the diameter of the array elements vary in order to produce optimal array antennas while keeping the number of controls to one (with respect to amplitude). Finally, it may be of interest to extend the convex optimisation algorithm when designing the array antennas of configuration 2. For example, the separate RX/TX array elements which lie in the same area for TX and RX may be replaced by a single common RX/TX array element type which could reduce the number of elements required.

Bibliography

[1] S. Johansson, "Design Study into Sparse Array Antenna Demonstrators for Future Satellite Systems", M.S thesis, Dept. of Signals and Systems, Chalmers University of Technology, Gothenburg, Sweden, 2014.

[2] C. Bencivenni, M. V. Ivashina, R. Maaskant and J. Wettergren, "Design of Maximally Sparse Array Antennas in the Presence of Mutual Coupling", *IEEE Antennas and Wireless Propagation Letters*, issn. 1536-1225, vol. 14, pp. 159–162, 2015.

[3] C. Bencivenni, M. Ivashina, R. Maaskant, and J. Wettergren, "Fast Synthesis of Wide-Scan-Angle-Maximally Sparse Array Antennas Using Compressive-Sensing and Full-Wave EM-Analysis", accepted by IEEE AP, 2015.

[4] P. Angeletti, G. Toso and G. Ruggerini, "Array Antennas With Jointly Optimized Elements Positions and Dimensions Part II: Planar Circular Arrays", *IEEE Transactions on Antennas and Propagation*, vol. 62, no. 4, pp. 1627-1639, April 2014.

[5] C. A. Balanis, "Antenna Synthesis and Continuous Sources" in *Antenna Theory: Analysis and Design*, 3rd ed., Hoboken, NJ, John Wiley, 2005, ch. 7, sec. 7.6, pp. 406-410.

[6] C. Bencivenni, "Sparse array synthesis of complex antenna elements", Lic. thesis, Dept. of Signals and Systems, Chalmers University of Technology, Gothenburg, Sweden, 2015.

[7] C. A. Balanis, "Fundamental Parameters of Antennas" in *Antenna Theory: Analysis and Design*, 3rd ed., Hoboken, NJ, John Wiley, 2005, ch. 2, sec. 2.1 - 2.15, pp. 27-87.

[8] P. S. Kildal, "Characterization of directive antennas" in *Foundations of Antennas A Unified Approach*, Lund, Sweden, Studentlitteratur, 2000, ch. 2, sec. 2.1 - 2.3, pp. 22-52.

[9] P. S. Kildal, "Equivalent circuits of two-port circuits and circuitss" in *Foundations of antennas: a unified approach for Lien-Of-Sight and Multipath*, Sweden, Kildal Antenn AB., 2015, ch. F, sec. F.4, pp. 406-407.

[10] S. J. Orfanidis, "S-parameters" in *Electromagnetic Waves and Antennas*, ch. 14, sec. 14.4, pp. 669-670, [Online], Available: `www.ece.rutgers.edu/~orfanidi/ewa`, Retrieved: 2016-03-05.

[11] J. Wettergren, private communication, June 2015.

[12] P.S Kildal, "Array antennas" in *Foundations of antennas: a unified approach.*, Lund, Sweden, Studentlitteratur, 2000, ch. 9, sec. 9.1, pp. 344-346.

[13] C. A. Balanis, "Arrays: Linear, Planar, and Circular" in *Antenna Theory: Analysis and Design*, 3rd ed., Hoboken, NJ, John Wiley, 2005, ch. 6, sec. 6.4, pp. 290-294.

[14] P.S Kildal, "Array antennas" in *Foundations of antennas: a unified approach*, Lund, Sweden, Studentlitteratur, 2000, ch. 9, sec. 9.3, pp. 367-368.

[15] Volakis, "Phased Arrays" in *Antenna Engineering Handbook*, 4th ed.,New York, McGraw-Hill, 2007, ch. 2, sec. 2.2., pp. 20-25 – 20-19.

[16] R. J. Mailloux, "Summary of Element Pattern and Mutual Impedance Effects" in *Phased array antenna handbook*, Boston, Artech House, 1994, ch. 6, sec. 6.2, pp. 192-194.

[17] C. A. Balanis, "Antenna Synthesis and Continuous Sources" in *Antenna Theory: Analysis and Design*, 3rd ed., Hoboken, NJ, John Wiley, 2005, ch. 7, sec. 7.1, pp. 385-387.

[18] T. T. Taylor, "Design of Line-Source Antennas for Narrow Beamwidth and Low Sidelobes," *IRE Trans. Antennas Propagat.*, vol. AP-3, no. 1, pp. 16–28, Jan. 1955.

[19] R. S. Elliott, "Design of Line-Source Antennas for Narrow Beamwidth and Asymmetric Low Sidelobes," *IEEE Trans. Antennas Propagat.*, vol. 23, no. 1, pp. 100–107, Jan. 1975.

[20] G. J. Van der Maas, "Simplified Calculation for Dolph-Tchebycheff Arrays", *Journal of Applied Physics*, vol. 12, pp. 121-124, 1954.

[21] P. Angeletti and G. Toso, "Aperiodic arrays for space applications: A combined amplitude/density synthesis approach," in 2009 *EuCAP 2009. 3rd European Conference on Antennas and Propagation*, pp. 2026-2030.,

[22] EM Software & Systems-S.A. (Pty) Ltd, "FEKO User's Manual", Stellenbosch, South Africa, pp. 1-1 –1-10, [Online], Available: `http://www.altairuniversity.com/wp-content/uploads/2015/03/UserManual.pdf`, Retrieved: 160305.

[23] M. C. Grant, S. P. Boyd, "The CVX Users' Guide", CVX Research Inc, June 10, 2015, pp. 1-3, [Online], Available: `http://web.cvxr.com/cvx/doc/CVX.pdf`, Retrieved: 160305.

A

Array Antennas of the FoV $5° - 7°$

Complementary results for FoV 5°-7° are given in this appendix to the results in Ch. 4. The array designs are shown along with the radiation patterns and imposed radiation masks. The separate TX array elements are depicted with empty circles, the RX array elements are shown in filled circles and the common RX/TX array elements are shown in semi filled circles.

A.1 Array Antennas Utilising Common and Separate RX/TX Apertures and Separate RX/TX Elements

This section gives the results for the array antennas of configuration 1 and 2.

A.1.1 Taylor Synthesised Array Antennas

In this section are the results for the arrays of configuration 1 depicted of Taylor synthesised array antennas.

A.1.1.1 Inter-beam Distance 1°

In Fig. A.1 are the array design and radiation pattern shown for the FoV 5 ° and inter-beam distance 1° of a Taylor synthesised array antenna.

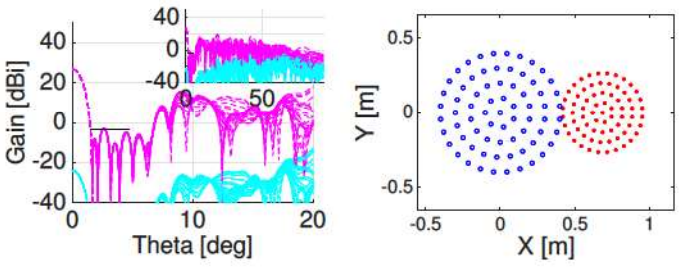

(a) Radiation pattern for the TX and RX.

(b) Array configuration 1.

Figure A.1: Array design and radiation pattern of the Taylor synthesised arrays with inter-beam distance 1° and the FoV 5°.

In Fig. A.2 are the array design and radiation pattern are shown for the FoV 6 ° and inter-beam distance 1° of a Taylor synthesised array antenna.

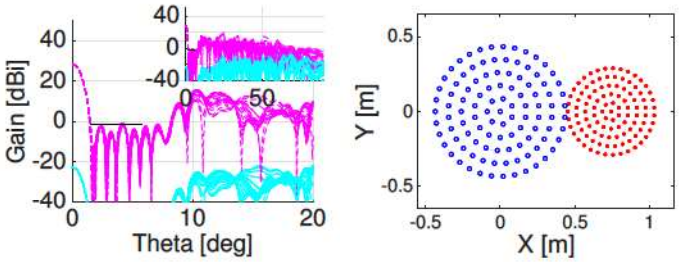

(a) Radiation pattern for the TX and RX.

(b) Array configuration 1.

Figure A.2: Array design and radiation pattern of the Taylor synthesised arrays with inter-beam distance 1° and the FoV 6°.

In Fig. A.3 are the array design and radiation pattern shown for the FoV 7 ° and inter-beam distance 1° of a Taylor synthesised array antenna.

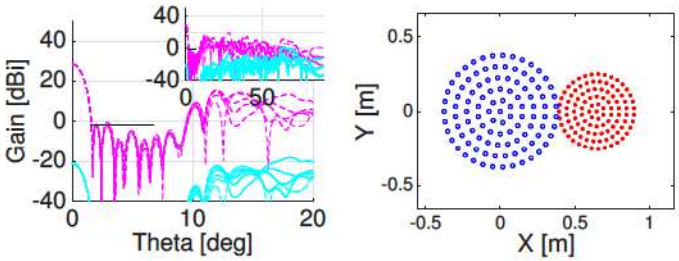

(a) Radiation pattern for the TX and RX.

(b) Array configuration 1.

Figure A.3: Array design and radiation pattern of the Taylor synthesised arrays with inter-beam distance 1° and the FoV 7°.

A.1.1.2 Inter-beam Distance 0.5°

In Fig. A.4 are the array design and radiation pattern shown for the FoV 5° and inter-beam distance 0.5° of a Taylor synthesised array antenna.

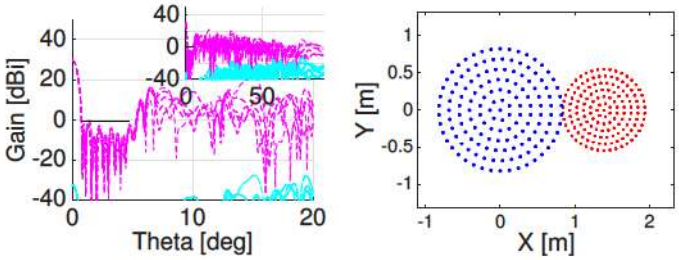

(a) Radiation pattern for the TX and RX. (b) Array configuration 1.

Figure A.4: Array design and radiation pattern of the Taylor synthesised arrays with inter-beam distance 0.5° and the FoV 5°.

In Fig. A.5 are the array design and radiation pattern shown for the FoV 6° and inter-beam distance 0.5° of a Taylor synthesised array antenna.

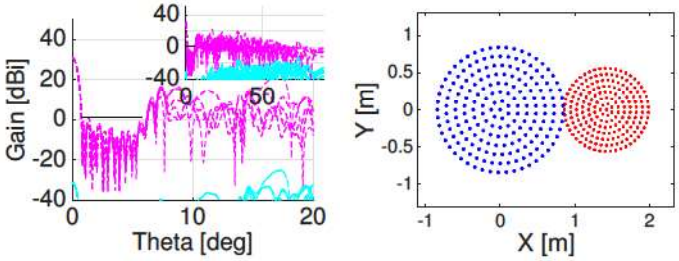

(a) Radiation pattern for the TX and RX. (b) Array configuration 1.

Figure A.5: Array design and radiation pattern of the Taylor synthesised arrays with inter-beam distance 0.5° and the FoV 6°.

In Fig. A.6 are the array design and radiation pattern shown for the FoV 7° and inter-beam distance 0.5° of a Taylor synthesised array antenna.

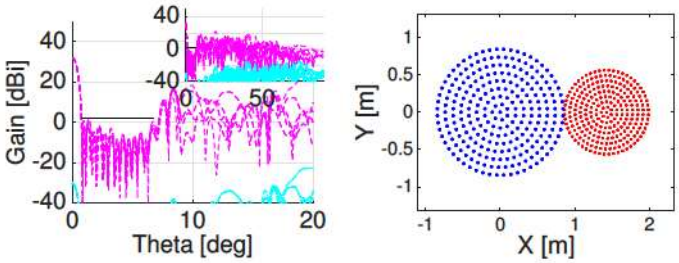

(a) Radiation pattern for the TX and RX.

(b) Array configuration 1.

Figure A.6: Array design and radiation pattern of the Taylor synthesised arrays with inter-beam distance 0.5° and the FoV 7°.

A.1.2 Density Tapered Array Antennas

In this section are the results for the array antennas of configuration 1 depicted of density tapered array antennas.

A.1.2.1 Inter-beam Distance 0.5°

In Fig. A.7 are the array design and radiation pattern shown with the FoV 5 ° and inter-beam distance 0.5° of a density tapered array antenna.

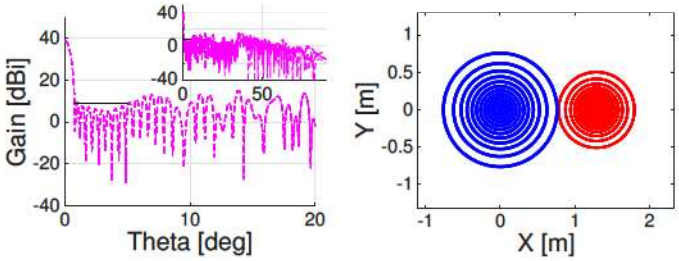

(a) Radiation pattern for the TX and RX.

(b) Array configuration 1.

Figure A.7: Array design of density tapered arrays and radiation pattern with inter-beam distance 0.5° and the FoV 5°.

In Fig. A.8 are the array design and radiation pattern shown with the FoV 6 ° and inter-beam distance 0.5° of a density tapered array antenna.

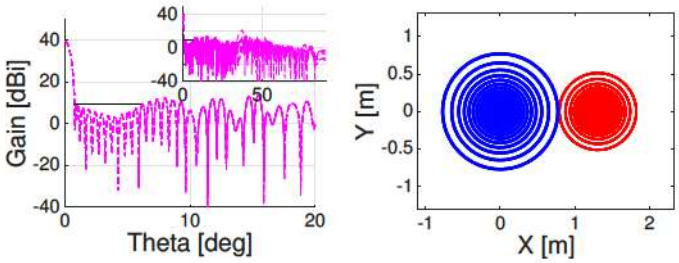

(a) Radiation pattern for the TX and RX.

(b) Array configuration 1.

Figure A.8: Array design of density tapered arrays and radiation pattern with inter-beam distance 0.5° and the FoV 6°.

In Fig. A.9 are the array design and radiation pattern shown with the FoV 7 ° and inter-beam distance 0.5° of a density tapered array antenna.

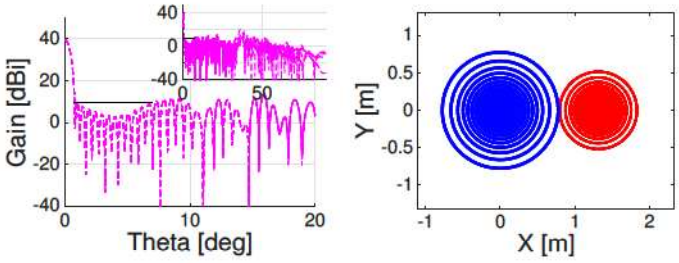

(a) Radiation pattern for the TX and RX.

(b) Array configuration 1.

Figure A.9: Array design of density tapered arrays and radiation pattern with inter-beam distance 0.5° and the FoV 7°.

A.1.3 Convex Optimised Array Antennas

In this section are the complimentary results for the arrays of configurations 1 and 2 depicted of convex optimised array antennas.

A.1.3.1 Inter-beam Distance 1°

In Fig. A.10 are the array designs and radiation patterns shown for convex optimised array antennas of the FoV 5 ° and inter-beam distance 1° with radiation mask range 8°.

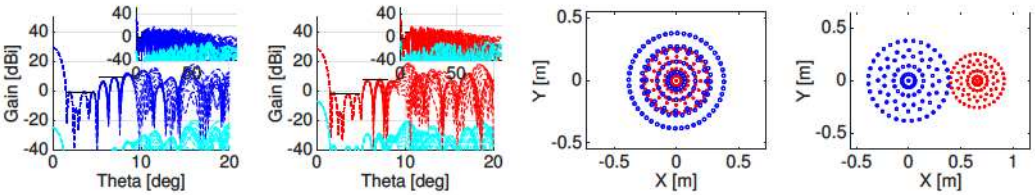

(a) Radiation pattern for the TX. (b) Radiation pattern for the RX. (c) Array configuration 2. (d) Array configuration 1.

Figure A.10: Array designs of convex optimised arrays and radiation patterns with inter-beam distance 1°, the FoV 5° and radiation mask range 8°.

In Fig. A.11 are the array designs and radiation patterns shown for convex optimised array antennas of the FoV 5 ° and inter-beam distance 1° with radiation mask range 15°.

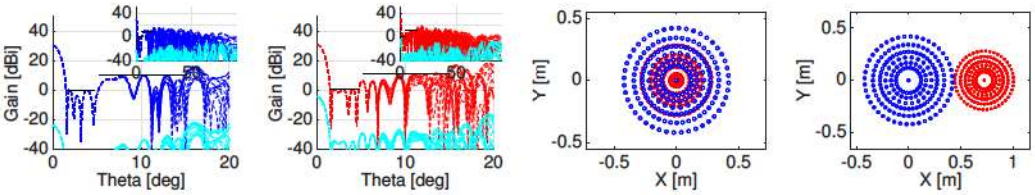

(a) Radiation pattern for the TX. (b) Radiation pattern for the RX. (c) Array configuration 2. (d) Array configuration 1.

Figure A.11: Array designs of convex optimised arrays and radiation patterns with inter-beam distance 1° and the FoV 5° and radiation mask range 15°.

In Fig. A.12 are the array designs and radiation patterns shown for convex optimised array antennas of the FoV 6 ° and inter-beam distance 1° with the radiation mask range 8°.

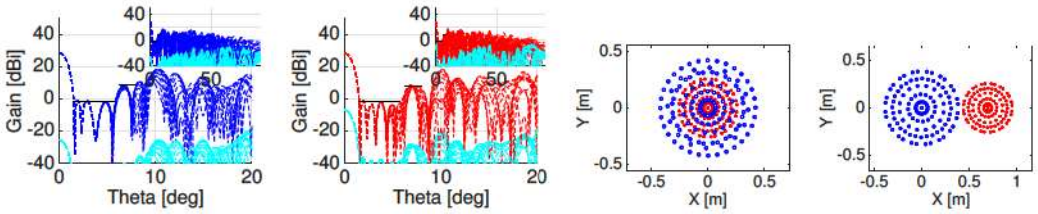

(a) Radiation pattern for the TX. (b) Radiation pattern for the RX. (c) Array configuration 2. (d) Array configuration 1.

Figure A.12: Array designs of convex optimised arrays and radiation patterns with inter-beam distance 1°, the FoV 6° and radiation mask range 8°.

In Fig. A.13 are the array designs and radiation patterns shown for convex optimised array antennas of the FoV 6 ° and inter-beam distance 1° with radiation mask range 15°.

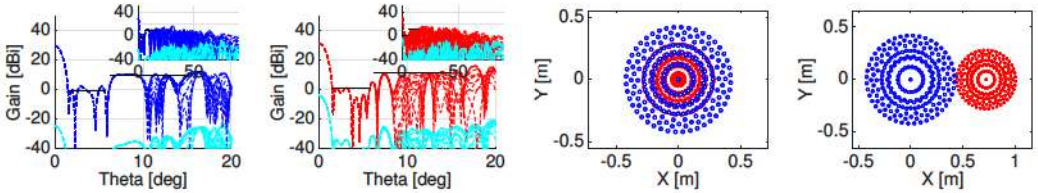

(a) Radiation pattern for the TX. (b) Radiation pattern for the RX. (c) Array configuration 2. (d) Array configuration 1.

Figure A.13: Array designs of convex optimised arrays and radiation patterns with inter-beam distance 1°, the FoV 6° and radiation mask range 15°.

In Fig. A.14 are the array designs and radiation patterns shown for convex optimised array antennas of the FoV 7 ° and inter-beam distance 1° with radiation mask range 8°.

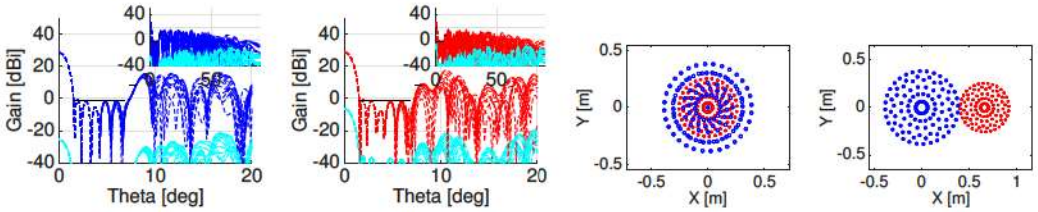

(a) Radiation pattern for the TX. (b) Radiation pattern for the RX. (c) Array configuration 2. (d) Array configuration 1.

Figure A.14: Array designs of convex optimised arrays and radiation patterns with inter-beam distance 1°, the FoV 7° and radiation mask range 8°.

In Fig. A.15 are the array designs and radiation patterns shown for convex optimised array antennas of the FoV 7 ° and inter-beam distance 1° with radiation mask range 15°.

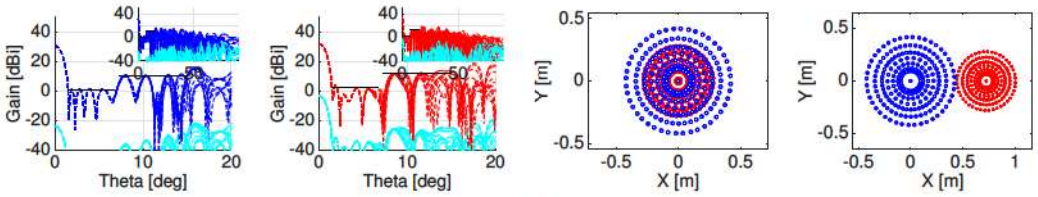

(a) Radiation pattern for the TX.
(b) Radiation pattern for the RX.
(c) Array configuration 2.
(d) Array configuration 1.

Figure A.15: Array designs of convex optimised arrays and radiation patterns with inter-beam distance 1°, the FoV 7° and radiation mask range 15°.

A.1.3.2 Inter-beam Distance 0.5°

In Fig. A.16 are the array designs and radiation patterns shown for convex optimised array antennas of the FoV 5 ° and inter-beam distance 0.5° with radiation mask range 8°.

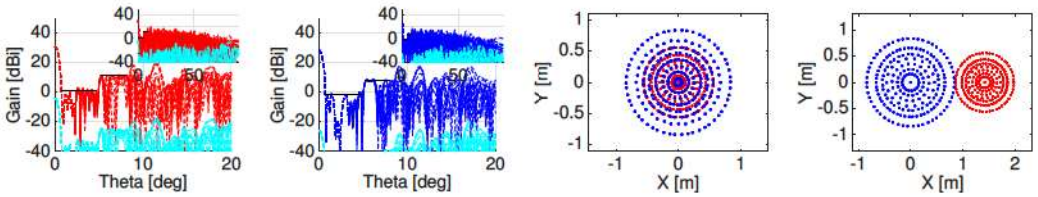

(a) Radiation pattern for the RX.
(b) Radiation pattern for the TX.
(c) Array configuration 2.
(d) Array configuration 1.

Figure A.16: Array designs of convex optimised arrays and radiation patterns with inter-beam distance 0.5° and the FoV is 5° with radiation mask range 8°.

In Fig. A.17 are the array designs and radiation patterns shown for convex optimised array antennas of the FoV 5 ° and inter-beam distance 0.5° with radiation mask range 15°.

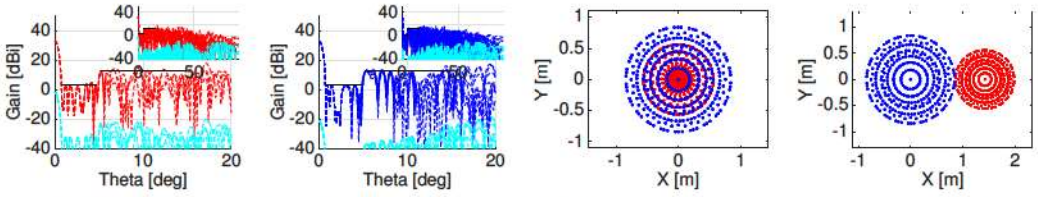

(a) Radiation pattern for the RX.
(b) Radiation pattern for the TX.
(c) Array configuration 2.
(d) Array configuration 1.

Figure A.17: Array designs of convex optimised arrays and radiation patterns with inter-beam distance 0.5° and the FoV is 5° with radiation mask range 15°.

In Fig. A.18 are the array designs and radiation patterns shown for convex optimised array antennas of the FoV 6 ° and inter-beam distance 0.5° with radiation mask range 8°.

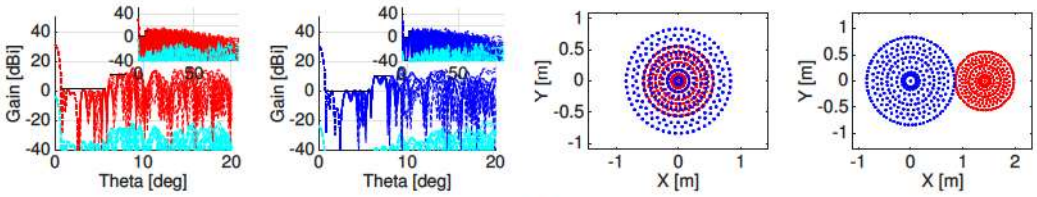

(a) Radiation pattern for the RX. (b) Radiation pattern for the TX. (c) Array configuration 2. (d) Array configuration 1.

Figure A.18: Array designs of convex optimised arrays and radiation patterns with inter-beam distance 0.5° and the FoV is 6° with radiation mask range 8°.

In Fig. A.19 are the array designs and radiation patterns shown for convex optimised array antennas of the FoV 6 ° and inter-beam distance 0.5° with radiation mask range 15°.

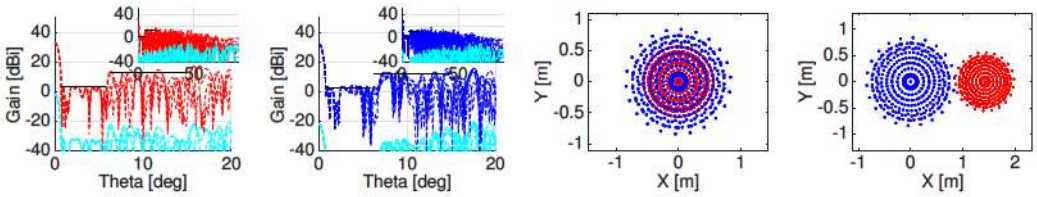

(a) Radiation pattern for the RX. (b) Radiation pattern for the TX. (c) Array configuration 2. (d) Array configuration 1.

Figure A.19: Array designs of convex optimised arrays and radiation patterns with inter-beam distance 0.5° and the FoV is 6° with radiation mask range 15°.

In Fig. A.20 are the array designs and radiation patterns shown for convex optimised array antennas of the FoV 7 ° and inter-beam distance 0.5° with radiation mask range 8°.

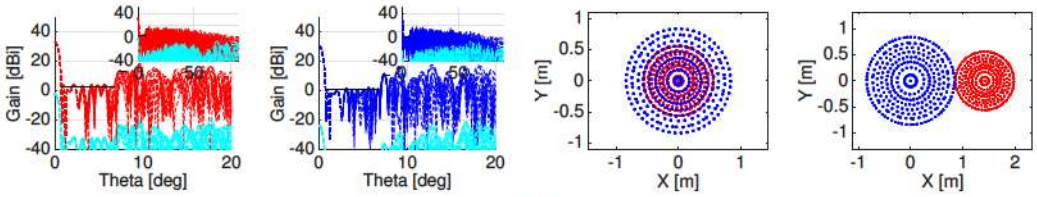

(a) Radiation pattern for the RX. (b) Radiation pattern for the TX. (c) Array configuration 2. (d) Array configuration 1.

Figure A.20: Array designs of convex optimised arrays and radiation patterns with inter-beam distance 0.5° and the FoV is 7° with radiation mask range 8°.

In Fig. A.21 are the array designs and radiation patterns shown for convex optimised array antennas of the FoV 7 ° and inter-beam distance 0.5° with radiation mask range 15°.

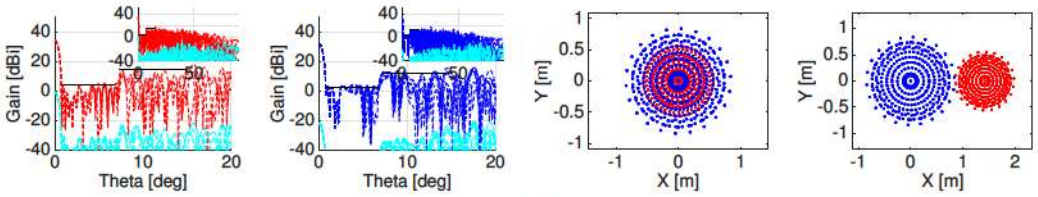

(a) Radiation pattern for the RX.

(b) Radiation pattern for the TX.

(c) Array configuration 2.

(d) Array configuration 1.

Figure A.21: Array designs of convex optimised arrays and radiation patterns with inter-beam distance 0.5° and the FoV 7° with radiation mask range 15°.

A.2 Array Antennas Utilising Common RX/TX Apertures and Common RX/TX Elements

In this section are the results for array antennas of configuration 3 given as a compliment to the results in Ch. 4.

A.2.1 Taylor Synthesised Array Antennas

In this section are the results for the arrays of configuration 3 depicted of Taylor synthesised array antennas.

A.2.1.1 Inter-beam Distance 1°

In Fig. A.22 are the array design and radiation patterns shown for a Taylor synthesised array antenna with inter-beam distance 1° and the FoV 5 °.

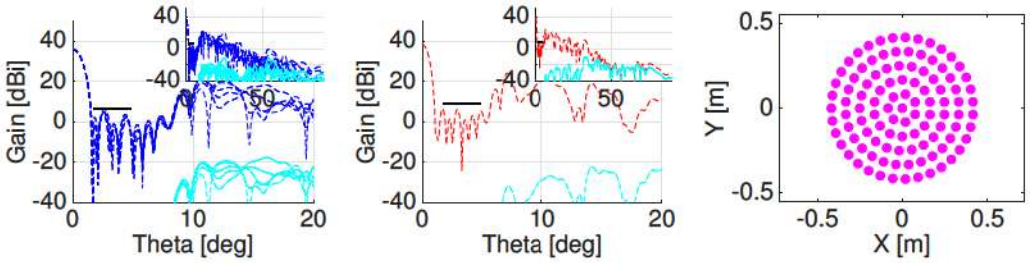

(a) Radiation pattern for the RX.

(b) Radiation pattern for the TX.

(c) Array configuration 3.

Figure A.22: Array design and radiation patterns of a Taylor synthesised array antenna with inter-beam distance 1° and the FoV 5°.

In Fig. A.23 are the array design and radiation patterns shown for a Taylor synthesised array antenna with inter-beam distance 1° and the FoV 6 °.

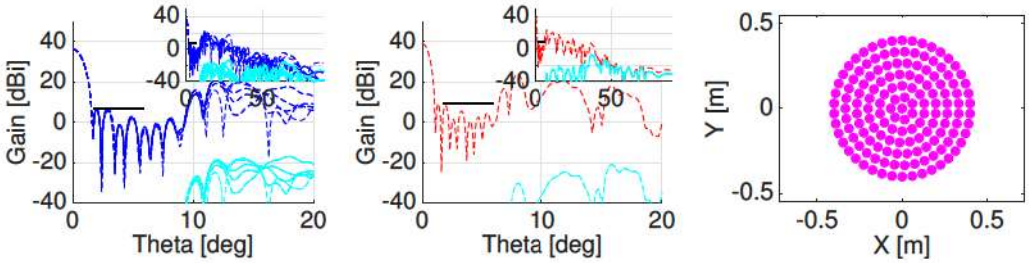

(a) Radiation pattern for the RX.

(b) Radiation pattern for the TX up to 20°

(c) Array configuration 3.

Figure A.23: Array design and radiation patterns of a Taylor synthesised array antenna with inter-beam distance 1° and the FoV 6°.

In Fig. A.24 are the array design and radiation patterns shown for a Taylor synthesised array antenna with inter-beam distance 1° and the FoV 7 °.

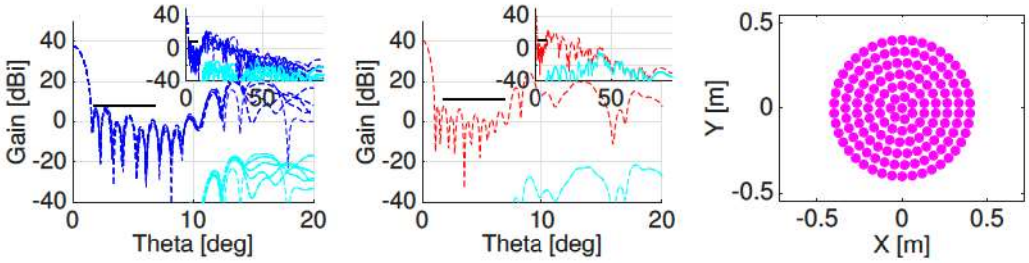

(a) Radiation pattern for the RX.

(b) Radiation pattern for the TX up to 20°

(c) Array configuration 3.

Figure A.24: Array design and radiation patterns of a Taylor synthesised array antenna with inter-beam distance 1° and the FoV 7°.

A.2.1.2 Inter-beam Distance 0.5°

In Fig. A.25are the array design and radiation patterns shown for a Taylor synthesised array antenna with inter-beam distance 0.5° and the for FoV 5 °.

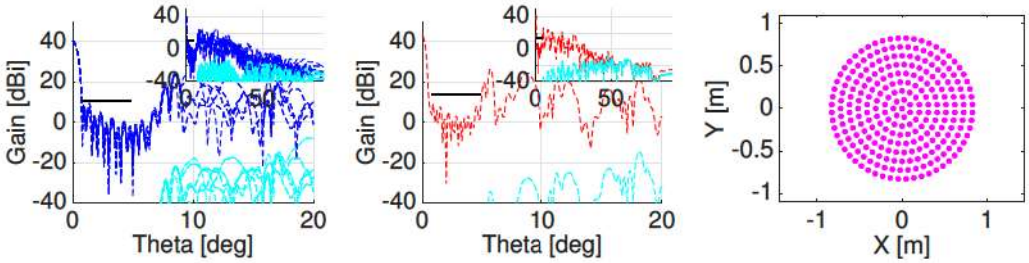

(a) Radiation pattern for the TX.

(b) Radiation pattern for the TX.

(c) Array configuration 3.

Figure A.25: Taylor synthesised array antenna and radiation patterns with inter-beam distance 0.5° and the FoV 5°.

In Fig. A.26are the array design and radiation patterns shown for a Taylor synthesised array antenna with inter-beam distance 0.5° and the for FoV 6 °.

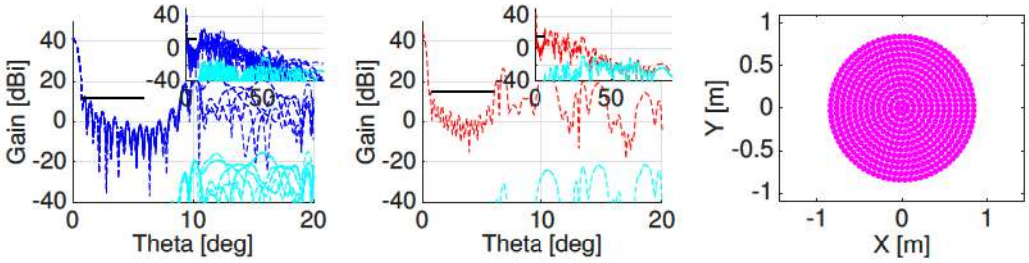

(a) Radiation pattern for the TX up to 20°.

(b) Radiation pattern for the TX up to 20°.

(c) Array configuration 3.

Figure A.26: Taylor synthesised array antenna and radiation patterns with inter-beam distance 0.5° and the FoV 6°.

In Fig. A.27are the array design and radiation patterns shown for a Taylor synthesised array antenna with inter-beam distance 0.5° and the for FoV 7 °.

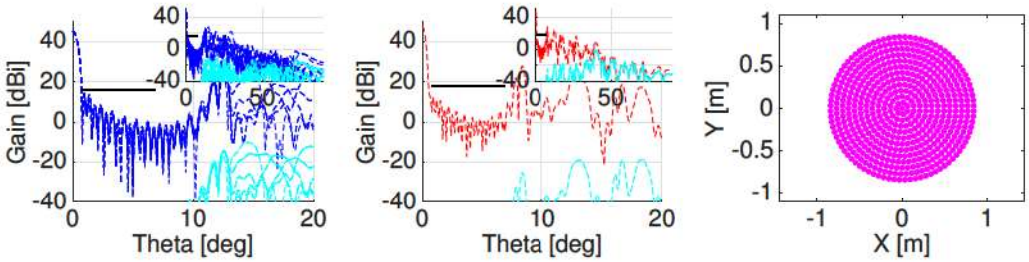

(a) Radiation pattern for the TX.

(b) Radiation pattern for the TX.

(c) Array configuration 3.

Figure A.27: Taylor synthesised array antenna and radiation patterns with inter-beam distance 0.5° and the FoV 7°.

A.2.2 Density Tapered Array Antennas

In this section are the results for the arrays of configuration 3 depicted of density tapered array antennas.

A.2.2.1 Inter-beam Distance 0.5°

In Fig. A.28 are the array design and radiation patterns shown for a density tapered array antenna with inter-beam distance 0.5° and the FoV 5 °.

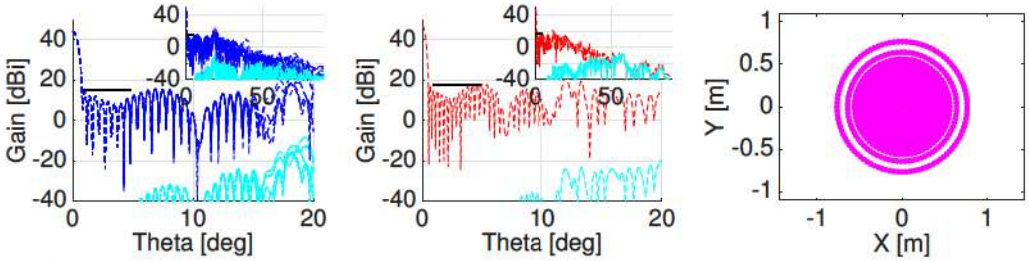

(a) Radiation pattern the TX.

(b) Radiation pattern the RX.

(c) Array configuration 3.

Figure A.28: Array design and radiation patterns of a density tapered array antenna with inter-beam distance 0.5° and the FoV 5°.

In Fig. A.29 are the array design and radiation patterns shown for a density tapered array antenna with inter-beam distance 0.5° and the FoV 6 °.

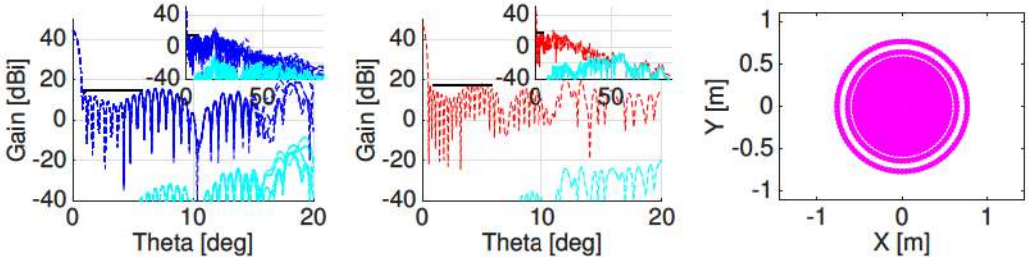

(a) Radiation pattern the TX.

(b) Radiation pattern the RX.

(c) Array configuration 3.

Figure A.29: Array design and radiation patterns of a density tapered array antenna with inter-beam distance 0.5° and the FoV 6°.

In Fig. A.30 are the array design and radiation patterns shown for a density tapered array antenna with inter-beam distance 0.5° and the FoV 7 °.

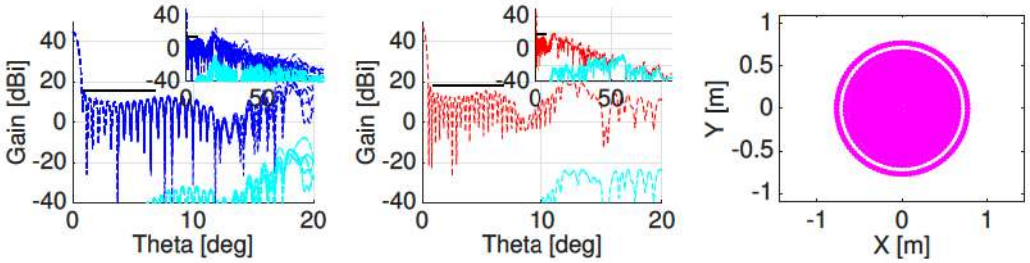

(a) Radiation pattern the TX.

(b) Radiation pattern the RX up to 20°

(c) Array configuration 3.

Figure A.30: Array design and radiation patterns of a density tapered array antenna with inter-beam distance 0.5° and the FoV 7°.

A.2.3 Convex Optimised Array Antennas

In this section are the results for the arrays of configuration 3 depicted of convex optimised array antennas.

A.2.3.1 Inter-beam Distance 1°

In Fig. A.31 are the array design and radiation patterns shown for a convex optimised array antenna with inter-beam distance 1° and the FoV 5°.

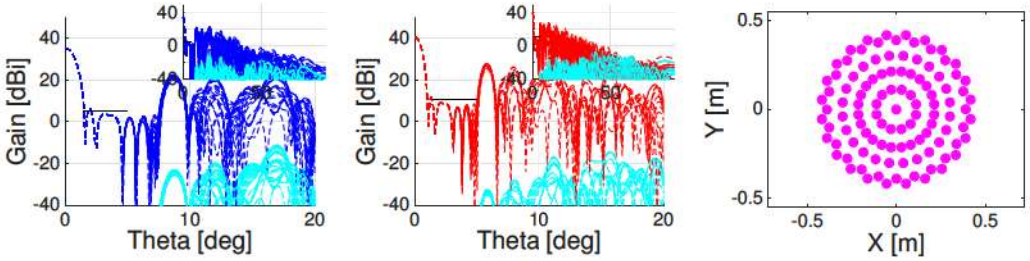

(a) Radiation pattern for the RX.

(b) Radiation pattern for the TX.

(c) Array configuration 3.

Figure A.31: Array design and radiation patterns of a convex optimised array antenna with inter-beam distance 1° and the FoV 5°.

In Fig. A.32 are the array design and radiation patterns shown for a convex optimised array antenna with inter-beam distance 1° and the FoV 6°.

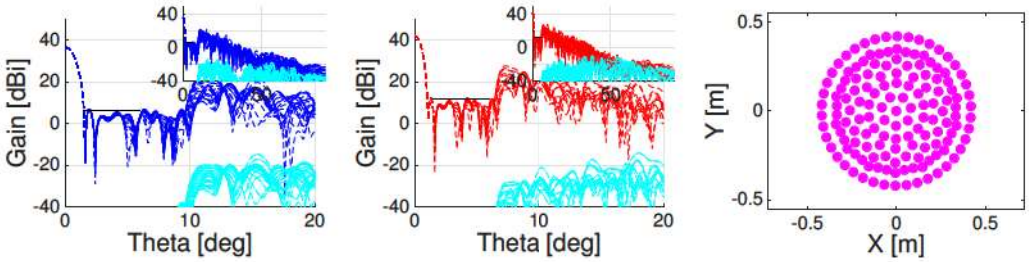

(a) Radiation pattern for the RX.

(b) Radiation pattern for the TX.

(c) Array configuration 3.

Figure A.32: Array design and radiation patterns of a convex optimised array antenna with inter-beam distance 1° and the FoV 6°.

In Fig. A.33 are the array design and radiation patterns shown for a convex optimised array antenna with inter-beam distance 1° and the FoV 7°.

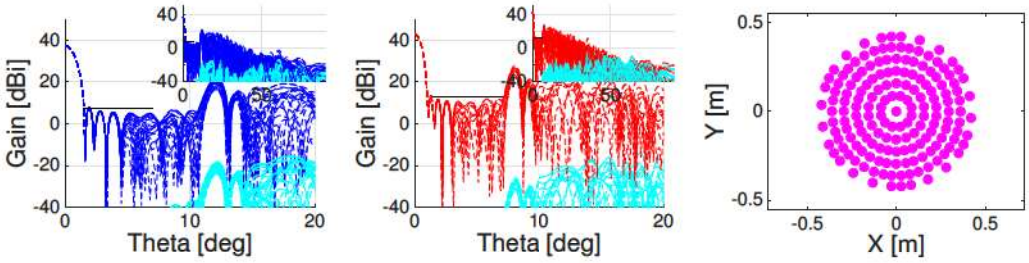

(a) Radiation pattern for the RX.

(b) Radiation pattern for the TX.

(c) Array configuration 3.

Figure A.33: Array design and radiation patterns of a convex optimised array antenna with inter-beam distance 1° and the FoV 7°.

A.2.3.2 Inter-beam Distance 0.5°

In Fig. A.34 are the array design and radiation patterns shown for a convex optimised array antenna with inter-beam distance 0.5° and the FoV 5°.

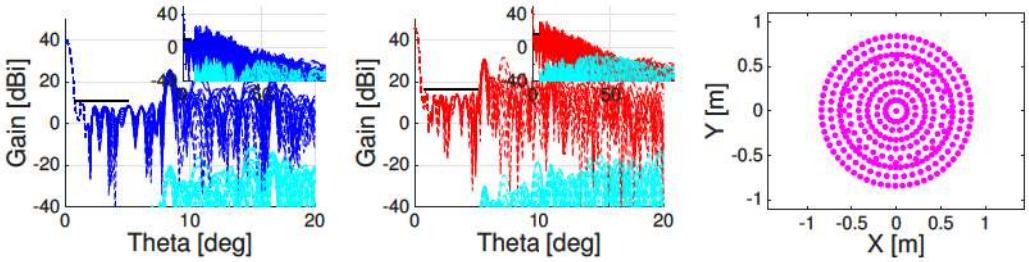

(a) Radiation pattern for TX.

(b) Radiation pattern for RX.

(c) Array configuration 3.

Figure A.34: Array design and radiation patterns of a convex optimised array antenna with inter-beam distance 0.5° and the FoV 5°.

In Fig. A.35 are the array design and radiation patterns shown for a convex optimised array antenna with inter-beam distance 0.5° and the FoV 6°.

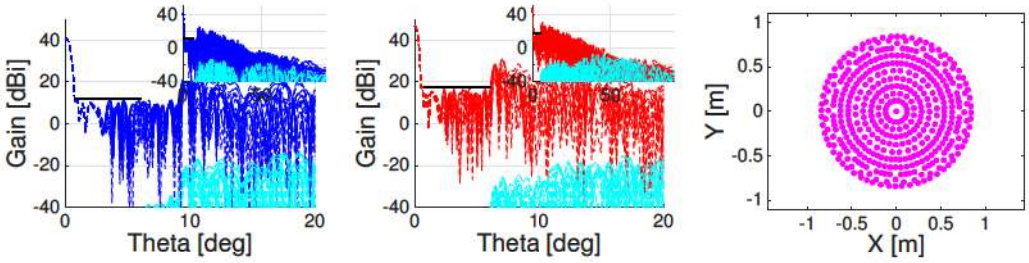

(a) Radiation pattern for TX.

(b) Radiation pattern for RX.

(c) Array configuration 3.

Figure A.35: Array design and radiation patterns of a convex optimised array antenna with inter-beam distance 0.5° and the FoV 6°.

In Fig. A.36 are the array design and radiation patterns shown for a convex optimised array antenna with inter-beam distance 0.5° and the FoV 7°.

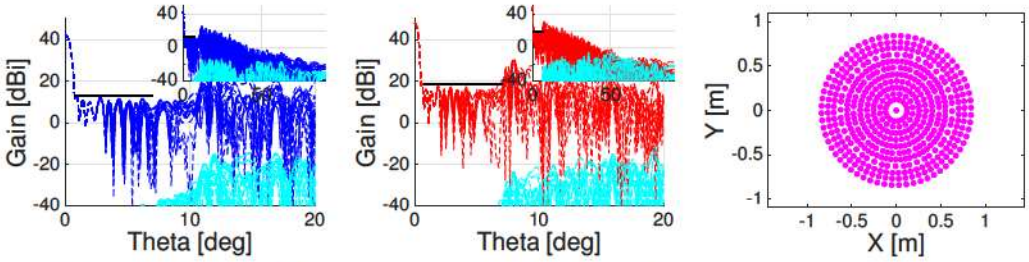

(a) Radiation pattern for TX.

(b) Radiation pattern for RX.

(c) Array configuration 3.

Figure A.36: Array design and radiation patterns of a convex optimised array antenna with inter-beam distance 0.5° and the FoV 7°.